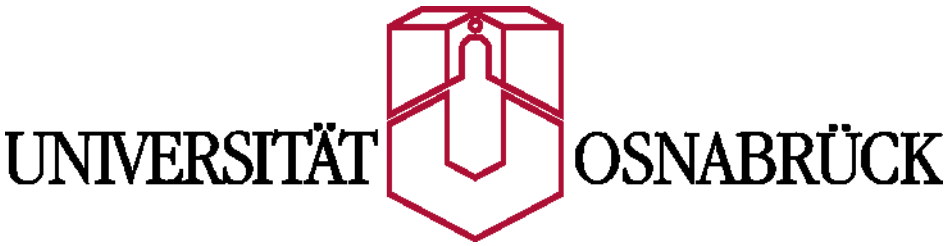

Click Functionalization of Carbon Nanotubes for Nano-Bio Applications

Doctoral Dissertation

by

Gririraj Manoharan

Department of Physics

University of Osnabrueck

Osnabrueck

October 2021

Dissertation to partially fulfill the requirements for the degree of

"**Doctor rerum naturalium**"

presented by Griririaj Manoharan

to the department of physics – University of Osnabrueck

Reviewer #1: Dr. Carola Meyer

Reviewer #2: Prof. Dr. Joachim Wollschläger

Acknowledgements

First and foremost, I would like to thank Dr. Carola Meyer for giving me the opportunity to work on the project and being available all the time for great discussions and supporting me throughout the whole time.

I wish to thank Prof. Dr. Wolfgang Harneit for his continuous support and motivating words during my tenure. Many thanks to Prof. Dr. Joachim Wollschläger for examining my thesis.

I would like to thank Dr. René Wieczorek and Petra Bösel for sharing their ideas and experience without hesitation for all my questions, especially chemistry. Thanks to Jannis Thien for sharing his knowledge about XPS measurements and analysis.

Many thanks to the CellNanos Celebrities Dr. Michael Holtmannspötter and Dr. Michael Phillipi for their constant support and assistance, especially during the latter half of my thesis. Not to forget Dr. Rainer Kurre for his support with instruments.

I would like to thank our collaborators Laura Meingast and Prof. Dr. Janina Maultzsch for carrying out Raman measurements and our fruitful discussions.

I thank all the other colleagues who helped me on different occasions Mercedes Runge, Qaiser Ali Khan, Lara Jorde, and Alida Meyer, for their assistance during my tenure. Thanks to Jan, our café relaxation talks are fun and unforgettable.

A huge thanks to all my friends and colleagues who helped me out during these hectic times where the world took a “pause”. Special thanks to my one and only lab partner Mykola Fomin for being part of my progress in most of my ON and OFF academia tasks. I thank my friend Suresh Maniarasu for assisting me with the XPS analysis and being a pillar of support during this challenging time.

Last but not least, I want to thank wholeheartedly my parents Manoharan and Vetrikodi, for always believing in me and supporting me no matter what. Special thanks to my lovely sister Sujitra for being my Jerry.

Abstract

One of the main subjects of this thesis is to design a novel synthetic route to covalently functionalize carbon nanotubes with various molecules in a non-toxic way on both surface and suspension. Functionalized carbon nanotubes are of great interest in the field of molecular electronics, materials science and nano-bio applications because of their remarkable structural, chemical and physical properties.

First, the single-walled carbon nanotubes are functionalized with gold nanoparticles by the route, which involves silanization and copper-free click chemistry (SPAAC). We characterize the functionalized nanotubes through XPS, IR and Raman spectroscopic techniques to identify the surface attachment of molecules after each step. We observe a drastic change in homogeneity and functionalization density of single-walled carbon nanotubes with gold nanoparticles concerning solvent through TEM.

Employing the same route, biomolecules such as fluorescent dyes and single-stranded DNA molecules are integrated with SWNTs. Fluorescence lifetime analysis of AF647 functionalized SWNTs is reduced compared to free dye due to the fluorescence quenching phenomenon of carbon nanotubes. Functionalized SWNTs are characterized with FLIM, SEM, and Raman for better correlation at the same area of interest. Furthermore, the nanotubes are resolved at the nanoscale level through STORM imaging technique with a limited photon budget. Single-stranded DNA molecules of different lengths are used to investigate the fluorescence quenching as they are distance-dependent. DNA-PAINT is engaged in imaging the functionalized SWNTs with an unlimited photon budget, overcoming STORM's challenge.

Lastly, the route is transferred to surface-grown CNTs through the CVD technique, in which both the gold nanoparticles and fluorescent dyes are grafted with nanotubes

selectively. CVD is carried out on different substrates Si/SiO_2, quartz substrate and quartz coverslip for substrate functionalization. Catalyst deposition plays a significant role in not only the CVD growth but also in the lifetime analysis of the substrate functionalized nanotubes. We observe similar fluorescence quenching of nanotubes in the substrate compared with nanotubes functionalized in suspension. Surface-grown nanotubes in the optically transparent substrate can be resolved through STORM at the nanoscale level.

In conclusion, we demonstrate a synthetic design to functionalize SWNTs which provides the possibility to be versatile and non-toxic. Moreover, we show that the nanotubes can be functionalized through this route homogeneously and selectively on both surface and suspension. This work lays the foundation for tailoring SWNTs with not only a wide range of molecules and to study their functional characteristics but also to carry out functionalization on different substrates for various applications.

Table of Contents

Chapter 1

Introduction

Nanotechnology has played a significant role in recent decades, delivering improvements in various disciplines such as medical, telecommunications, and electronics and dramatically accelerating the progress in our society. Nanotechnology is a highly interdisciplinary field that brings together chemists, physicists, biologists, material scientists, and physicians. The idea of genuinely directing the structure at the nanoscale, as envisioned by Feynman in his 1960 speech "There's Plenty of Room at the Bottom," marked the beginning of modern nanotechnology[1]. Binnig and Rohrer's discovery of the scanning tunneling microscope in 1981 made it possible to investigate and manipulate surfaces with atomic precision[2]. One of the examples of ancient nanotechnology, which has been discovered very recently, is the keeladi pottery from Tamil Nadu, India.

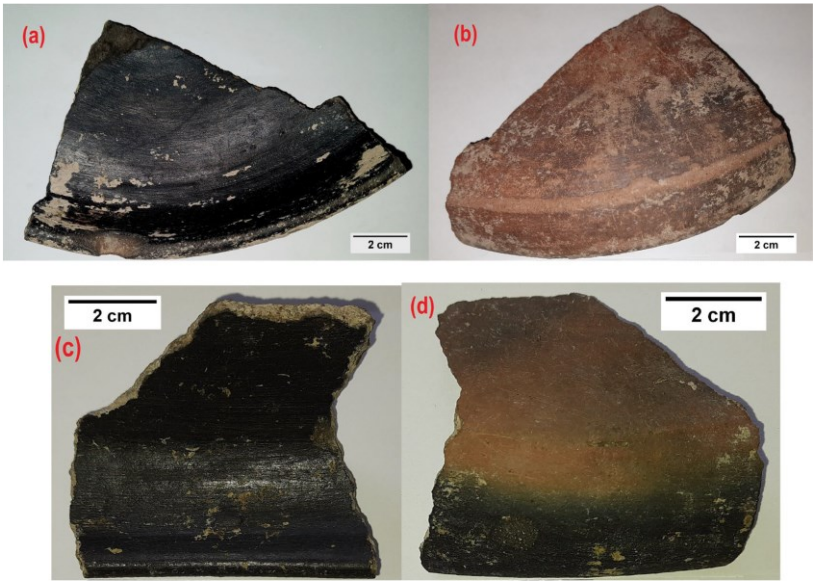

Figure 1.1 Keeladi Pottery Shards. The inner portion showed the shining black coating, which was later revealed to be a mix of single-walled and multi-walled carbon nanotubes that dated back to the 6th century B.C[3].

A combination of single-walled and multi-walled carbon nanotubes was found after analyzing the outlandishly intense pottery shreds. Later it was discovered that the carbon nanotubes were coated inside the pottery that dates back to the sixth century BC, and it still retains their stability and adhesion[3]. Over the past 25 years, carbon nanomaterials and their physics have evolved into one of the most studied nanomaterials in the research world. Depending on the degree of hybridization, carbon can be divided into three types: sp^3-hybridized diamond, sp^2-hybridized graphite with delocalized π-electrons, and sp^2-hybridized fullerenes. Iijima is credited with discovering carbon nanotubes (CNTs) in 1991[4], when he first recognized their graphitic structure, despite Radushkevich having previously made CNTs in 1952 and Oberlin in 1976[5,6]. Concentric graphite layers, today known as multi-walled carbon nanotubes, were discovered by Iijima (MWNTs). Two years later, two groups of researchers independently synthesized single-walled carbon nanotubes (SWNTs): Iijima et al.[7] and Bethune et al.[8]. Novoselov et al.[9] isolated graphene, a one-atom-thick sheet of sp^2-hybridized carbon atoms, in 2004 via mechanical exfoliation, later awarded the Nobel prize in 2010.

Since then, CNTs have attracted tremendous interest for their unique and promising physical, chemical, electronic, mechanical and optical properties[10], influencing greatly in applications such as the semiconductor industry, especially in sensing devices[11] and electronic circuits[12]. These extraordinary properties can be enhanced to a different level when one tailors a variety of molecules with nanotubes for different applications such as molecular electronics[13,14], advanced nanocomposite materials[15] and biomedical systems[16–18]. Although numerous prototypes have been manufactured, technological obstacles, particularly the difficulties in large-scale processing CNTs, have hampered their commercialization because of the inappropriate handling in their dry state and their low solubility with common

solvents needed for deposition[19]. Carbon nanotubes have to be integrated with other nanostructures such as nanoparticles or molecules to develop highly engineered functionalities. Depending on the application, this has to be implemented on individual CNTs on a surface or with CNTs in suspension. Chemical functionalization is an effective strategy to graft various molecules to the surface of the carbon nanotubes for various applications. As swiftly recognized, chemical functionalization of the CNT surface is a critical step in overcoming the barrier and laying the groundwork for the later processability of CNT derivatives.

Two main strategies are employed to make the nanotubes into functional materials: the covalent sidewall coupling reactions and non-covalent functionalization through hydrophobic interactions. Non-covalent functionalization involves biomacromolecules or wrapping with polymers. In contrast, covalent functionalization via "*grafting to"* or "*grafting from"* routes are the techniques used to alter the nanotubes' surface characteristics to achieve better dispersion and further interactions with molecules[20,21].

Among these functionalization techniques, click chemistry, a covalent way of attaching molecules to nanotubes, offers us versatility with high efficiency in a simple manner. Click chemistry defines several different, unique, and simple chemical reactions compatible with aqueous media (green chemistry) and has a simple purification method (the absence of by-products)[22–24].

Adronov and co-workers are the first ones to functionalize the carbon nanotubes through click chemistry with metal catalyst[25]. There is, however, a desire to develop new click-reactions incorporating living systems and biomolecules without metal catalysis, as they could be cytotoxic. The impairment of these metal ions could harm biological activities as well as electrical and optoelectronic systems. It has been reported in several pieces of literature that metal ions such as copper influence the

genetic structure of the DNA and its process, affecting the fluorescence quenching of quantum dots and can alter the structure of protein repelling organic moieties apart from toxicity[26–28].

The copper-free [3+2] Huisgen cycloaddition, also known as strain-promoted alkyne-azide cycloaddition (SPAAC), is one of the effective reactions. C.R. Bertozzi and co-workers pioneered the use of cyclic alkynes and azides in this process[29]. This copper-free click reaction, which does not require a metal catalyst, uses the ring strain energy of a cyclooctyne group as a substantial geometrical distortion of the C≡C bond to allow the 1,3-dipolar cycloaddition to proceed quickly.

However, the grafting density with these reactions is still challenging due to their poor solubility of strained alkynes in aqueous media and relatively slower than the CuAAC[30]. Here, we design a hybrid synthetic route that involves silanization and SPAAC click reaction to functionalize carbon nanotubes with versatile molecules like metal nanoparticles and biomolecules. This route enhances the functionalization density through silanization and allows the cycloaddition to proceed efficiently without the influence of metal catalysts.

Surface characterization like X-ray photoelectron spectroscopy is in place after every chemical reaction to achieve gold nanoparticle functionalized SWNTs. For the further process of grafting versatile molecules, this acts as the base to understand the feasibility of the synthetic route.

Many uses of SWNTs for advanced biomedical sensing rely on the grafted analytes present in the surface of the nanotubes. One of the significant challenges in the carbon nanotube world is understanding the fluorescence quenching behavior of the functionalized nanotubes. There are a variety of reasons for this phenomenon. Therefore, it is essential to gain more profound knowledge about the SWNTs and

their conjugates and properties, such as the energy transfer between the SWNTs and the attached fluorescent dye.

A part of this work deals with functionalized carbon nanotubes, which are scrutinized to understand the photophysical properties like fluorescence lifetime and fluorescence quenching through advanced microscopic techniques like FRET-FLIM, STORM and DNA-PAINT. Single-molecule localization techniques assist us to image the ultrastructure in high resolution and study the fluorescence properties of the functionalized CNTs. Single-stranded DNA molecules of different lengths provide us with a systematic way of investigating the photophysical properties of the functionalized SWNTs as they are distance-dependent. In addition to this, we transfer this synthetic route to CVD grown nanotubes as they widen the carbon nanotube field-effect transistor (CNTFET) device fabrication in molecular electronics, especially in biosensing applications and localize the fluorescent dye functionalized CNTs in optically transparent substrates for the investigation of photophysical properties.

One of the main objectives of this thesis is to establish a functionalization route that will not only enhance the functionalization density but also be compatible with bioapplications. This should be appropriate for grafting versatile molecules like metal nanoparticles and fluorescent dyes with nanotubes. The following work aims to understand better the properties of functionalized SWNTs with different molecules of high relevance in various fields like nanoelectronic devices, nano biosensing devices, and advanced optical imaging in biosystems.

The outline of the thesis is as follows:

Chapter 2 presents carbon nanotubes and their promising properties, focusing on the versatility of the carbon nanomaterial in different applications. Various forms of functionalization, especially click chemistry, are discussed as they widen the application window in nanoelectronic devices and nanobiotechnology fields. The design of our synthetic route and experimental techniques are also described in this chapter.

Chapter 3 establishes the unique functionalization route that involves silanization and strain-promoted azide-alkyne cycloaddition, also known as copper-free click chemistry for single-walled carbon nanotubes with gold nanoparticles. Characterization of the gold functionalized carbon nanotubes is discussed after every step of the synthetic route with spectroscopic and microscopic techniques. This chapter forms the base by introducing the functionalization procedure used in the following chapters with versatile molecules.

Chapter 4 continues the functionalization of single-walled carbon nanotubes but with fluorescent dyes like Cyanine 3 and AF647. The central part of this chapter deals with the post-functionalization characteristics of the SWNTs like microscopic fluorescence imaging and fluorescence lifetime analysis. In addition to this, the correlation between SEM and Raman spectroscopy assists us with the chirality assignment and structural characterization of the functionalized carbon nanotubes. Single-molecule localization microscopic technique STORM is introduced to image the fluorescent dye functionalized nanotubes to study their photophysical properties.

In **Chapter 5**, the functionalization of single-stranded DNA molecules with carbon nanotubes will be demonstrated, along with their photophysical properties. DNA-PAINT, an interesting single-molecule localization microscopic technique, is

engaged to investigate photophysical properties like fluorescence quenching. Various DNA strands of different lengths and their corresponding characteristics are discussed via the DNA-PAINT approach.

Chapter 6 introduces the designed synthetic route for grafting single-walled carbon nanotubes in the previous chapters transferred to the CVD grown nanotubes on a substrate. Different substrates like Si/SiO_2 are used to perform substrate functionalization for nano electron devices. Additionally, transparent optical substrates are employed to understand better the high-resolution fluorescence imaging and lifetime analysis of the fluorescent dye functionalized CVD grown nanotubes.

Furthermore, the final chapter 7 concludes the thesis with a summary and discussion for future investigations.

References

(1) Feynman, R. P. There's Plenty of Room at the Bottom. *Eng. Sci.* **1960**, *23* (5), 22–36. https://resolver.caltech.edu/CaltechES:23.5.1960Bottom.

(2) Binnig, G.; Rohrer, H.; Gerber, C.; Weibel, E. Surface Studies by Scanning Tunneling Microscopy, *Phys.Rev.Lett.* **1982**, *49* (1), 57 - 61. https://doi.org/10.1103/PhysRevLett.49.57.

(3) Kokarneswaran, M.; Selvaraj, P.; Ashokan, T.; Perumal, S.; Sellappan, P.; Murugan, K. D.; Ramalingam, S.; Mohan, N.; Chandrasekaran, V. Discovery of Carbon Nanotubes in Sixth Century BC Potteries from Keeladi, India. *Sci. Rep.* **2020**, *10* (1), 19786. https://doi.org/10.1038/s41598-020-76720-z.

(4) Iijima, S. Helical Microtubules of Graphitic Carbon. *Nature* **1991**, *354* (6348), 56–58. https://doi.org/10.1038/354056a0.

(5) Radushkevich, L. V.; Lukyanovich, V. M. On the Carbon Structure Formed during Thermal Decomposition of Carbon Monoxide in the Presence of Iron. *Zh. Fiz. Khim* **1952**, No. 26, 88-95.

(6) Oberlin, A.; Endo, M.; Koyama, T. Filamentous Growth of Carbon through Benzene Decomposition. *J. Cryst. Growth* **1976**, *32* (3), 335–349. https://doi.org/https://doi.org/10.1016/0022-0248(76)90115-9.

(7) Iijima, S.; Ichihashi, T. Single-Shell Carbon Nanotubes of 1-Nm Diameter. *Nature* **1993**, *363* (6430), 603–605. https://doi.org/10.1038/363603a0.

(8) Bethune, D.S.; Kiang, C.H.; de Vries, M.S.; Gorman, G.; Savoy, R.; Vazquez, J.; Beyers, R. Cobalt-Catalysed Growth of Carbon Nanotubes with Single-Atomic-Layer Walls. *Nature* **1993**, *363* (6430), 605–607. https://doi.org/10.1038/363605a0.

(9) Novoselov, K. S.; Geim, A. K.; Morozov, S. V; Jiang, D.; Zhang, Y.; Dubonos, S. V; Grigorieva, I. V; Firsov, A. A. Electric Field Effect in Atomically Thin Carbon Films. *Science (80).* **2004**, *306* (5696), 666–669. https://doi.org/10.1126/science.1102896.

(10) Rathinavel, S.; Priyadharshini, K.; Panda, D. A Review on Carbon Nanotube: An Overview of Synthesis, Properties, Functionalization, Characterization, and the Application. *Mater. Sci. Eng. B* **2021**, *268*, 115095. https://doi.org/https://doi.org/10.1016/j.mseb.2021.115095.

(11) Kruss, S.; Hilmer, A. J.; Zhang, J.; Reuel, N. F.; Mu, B.; Strano, M. S. Carbon Nanotubes as Optical Biomedical Sensors. *Adv. Drug Deliv. Rev.* **2013**, *65* (15), 1933–1950. https://doi.org/10.1016/j.addr.2013.07.015.

(12) Baughman, R. H.; Zakhidov, A. A.; Heer, W. A. De. Carbon Nanotubes — the Route Toward Applications. Science, **2002**, *297*, 787–793. https://doi.org/10.1126/science.1060928.

(13) Avouris, P. Molecular Electronics with Carbon Nanotubes. *Acc. Chem. Res.* **2002**, *35* (12), 1026–1034. https://doi.org/10.1021/ar010152e.

(14) Collins, P. G.; Avouris, P. Nanotubes for Electronics. *Sci. Am.* **2000**, *283* (6), 62–69. https://doi.org/10.1038/scientificamerican1200-62.

(15) Ajayan, P. M. Nanotubes from Carbon. *Chem. Rev.* **1999**, *99* (7), 1787–1800. https://doi.org/10.1021/cr970102g.

(16) Katz, E.; Willner, I. Biomolecule Functionalized Carbon Nanotubes: Applicat ions in Nanobioelectronics. *ChemPhysChem* **2004**, *5* (8),1084–1104. https://doi.org/10.1002/cphc.200400193.

(17) Kotov, N.A.; Winter, J.O.; Clements, I.P.; Jan, E.; Timko, B.P.; Campidelli,

S.; Pathak, S.; Mazzatenta, A.; Lieber, C.M.; Prato, M.; Bellamkonda, R.V.; Silva, G.A.; Kam, N.W.S.; Patolsky, F.; Ballerini, L. Nanomaterials for Neural Interfaces. *Adv. Mater.* **2009**, *21* (40), 3970–4004. https://doi.org/10.1002/adma.200801984.

(18) Ménard-Moyon, C.; Kostarelos, K.; Prato, M.; Bianco, A. Functionalized Carbon Nanotubes for Probing and Modulating Molecular Functions. *Chem. Biol.* **2010**, *17* (2), 107–115. https://doi.org/10.1016/j.chembiol.2010.01.009.

(19) Ma, P.C.; Siddiqui, N.A.; Marom, G.; Kim, J. K. Dispersion and Functionaliz ation of Carbon Nanotubes for Polymer-Based Nanocomposites: A Review. *Compos. Part A Appl. Sci. Manuf.* **2010**, *41*(10), 1345–1367. https://doi.org/https://doi.org/10.1016/j.compositesa.2010.07.003.

(20) Richard, C.; Balavoine, F.; Schultz, P.; Ebbesen, T. W.; Mioskowski, C. Supramolecular Self-Assembly of Lipid Derivatives on Carbon Nanotubes. *Science* **2003**, *300* (5620), 775–778. https://doi.org/10.1126/science.1080848.

(21) Nakashima, N.; Tomonari, Y.; Murakami, H. Water-Soluble Single-Walled Carbon Nanotubes via Noncovalent Sidewall-Functionalization with a Pyrene-Carrying Ammonium Ion. *Chem. Lett.* **2002**, *31* (6), 638–639. https://doi.org/10.1246/cl.2002.638.

(22) Campidelli, S. Click Chemistry for Carbon Nanotubes Functionalization. *Curr. Org. Chem.* **2012**, *15* (8), 1151–1159. https://doi.org/10.2174/138527211795203004.

(23) He, Z.; Huang, H.; Jiang, R.; Mao, L.; Liu, M.; Chen, J.; Deng, F.; Zhou, N.; Zhang, X.; Wei, Y. Click Multiwalled Carbon Nanotubes: A Novel Method for Preparation of Carboxyl Groups Functionalized Carbon Quantum Dots. *Mater. Sci. Eng. C* **2020**, *108*, 110376.

https://doi.org/10.1016/j.msec.2019.110376.

(24) Kolb, H. C.; Finn, M. G.; Sharpless, K. B. Click Chemistry: Diverse Chemical Function from a Few Good Reactions. *Angew. Chemie - Int. Ed.* **2001**, *40* (11), 2004–2021. https://doi.org/10.1002/1521-3773(20010601)40:11<2004::AID-ANIE2004>3.0.CO;2-5.

(25) Li, H.; Cheng, F.; Duft, A.M.; Adronov, A. Functionalization of Single-Walled Carbon Nanotubes with Well-Defined Polystyrene by "Click" Coupling. *J. Am. Chem. Soc.* **2005**, *127* (41), 14518–14524. https://doi.org/10.1021/ja054958b.

(26) Tajmir-Riahi, H. A.; Langlais, M.; Savoie, R. A Laser Raman Spectroscopic Study of the Interaction of Calf-Thymus DNA with Cu(II) and Pb(II) Ions: Metal Ion Binding and DNA Conformational Changes. *Nucleic Acids Res.* **1988**, *16* (2), 751–762. https://doi.org/10.1093/nar/16.2.751.

(27) Shey, M.S.; Hughes, E.J.; de Kock, M.; Barnard, C.; Stone, L.; Kollmann, T. R.; Hanekom, W.A.; Scriba, T. J. Optimization of a Whole Blood Intracellular Cytokine Assay for Measuring Innate Cell Responses to Mycobacteria. *J. Immunol. Methods* **2012**, *376* (1–2), 79–88. https://doi.org/10.1016/j.jim.2011.11.011.

(28) Jewett, J.C.; Bertozzi, C. R. Cu Free Click Cycloaddition Reactions in Chemi cal Biology. *Chem. Soc. Rev.* **2010**, *39* (4), 1272–1279. https://doi.org/10.1039/b901970g.

(29) Agard, N. J.; Prescher, J. A.; Bertozzi, C. R. A Strain-Promoted [3 + 2] Azide-Alkyne Cycloaddition for Covalent Modification of Biomolecules in Living Systems. *J. Am. Chem. Soc.* **2004**, *126* (46), 15046–15047. https://doi.org/10.1021/ja044996f.

(30) Escorihuela, J.; Marcelis, A. T. M.; Zuilhof, H. Metal-Free Click Chemistry Reactions on Surfaces. *Adv. Mater. Interfaces* **2015**, *2* (13), 1–42. https://doi.org/10.1002/admi.201500135.

Chapter 2
Materials and Methods

2.1 Carbon nanotubes and properties

2.1.1 Atomic Structure

Carbon nanotubes are a honeycomb lattice of the graphene sheets, also known as pseudo-one-dimensional fullerenes, rolled up into a hollow cylinder. A single-walled carbon nanotube (SWNT) has all of its atoms on the surface and is thus thought of as the cylindrical form of a single sheet of graphene, whereas multi-walled carbon nanotubes are made up of multiple layers of graphite. Owing to their chirality, CNTs may behave either metallic or semiconducting. SWNTs give structural confinement due to their substantial aspect ratio, featuring diameters in the order nanometers, lengths up to several centimeters[1].

In graphene, the carbon atoms are organized in a hexagonal lattice, with each atom having three closest neighbors separated by an interatomic distance of C-C = 1.421Å. The unhybridized Pz-orbitals create π-bonds with delocalized electrons, whereas the sp^2-hybridized orbitals form σ-bonds with delocalized electrons, which are responsible for graphene's peculiar electrical characteristics.

Individual walls are held together by van der Waals interactions and have an inter shell spacing of ~0.34 nm, close to the graphite interlayer distance of 0.344nm.

SWNTs with various unit cells and symmetries, called "chiralities," are the primary source of the rolling angle of a theoretical graph plate. Carbon nanotubes have unique characteristics because of their graphic structure and their extensive range of conjugated π-bonding orbitals.

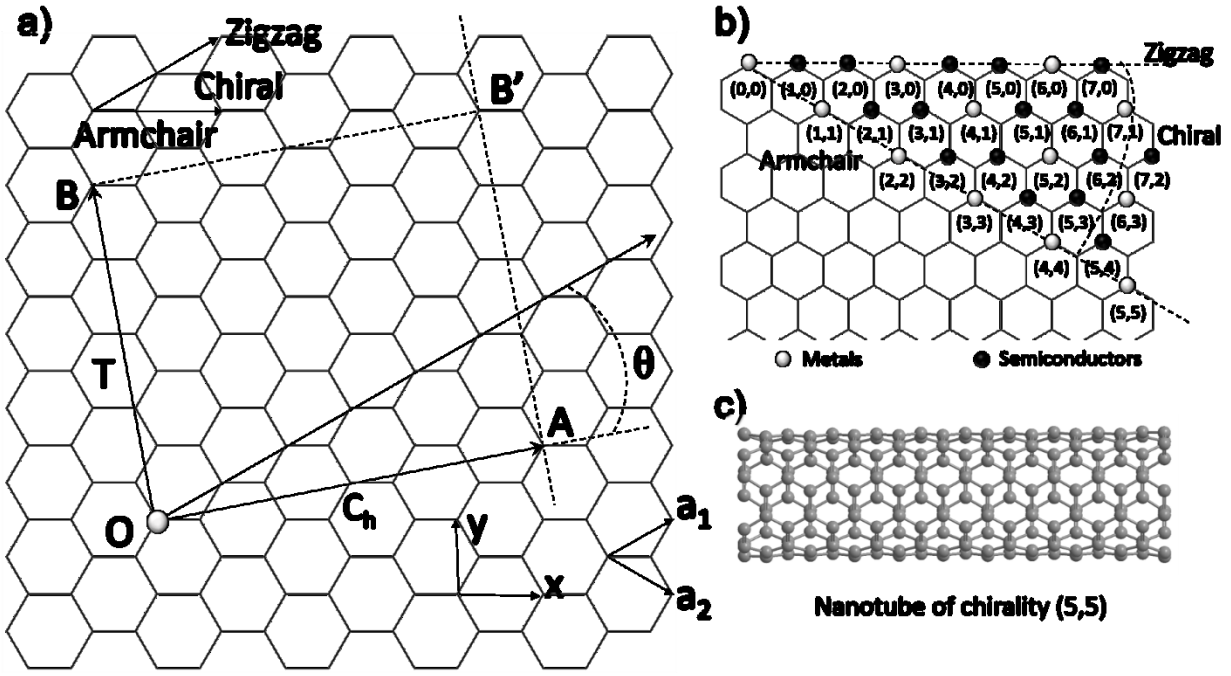

Figure 2.1 a) Schematic design of the chiral vector (C_h) in Graphene Lattice. b) Relationship between the integers (n,m) and nanotubes' metallic or semiconducting behavior. c) Structure of a nanotube with an Armchair chirality (5,5).

Single-walled carbon nanotubes can be classified accordingly with the way graphene sheet is rolled up. The unit cell of the vectors of a graphene sheet $\vec{a}_1$ and $\vec{a}_2$ define the chiral vector $\overrightarrow{C_h}$:

$$\overrightarrow{C_h} = n\vec{a}_1 + m\vec{a}_2 \qquad 2.1$$

with $n \geq m$. $\overrightarrow{C_h}$ is represented by the integer pair (n,m) and uniquely defines a particular nanotube. Based on this, the chiral vector $\overrightarrow{C_h}$ is the one along which the graphene sheet is rolled up to form a SWNT, which means that $\overrightarrow{C_h}$ connects two equivalent atomic sites along the circumference of the tube. The resulting nanotubes are classified as armchair, zigzag or chiral nanotubes. To acquire an armchair nanotube, $n = m$ has to be fulfilled, while for a zigzag nanotube $n = 0$. The

remaining groupings of indices n and m lead to chiral nanotubes exhibiting no specific periodicity along the chiral vector, but instead, the organization of carbon atoms shapes a spiral around the nanotube axis. From the chiral index, chiral angle $\theta_{(n,m)}$ between $\overrightarrow{C_h}$ and $\vec{a}_1$ and the diameter of the nanotube can be calculated through the following equations[2,3].

$$d_{CNT} = \frac{\overrightarrow{C_h}}{\pi} = \frac{\sqrt{3a_{cc}}}{\pi}\sqrt{n^2 + nm + m^2} \qquad 2.2$$

where $\sqrt{3a_{cc}}$ is the length of the unit vectors.

$$\cos\theta_{(n,m)} = \frac{\vec{a}_1 . \overrightarrow{C_h}}{|\vec{a}_1| . |\overrightarrow{C_h}|} = \frac{n + m/2}{\sqrt{n^2 + nm + m^2}} \qquad 2.3$$

The geometry of the carbon nanotubes is significant for understanding their physical characteristics and making computations easier. The electronic characteristics of carbon nanotubes with neighboring chiral indices considerably. Carbon nanotubes have distinctive aspects depending on their chiral indices, explored in the following sections. Because of the similarity in atomic structure, many of these attributes can be obtained from graphene.

2.1.2 Electronic Band Structure

The method of deriving the band structure of the carbon nanotube from the graphene is called the zone-folding approximation[4]. Graphene's electronic band structure may be estimated using an empirical tight-band model that contains only π-orbitals perpendicular to and interacting with the graphene surface, leading to electronic bands near Fermi levels[5]. The energy dispersion in graphene, if only nearest neighbors are considered, is given by

$$E_{\pm}(\vec{k}) = \gamma_0 \sqrt{3 + 2\cos\vec{k}.\vec{a}_1 + 2\cos\vec{k}.\vec{a}_2 + 2\cos\vec{k}(\vec{a}_1 - \vec{a}_2)} \qquad 2.4$$

where γ_0 defines the interaction between two neighboring π-electrons and $\vec{k}$ is the reciprocal wave vector in the Brillouin zone (BZ) of graphene[6]. E- represents the energy of the π-states of the valence band, while E+ is the energy of the π*-states in the conduction band.

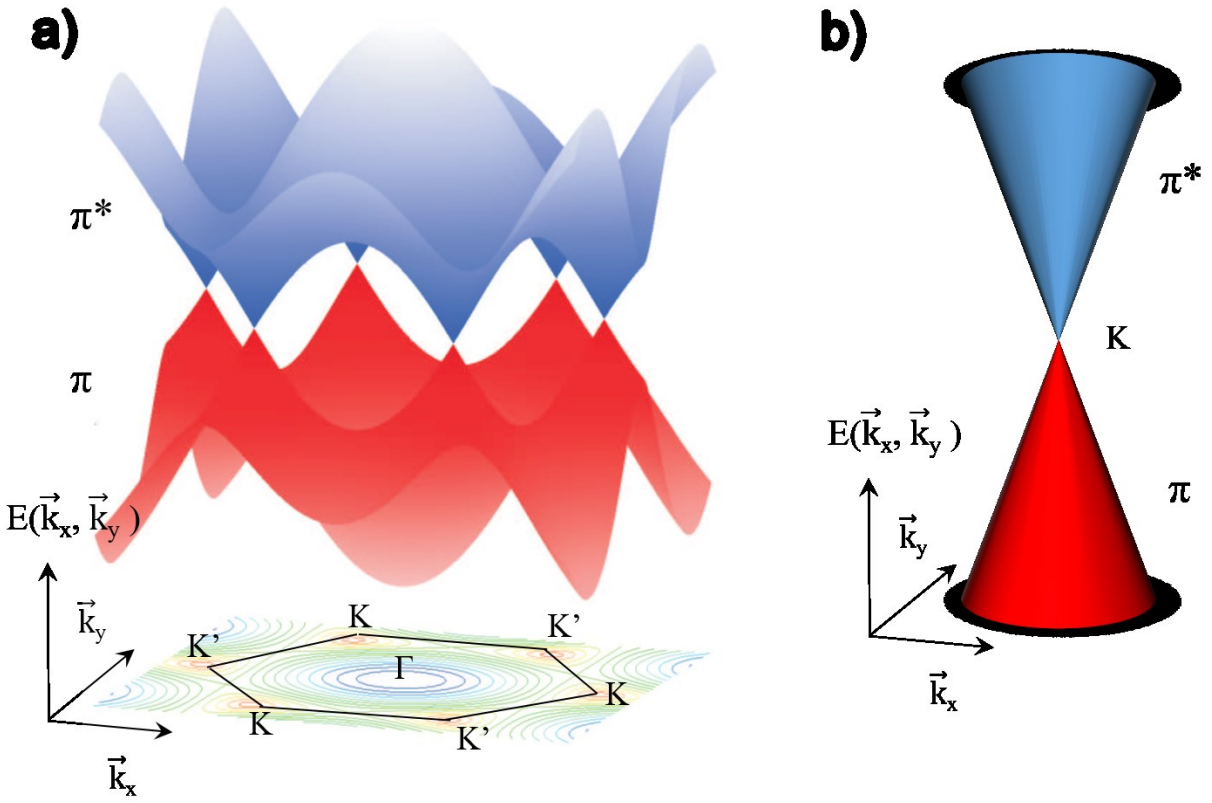

Figure 2.2 a) & b) Tight binding calculation of the band structure of graphene around their hexagonal Brillouin zone. The valence band is labeled with π (π*). (Redrawn from *K. Goss,2011, p 8*)[6a]

Figure 2.2 shows this electronic dispersion of graphene within their hexagonal Brillouin zone depending on the Cartesian reciprocal basis vectors $\vec{k}_x$ and $\vec{k}_y$.

The π - and π*-bands only contact at the six so-called K-points in the hexagonal BZ's corners, indicating that graphene is a semimetal. Around these points, both bands are nearly linear with $\vec{k} = k_x\vec{k}_x + k_y\vec{k}_y$ and can be explained as cones centered at the K points of the BZ, as shown in figure 2.2 b**.**

For SWNTs, the two-dimensional band structure of graphene is further reduced, and the following zone folding approximation may be used to explain it. Their circumference permits only discrete reciprocal wave vectors $\vec{k}_\perp = k_\perp\vec{e}_{k_\perp}$ perpendicular to the tube axis is given by

$$\overrightarrow{C_h}.\vec{k}_\perp = 2\,\pi m;\ \vec{T}.\vec{k}_\perp = 0;\ \overrightarrow{C_h}.\vec{k}_{||} = 0;\ \ \vec{T}.\vec{k}_{||} = 2\pi \qquad 2.5$$

with the wave, vector parallel to the tube axis $\vec{k}_{||}=k_{||}\,\vec{e}_{k||}$ and $m \in N$, which satisfy the boundary conditions. This results in a $\vec{k}$-space consisting of lines parallel to the tube axis, with line lengths determined by $2\pi/T$ and continuous for long SWNTs. With a spacing between the lines of $\Delta k = 2/d_T$, each line cuts the cones around the K-points. Thus, the electronic dispersion of graphene along these permitted states determines the actual band structure of a SWNT, with each line resulting in a distinct band defined by the quantum number m in the equation above. SWNT becomes (semi)metallic when a K-point of the BZ sits on such a line; otherwise, it is semiconducting. The K-point of graphene is situated at $1/3(\vec{k}_1-\vec{k}_2)$, where the reciprocal basis vectors $\vec{k}_1$ and $\vec{k}_2$ are associated to the basis vectors in real space $\vec{a}_1$ and $\vec{a}_1$ by $\vec{a}_i \,.\, \vec{k}_i = 2\pi\delta_{ij}$. Thus, a SWNT is (semi) metallic if

$$\vec{k}\,.\,\overrightarrow{C_h} = 2\pi m = \frac{1}{3}\left(\overrightarrow{k_1} - \overrightarrow{k_2}\right)(n_1\,\overrightarrow{a_1} + n_2\overrightarrow{a_2}) = \frac{2\pi}{3}(n_1 - n_2), \qquad 2.6$$

with the quantum number m. This is fulfilled for $3m = n_1 - n_2$ and explains the relation of the equation.

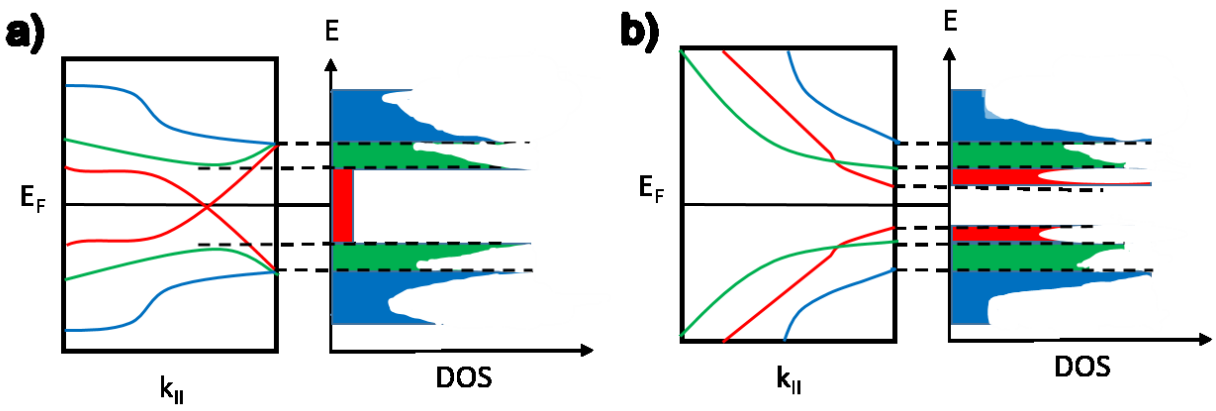

Figure 2.3 Schematic band structure obtained by the zone folding approximation for (a) metallic SWNT and (b) semiconducting SWNT.

Figure 2.3 illustrates the band structure of the SWNTs obtained by the zone folding approximation schematically a) metallic SWNT and b) semiconducting SWNT. On the right-hand side for each SWNT is their one-dimensional density of states, which is characterized by sharp van Hove singularities (vHSs) due to their one-dimensional confinement. Because their π- and π* -bands overlap at the Fermi level, metallic SWCNTs have a finite DOS, but semiconducting SWNTs have a bandgap between the first vHS of the valence and conduction bands. The energy between the corresponding vHSs is proportionate to $1/d_T$ since the distance between the lines of permissible states that cut the BZ of graphene is $\Delta k = 2/d_T$, and the dispersion falls linearly with k around the K-points.

2.1.3 Optical Properties

The electronic band structure of a nanotube can contain numerous sub-bands, but an incoming photon can only cause transitions between certain bands. Because of the antenna effect, the only light that is polarized parallel to the tube axis may interact with the one-dimensional nanotube[7]. However, the light polarized perpendicular to the tube axis can only change the band index[7,8].

Hence, optical transitions are estimated only between sub-bands with the same band index. The energy of an optical transition is denoted by the letters E_{ii}, where *i* denotes the index of the relevant band and counting begins with the band closest to the Fermi level. This corresponds to the energy between two van Hove singularities in the situation of negligible exciton binding energies, as illustrated in Figure 2.4.

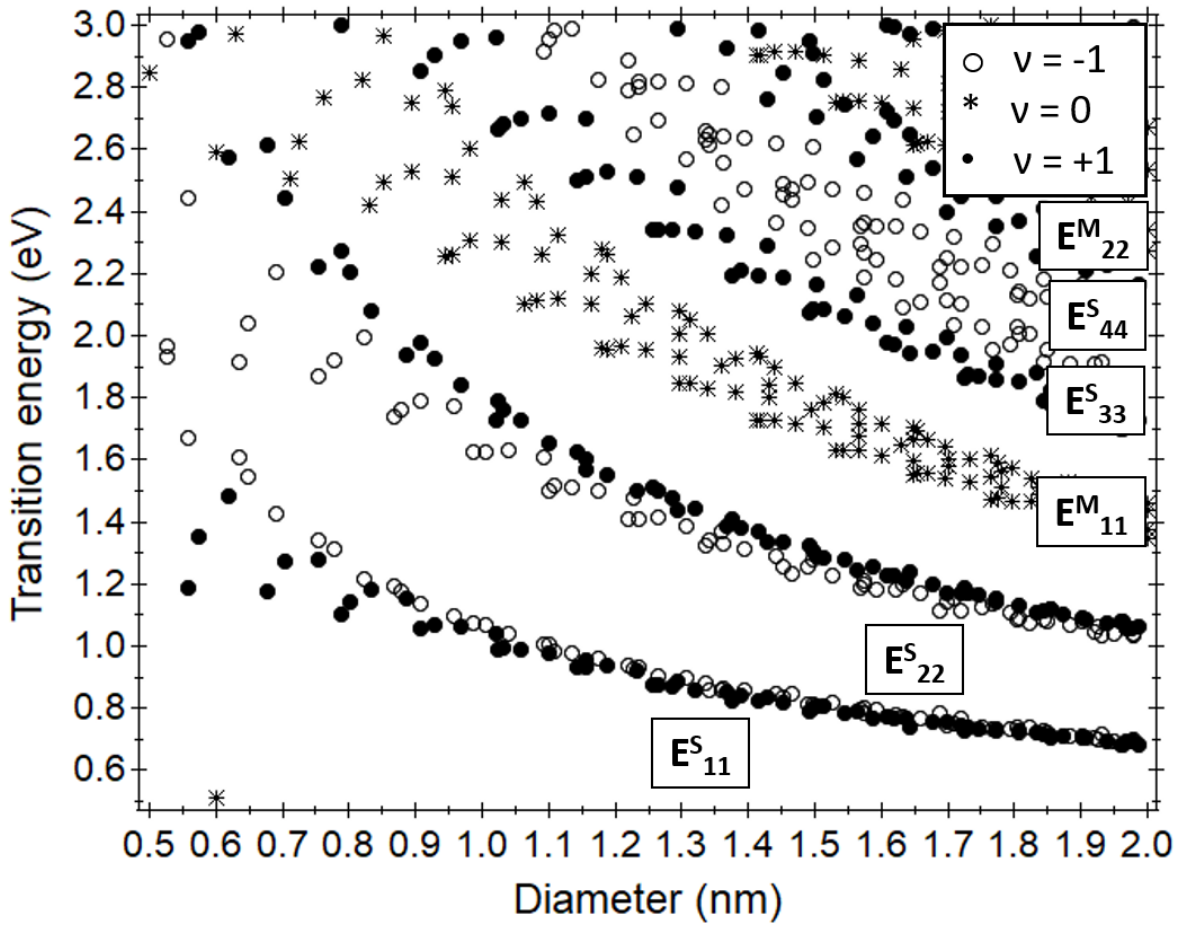

Figure 2.4 Optical transition energies as a function of nanotube diameter calculated within a non-orthogonal tight-binding model[9]. Asterik sign denotes (semi) metallic nanotubes (ν =0), circles represent semiconducting nanotubes. The latter divide into two families ν=-1 and ν=+1 plotted open and dark circles, respectively.

As illustrated in Figure 2.4, transition energies E_{ii} plotted as a nanotube diameter function to form the Kataura-Popov plot. This plot shows the relationship between the energy of band gaps in carbon nanotubes and their diameter. A nanotube of a particular diameter can be metallic or semiconducting, with many band gaps designated. The data points for a detailed band index *i* are organized together, displaying a 1/d dependence and are parted for metallic (E_{ii}^{M}) and semiconducting (E_{ii}^{S}) nanotubes.

The "V" shaped branches are produced within one of these groups, pointing to both sides of the group. A partition of the families ν = +1 and −1 can be observed in the semiconducting groups. The energies of the family always point to one side of the 1/d dependence. Because the metallic groups are made up of nanotubes from the ν = 0 family, semi-metallic nanotubes are included.

Within a single branch, the nanotubes have the same index,

$$b = 2n + m \qquad 2.7$$

The adjacent transition energies correspond to nanotubes for a particular branch, whose chiral indices relate as

$$(n_2, m_2) = (n_1 - 1, m_1 + 2) \qquad 2.8$$

The (n_1,m_1) are the smaller diameter chiral indices of the nanotubes in the Kataura-Popov plot, i.e. Left side of the (n_2,m_2) nanotube in the plot.

Popov computed the transition energies using asymmetry adapted non-orthogonal tight-binding, which is illustrated in figure 1.5[9]. In contrast to Kataura-Popov plots derived using the zone-folding approximation of tight-binding models for graphene, this model includes curvature-induced effects on the electrical band structure[10–12] and therefore delivers an upright database of carbon nanotube transition energies. Excitonic effects and electron correlations can be incorporated by strong upshifts of

the energy by 0.32 eV[9,13] of the calculated data in energy to match the transitional energies found experimentally.

The pattern recognition of the optical transitions studied by resonant Raman scattering on bulk materials having several distinct chiralities is used to generate experimental Kataura-Popov plots[14]. Optical transitions, on the other hand, are impacted by environmental factors. A further red-shift of the transition energies has been detected in bundled nanotubes and ascribed to mutual dielectric nanotubes screening inside a rope[17–19]. The degree of this shift is under discussion and ranges from 50 to 160 meV. Within multi-walled carbon nanotubes, a screening by several walls is also possible.

However, Kataura-Popov plots can be utilized to recognize a specific carbon nanotube with a certain diameter whose transition energy is acquired by resonant Raman or Rayleigh scattering[20]. The effectiveness of this index identification significantly depends on experimental conditions and precision of the input values: tube diameter and optical transition energy.

In this work, SWNTs are a mix of different chiralities, and thus it is significant to understand the chiral assignment with respect to the diameter of the nanotubes. Energy bands in metallic and semiconducting nanotubes have obvious differences and thus influence the optical properties of the functionalized SWNTs, especially in fluorescence characteristics[5]. As purchased nanotubes range in the diameter of 1.5 nm and 5 nm for individual SWNT and bundle, respectively. We discuss the functionalized SWNTs and their optical properties in upcoming experimental chapters through Raman spectroscopy.

2.2 Functionalization of carbon nanotubes

Aside from the aforementioned excellent characteristics of CNTs, due to their rigidity, chemical inertness, and strong π-π interactions, pure CNTs are difficult to dissolve or disperse in typical volatile organic solvents (VOS) or polymeric matrices. Because of the van der Waals forces of CNTs, nanotubes tend to cluster with one another, making dispersion problematic. Aside from the size effect of CNTs, the physical nature of the particles is also significant in dispersing them into a polymer matrix. Carbon nanotubes are kept together in bundles or entanglements of 50 to a few hundred individual CNTs by van der Waals forces when they are manufactured[21]. It has been demonstrated that these bundles and agglomerates reduce composites' electrical and mechanical characteristics compared to theoretical predictions based on individual CNTs[22]. The problem is figuring how to integrate individual carbon nanotubes, or at least reasonably thin nanotube bundles or disentangled nanotubes, into various molecules such as metal nanoparticles and biomolecules like fluorescent dyes and DNA molecules.

Functionalization of the CNT surface is a potential method of addressing these issues and plays a significant role in further applications of CNTs. Chemical, electrochemical, mechano-chemical, and plasma treatment are all methods of functionalization[23–26].

CNTs can be functionalized to functionalize their surfaces and side chains. The most frequent chemical functionalization procedure with strong acids eliminates the end caps while simultaneously shortening the length of the CNTs. Acid treatment also adds oxide groups to the tube ends and defect sites of CNTs, particularly carboxylic acids, carbonyl, and hydroxyl groups[27]. Different chemical processes on these oxide groups can be conducted to functionalize them with amides, thiols, or other groups. Figure 2.5 illustrates the different methods of functionalization of carbon nanotubes.

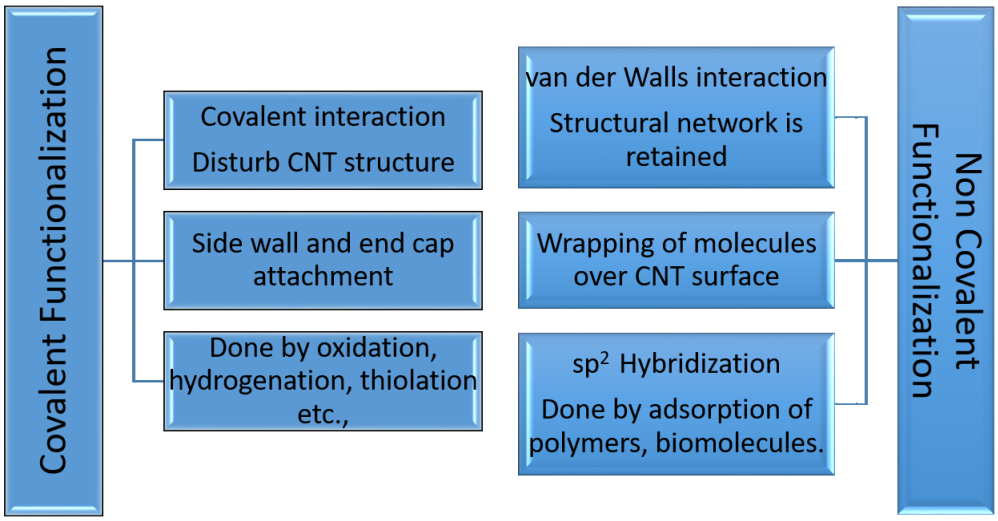

Figure 2.5 Different types of Covalent and Non-Covalent functionalization.

Chemical techniques are used to change the surface energy of CNTs, which improves their wetting or adhesion properties and their dispersion stability. These approaches seek to alter the surface chemistry of CNTs either non-covalently (adsorption) or covalently (covalent bonding). Functionalized carbon nanotubes may have electrical, optical, or mechanical characteristics that differ from the original nanotubes[28,29]. As a result, it is an exciting study to understand the different ways of functionalizing CNTs for various applications.

2.2.1 Covalent Functionalization

The establishment of a covalent coupling between functional entities and the carbon skeleton of nanotubes is the basis for covalent functionalization. Direct covalent sidewall functionalization and indirect covalent functionalization with carboxylic groups on the surface of CNTs could also be distinguished. Direct covalent sidewall functionalization is related to a shift in hybridization from sp^2 to sp^3 and a loss of conjugation at the same time[30,31]. Chemical changes of carboxylic groups at the open ends and holes in the sidewalls are used in indirect covalent functionalization. These

carboxylic groups may have originated on the as-grown CNTs and may have been produced further during oxidative purification. Chemical groups, fluorescently tagged molecules, DNA, anticancer medicines, and other functional groups can be added to the CNT surfaces to attach further the derivative reaction of the target product to the CNTs.

To enhance the reactivity of CNTs, the carboxylic acid groups are generally transformed into acid chloride and subsequently undergo an esterification or amidation process[32,33]. The disadvantage of covalent functionalization is that it may destroy the structural integrity of the nanotubes during the process, resulting in substantial changes in their physical characteristics. The effect of the disrupted π conjugation on mechanical and perhaps thermal characteristics is minimal, and the influence on electrical properties is expected to be strong since electrons are scattered throughout each covalent function site[34]. In contrast, the SWNTs with 3 atom% of carboxyl groups we use for functionalization retain most of their properties. This statement is backed by our Raman measurements as there is no drastic difference in the D mode after functionalization. Additionally, the surface grown nanotubes lead to functionalization after short oxidation, and the transport is still fine.

2.2.2 Non-Covalent Functionalization

CNTs are functionalized non-covalently by aromatic compounds, surfactants, and polymers, with most interactions via π-π stacking or hydrophobic interactions. Supramolecular complexation with different adsorption forces, such as van der Waals forces, hydrogen bonds, electrostatic force, and π-stacking interactions, is the mainstay of non-covalent functionalization[35–39]. Polymers and conjugated polymers, as the result of π-π stacking and van der Waals contact between the conjugated

polymer chain comprising aromatic rings and CNT surfaces, have proven to be excellent wrappings for the non-covalent functioning of CNTs[40–42].

Non-covalent functionalization has the benefit of working under very moderate reaction conditions and maintaining the excellent graphitic structure of CNTs compared to chemical functionalization. The reversibility and structural integrity of the nanotube are critical benefits of this type of functionalization since no covalent connections between the addend molecules and the nanotube surface are created. Another significant benefit is that, other than the design of the appropriate addend molecules, no additional chemical equipment or knowledge is required, making this technique extremely simple and scalable.

The primary downside of non-covalent attachments is that the forces between the wrapping molecule and the nanotube may be minimal, and the load transfer effectiveness may be low[43]. Significantly, the functionalization way has to be highly stable for the carbon nanotubes to be grafted with highly engineered multiple molecules. And thus, we opt for the covalent way of functionalization to proceed with functionalizing carbon nanotubes as this is the suitable route.

2.2.3 Silanization of carbon nanotubes

Silanization is one of the effective techniques to improve the surface properties of carbon nanotubes by using organosilanes as a coupling agent. Silanization allows carbon nanotubes to have different surface properties based on the organic component of the organosilanes attached to the nanotube surface[44,45]. Silanized nanotubes exhibit a variety of characteristics depending on the silane employed for functionalization. Functional groups like carboxyl and hydroxyl groups generated during the oxidation process of nanotubes have been used to achieve silanization in nanotubes. Moreover, silanized CNTs are utilized to bind other nanoparticles and molecules to the nanotube surface. This is important for developing new ways to

functionalize or integrate CNTs in other inorganic or highly engineered organic nanoscale structures. Velasco-Santos et al. reported the first report about the silanization of carbon nanotubes.

Organosilanes are of indifferent analogs such as mono, di and trifunctional silanes. Among these, tri-functional organosilanes are more reactive and multifunctional comparatively concerning the reaction parameters[46]. The silane coupling agents for organic functions are substances that allow two materials to be chemically combined. This 'link' can be made via chemical connections or by physical interactions. The organosilanes are chemically described as R-Si-R'$_{3,}$ where R is an organo-functional group attached to silicon. R' group reacts readily with the functional groups created on the surface of the CNTs[47].

2.3 Click Chemistry

The evolving "click chemistry" area offers an elegant protocol for producing carbon nanotubes based on advanced functional materials. The phrase "click chemistry" refers to a series of chemical reactions that are flexible, specific, and easy to perform and compatible with aqueous media, displaying a simple purification procedure without generating by-products. Sharpless and co-workers presented this innovative idea in 2001[48]. It gained immediate attention in various applications such as biotechnology, materials and polymer science, medicinal chemistry, etc. Researchers may readily introduce hydroxyl, carboxyl, and amino groups to conjugate compounds applying this process, thanks to their exceptional functional group tolerance. Different reactions with various mechanisms can be considered click reactions, provided they follow the conditions mentioned above, such as cycloaddition reactions like Diels-Alder, tetrazine cycloaddition, photo click reaction and azide-alkyne 1,3 dipolar cycloaddition[49–51]. In those, two of the most significant and widespread click reactions are discussed below.

2.3.1 Copper-catalyzed azide-alkyne [3 + 2] cycloaddition (CuAAC)

One of the most popular and studied click reactions is the Cu(I) catalyzed azide-alkyne [3 + 2] cycloaddition explained simultaneously by Meldal and Sharpless[52]. This bio-orthogonal reaction is the catalyzed version of Huisgen 1,3 dipolar cycloaddition and has been successfully used in many chemistries, materials science and biochemistry. Utilizing the copper(I) catalyst, the reaction may also be carried out selectively at room temperature onto the 1,4-regioisomer of the triazole, and this allows the reaction to be performed at room temperature. For use in bioorganic chemical applications, the CuAAC reagents have the major benefit of being entirely bio-orthogonal to all functional chemical groups in living organisms[53,54]. In addition, the 1.4-triazole ring functioning as a rigid linking unit between two amino acids can

imitate the atomic position and the electronic characteristics of peptide bonds without the same susceptibility to hydrolysis. The copper-catalyzed the Huisgen [3+2] cycloaddition reaction has emerged as a strategy for the quick and efficient assembly of molecules in both the industrial and the university sectors, thanks to its high region selectivity, high yield, simple reaction conditions, good reliability and tolerance to a broad range of functional groups[55–58].

Adronov and co-workers reported the first functionalization of carbon nanotubes through Cu(I) catalyzed azide-alkyne [3 + 2] cycloaddition[53]. The synthesis of Cu(I)-catalyzed 1, 2, 3-triazoles was shown to occur under various circumstances efficiently through the combination of the azide-terminated polymer and the alkyne-functionalized SWNT. This process effectively generated organic-soluble polymer – nanotube conjugates with a high grafting density and regulated molecular polymer weight at low temperatures and short reaction time. In 2007, the C.N.R. Rao group published an example of nanotubes being functionalized using 'click chemistry' with gold nanoparticles. This study employed a pretty different technique: the golden nanoparticles carrying alkyne function were synthesized and reacted to SWNTs bearing azide functional groups[59].

The click reaction was also utilized to functionalize biomolecules for nanotechnology in bio-applications, particularly for medication delivery. Cho et al. focused on the functionalization of SWNTs with bioactive molecules through the same functionalization technique. Using the Cu(I)-catalyzed Huisgen [3+2] cycloaddition process involving alkynes and an excess of azides, azides generated from various amino acids were linked with alkyne-functionalized SWNTs through the 1, 2, 3-triazole ring[60]. In the field of optoelectronic devices, hybrid materials based on phthalocyanines and nanotubes are particularly appealing[61,62]. To make

phthalocyanine functionalized SWNTs, Campidelli et al. employed the Cu(I)-catalyzed Huisgen [3+2] cycloaddition process[63].

2.3.2 Strain Promoted Azide Alkyne Cycloaddition (SPAAC)

The strain-promoted alkyne–azide cycloaddition (SPAAC) is a bio-orthogonal process that may be used to image and monitor biomolecules *in vivo*. The fast kinetics, chemoselectivity, and biocompatibility of this process contribute to its effectiveness. As a result, it represents a significant technical advance that allows for the spatial resolution of living creatures and provides unique temporal features of in vivo bioprocesses. A copper-free [3+2] huisgen cycloaddition is the most renowned bio-orthogonal reaction, also known as a strain-promoting alkyne–azide cycloaddition (SPAAC), demonstrated by C.R. Bertozzi[64].

The 1,3-dipolar cycloaddition can happen quickly without a metal catalyst because the ring strain energy of a cyclooctyne group is released due to the geometrical distortion of the C≡C bond. In the strain-promoted azide-alkyne cycloaddition (SPAAC), however, the synthesis of triazole rings is generally slower than in the analogous CuAAC process. Consequently, many ways to overcome this disadvantage have been developed. The reaction rates can be increased by boosting the reactivity of alkynes, allowing the cycloaddition to happen under moderate circumstances.

This reaction has been devised rapidly and selectively to solve issues associated with the usage of copper in the Cu-catalyzed form of this reaction inside bio-systems. In the recent decade, interest in developing new click reactions that do not involve metallic catalysts has increased. The interference of a wide variety of metal ions, specifically copper, is responsible for this development with numerous biological processes and a range of electrical and (opto) electronic phenomena. DNA interaction with heavy metal ions, including Cu, Pb, Cd, Pt, Pd, and Ni, can cause

damage to the DNA, modify the structure of and above all, a function of the genetic material. Metal ions can be troublesome in this context since they bind strongly to guanosine bases, break A-T pairings and damage the double-helical structure of DNA[65–67]. Besides the toxicity of Cu ions, metal ions could also alter the protein-repelling structure of the ethylene oxide moieties, change the essential functional properties of surfaces, such as a monolayer conductivity on the semiconductor surfaces, and cause dramatic effects like fluorescence quenching in quantum dots. Fortunately, alternative click reactions that do not require metal catalysts yet offer good and mild surface functionalities have developed in recent years, and SPAAC is one among them[68].

The chemical structure of the cyclooctyne has a significant impact on the reaction rates and conversion of SPAAC reactions[68]. Improvements in reaction rates reported by Bertozzi and others were based on the presence of electron-withdrawing substituents on the position in the alkyne (DIFO)[69], or by increasing the ring strain by incorporating sp^2 centers (dibenzocyclooctynes (DBCO))[70], or adding three-membered ring (BCN)[71] to the cyclooctyne ring. Using dibenzocyclooctynes derivatives as efficient alkynes in the SPAAC reaction for surface modification has gained favor because of the improvement in reaction kinetics reported by Popik and van Delft[72,73]. Despite the remarkable effectiveness of this method, it needed extended reactions (24 h), which might be a significant disadvantage. According to reports, the DBCO group withstood the usual acidic and oxidative processes of solid-phase oligonucleotide synthesis (SPOS) and the heat cycling and customary conditions of the polymerase chain reaction (PCR)[74].

Workentin and co-workers reported implementing this SPAAC route with single-walled carbon nanotubes where Au NPs-CNT hybrid by coupling the DBCO-modified single-wall carbon nanotubes (SWCNT) to the azide-modified gold

nanoparticles[75,76]. This copper-free click chemistry technique is used to functionalize single-stranded DNA oligonucleotides for sensing and nanomedicine applications by Antonios G. Kanaras[77]. Adronov and co-workers developed a non-covalent way of employing strain promoted azide-alkyne cycloaddition in functionalizing polymer attached single-walled carbon nanotubes thin films[78].

In this work, we design a novel and hybrid synthetic route of functionalizing carbon nanotubes through silanization and the SPAAC method. This route yields not only dense and homogeneous grafting but is also biocompatible due to its non-toxic nature. Additionally, we present that the route can be transferred to different substrates to functionalize CVD grown nanotubes on the surface. Since the route is selective and specific, integrating various molecules with nanotubes becomes more accessible, especially in device fabrication of individual CNTs.

2.4 Experimental Methods

2.4.1 Click Functionalization of Single-Walled Carbon Nanotubes

Carboxylated SWNTs (Carboxylated SWNTs-COOH 1-3 atomic %) were used from Carbon Solutions, Inc. USA. 100 mg of nanotubes were sonicated with 20 ml of extra dry toluene for about 30 minutes on a 40 ml falcon tube. After the sonication, the suspension was transferred to a new vail to separate the solution from carbon residues. 500 µl of 11-Bromoundecyltrichlorosilane (ABCR GmbH, Germany) were added, and the suspension was stirred for 18 hours in an argon environment as the silane is sensitive to ambient atmosphere. After silanization, the suspension was centrifuged at 4000 rpm for 10 minutes, and the supernatant was discarded. The suspension was dispersed again with 20 ml of toluene, sonicated for 5 minutes, and centrifuged at 4000 rpm. The washing procedure was carried out three more times with the silanized SWNTs with 20 ml toluene and centrifuged to remove the unreacted silane and amorphous carbon along with the excess solvent present in the suspension. Then, the same washing procedure was continued with 20 ml of N, N-Dimethylformamide (extra dry DMF) (Acros Organics, Germany) twice before the subsequent reaction.

Silanized SWNTs were dispersed in 20 ml of DMF (extra dry) with a spatula of Sodium Azide (NaN_3) (Merck KGaA, Germany) and stirred in an oil bath at 60 °C for 18 hours in an argon environment. After the reaction, the suspension was vacuum filtrated after 5 minutes of sonication to separate the azidized SWNTs from excess solvents and residues. The same washing procedure was carried out with 20 ml of distilled water, and the process was repeated thrice. Then the suspension was washed in 20 ml of Isopropanol (IPA) twice before the final reaction.

As this synthetic route can graft versatile molecules, molecules of our interest attached with Dibenzocyclooctyne (DBCO) were functionalized with azidized

SWNTs such as gold nanoparticles, Cyanine 3, AF647 fluorescent dyes and single-stranded DNA molecules of different lengths for various studies.

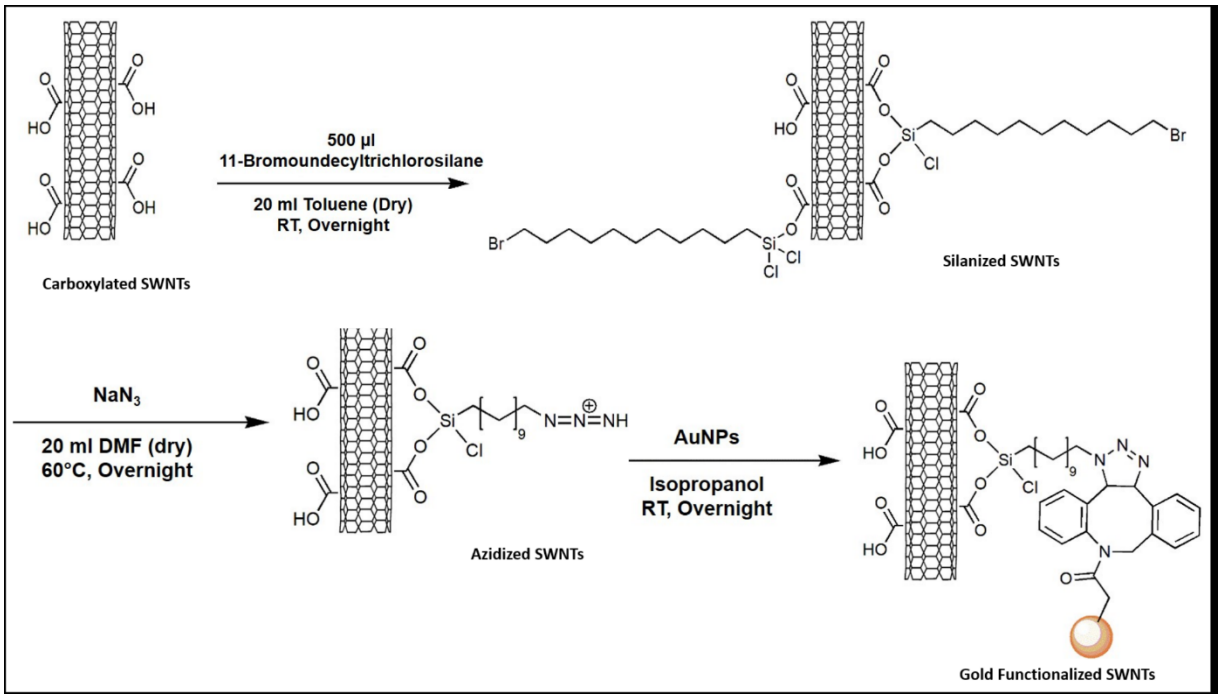

Figure 2.6 Synthetic route for functionalizing SWNTs with gold nanoparticle-DBCO. Carboxylated SWNTs are silanized. After azidization, the AuNP-DBCO is clicked through the SPAAC reaction.

Gold Nanoparticles (Au NPs-DBCO) (Nanopartz, Inc. USA) (dry 1 mg) were dissolved in 1 ml of distilled water to make it a colloid. Azidized SWNTs and AuNPs-DBCO solution were dispersed in 10 ml of IPA, and the suspension was stirred for 18 hours at room temperature. After the click reaction, the suspension was centrifuged at 4000 RPM for 10 minutes to discard the supernatant and then sonicated with 20 ml of IPA for the further washing process. The same procedure was repeated five times to eradicate the unreacted elements and excess solvent from

the suspension. Finally, the suspension was vacuum dried to remove the solvent present in the precipitate after washing.

Other fluorescent dyes such as Cyanine 3 and AF647 were dispersed to make a solution of concentration 1 mM in DMSO (Dimethylsulfoxide), and 10 µl of this solution was added to click the molecules with azidized SWNTs. Fluorescent functionalized SWNTs were washed with IPA five times to eliminate the unreacted residues present in the final solution. However, the single-stranded DNA molecules were clicked and washed under a different environment (H_2O) as they are sensitive to alcohol.

2.4.2 Click Functionalization of CVD grown Carbon Nanotubes

The schematic route to functionalize the CVD grown carbon nanotubes on substrates such as Si/SiO_2, Quartz substrate and Quartz Coverslips (thickness ~0.15 mm) was almost as same as that of the bulk material with minor changes. Carbon nanotubes were grown at the temperature of T = 900 °C for 10 min with methane as carbon feedstock on a catalyst drop cast substrate. After growth, the substrate was silanized with thermally stable Perfluorodecyltrichlorosilane (FDTS) (ABCR GmbH, Germany) through vapor deposition at 80 °C for 2 h. FDTS will act as a passivation layer for the substrate to avoid unwanted attachment on the substrate during further functionalization. FDTS silanized substrate was oxidized at 450 °C for 30 min to create carboxylic groups, which are the binding sites for further functionalization. The density of the functional groups created in CVD grown nanotubes after oxidation can be controlled by varying the oxidation duration[79]. Moreover, the density of covalent functionalization was relatively low on CVD grown carbon nanotubes which did not affect the transport properties[80].

After oxidization, the substrate was silanized with Bromoundecyltrichlorosilane through vapor deposition at 80 °C for 2 h, knowing that the silane will attach to the

carboxylic groups created on the surface of the nanotubes. Sodium Azide solution was prepared in DMF (1 mg in 5 ml) for the azidization reaction at 60 °C for 18 hours on the substrate.

Finally, the gold nanoparticles of 0.5 mg (dry) were dispersed with distilled water, and the solution was treated with the substrate for 18 hours at room temperature. The substrate was washed after the click reaction with water and then through sonication for 5 min with acetone and IPA alternatively.

Likewise, the fluorescent dyes such as Cyanine 3 and AF647 were also functionalized with the transparent substrates (quartz substrate and quartz coverslips) after following the same route till azidization. Fluorescent dyes were dispersed in DMSO solution and treated with azidized CVD grown nanotubes. Finally, the washing procedure was followed as same as that of gold nanoparticle functionalization.

2.5 Experimental Techniques

2.5.1 Chemical Vapor Deposition (CVD)

CVD is the most versatile method for producing massive, controllable amounts of CNTs. From thin films to entangled strands, the approach allows for a wide range of CNT development. The technique's general architecture comprises a mass flow controlled chamber containing a catalyst precursor and a nucleation surface. For the growth of CNTs, CVD relies on the catalytic decomposition of a carbon precursor gas. CNTs are grown at a specific temperature window in the range of 700 to 2500 °C for a specific mixture of hydrocarbon gases such as methane, ethylene, carbon monoxide etc., and the carrier gas such as hydrogen, nitrogen etc., which is reacted over the catalyst for a calculated time of 15 minutes to 90 minutes depending on the desired output. CVD process and catalyst material were followed from the J.Kong route and comprise $Fe(NO_3)_3$, Al_2O_3, and $MoO_2(C_5H_5O_2)_2$ nanoparticles in methanol solution, which are sonicated to produce solution-based iron catalyst[81].

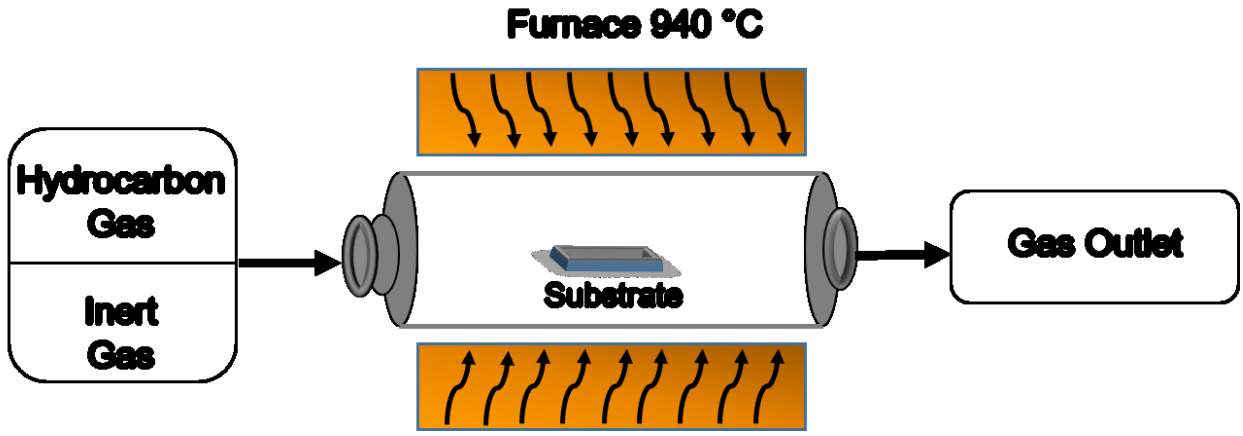

Figure 2.7 Schematic diagram of chemical vapor deposition (CVD) set up.

Molybdenum attracts amorphous carbon, preventing it from covering the active catalyst and preserving its catalytic properties. Changing the amount of Mo affects the amount of CNT growth with a given catalyst. The alumina acts as a scaffolding material, bringing the other particles together to form islands, while the active

catalyst is iron. Methane degrades to release carbon during the growth process, while hydrogen promotes CNT growth by acting as a reducing agent for the catalyst. Catalytic decomposition of methane results in carbon nanotubes at the Fe-based catalyst clusters. When the growth is complete, the samples are cooled to room temperature in an argon atmosphere to prevent the CNTs from oxidizing. Once the growth is complete, CNTs are present, beginning with the catalyst islands and spreading in any direction. Here, we used the CVD technique to grow nanotubes and functionalize them with a variety of molecules on the surface. Catalyst is diluted to grow long, elongated individual nanotubes which can be of good interest to fabricate devices.

2.5.2 X-ray Photoelectron Spectroscopy

X-ray Photoelectron Spectroscopy (XPS) is a surface characterization tool that provides information about the chemical structure and determines the surface-modified material's elemental composition. Most suitable for chemically modified surfaces, in our case, functionalized carbon nanotubes[82]. XPS analyzes several atomic layers at the surface of the materials between 1 and 10 nm. This technique is based on the photoexcitation process, which explains the excitation of an electron in investigated material by an incoming photon. The ejection of electrons from the material's surface upon exposure to electromagnetic radiation of sufficient energy is known as the photoelectric effect. According to the equation, KE is the kinetic energy of the electron, h is the Planck's constant, v is the frequency of the incident radiation, Eb is the binding energy, and ϕ is the work function, electrons emitted have characteristic kinetic energies proportional to the energy of the radiation.

$$KE = hv - Eb - \phi \qquad 2.9$$

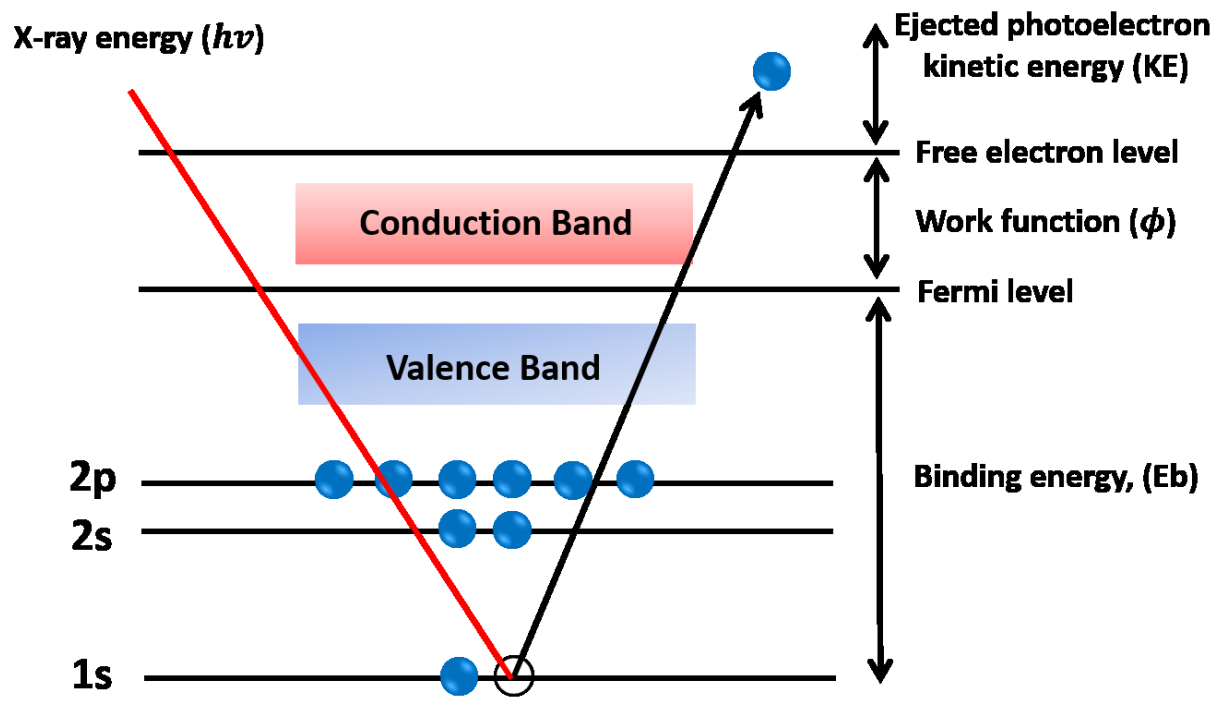

Figure 2.8 Principle of X-ray Photoelectron Spectroscopy

In XPS, high energy radiation is used to eject core electrons from the sample, and the corresponding kinetic energies of the core electrons were measured. XPS measurements are implemented under ultra-high vacuum in an ESCA-unit Phi 5000 VersaProbe III with a base pressure of 10^{-9} mbar. Al Kα radiation of a monochromatized Al anode (hν = 1486.6 eV) is used as the X-ray source. The sample solutions are prepared in IPA and coated on the copper substrate for the measurements. In this work, XPS measurements for the functionalized SWNTs play a significant role in understanding the grafting of the molecule after every reaction in our synthetic route. Additionally, the specific bonding between two different molecules, composition, and atomic concentration percentage is also identified and quantified through XPS analysis.

2.5.3 Raman Spectroscopy

Raman spectroscopy is one of the most efficient and non-destructive characterization techniques for sample analysis, especially carbon nanomaterials and their functional derivatives. Raman scattering can ensue with a change in vibrational, rotational or electronic energy of a molecule[83]. There are two types of scattering in Raman spectroscopy based on whether the excitation starts from the ground state or vibrationally-excited states. When the molecules gain energy from the ground state to a higher energy level, the type is known as Stokes Raman scattering.

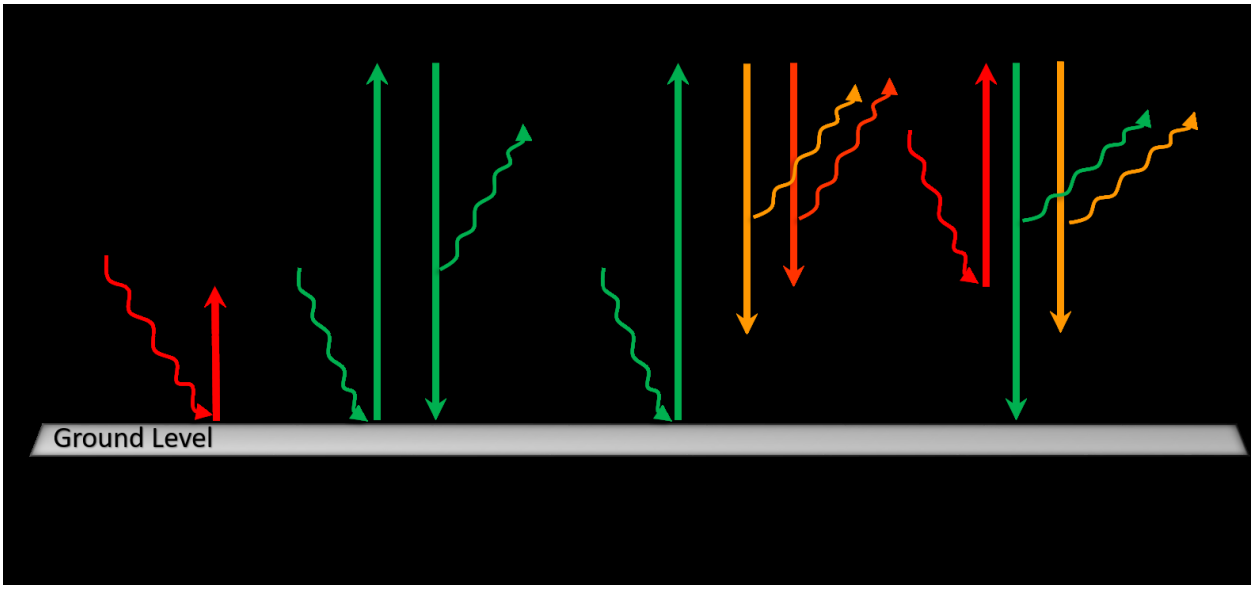

Figure 2.9 Principle of IR and Raman spectroscopy

If the molecule loses energy from the excited state to the lower energy level, they are named Anti-Stokes Raman scattering. Additionally, most of the molecules are initial excited ground state at room temperature, and thus the intensity of the stokes lines is always higher than that of the anti-stokes. For this discovery, this phenomenon of observing vibrational transition due to the exchange of energy is called Raman scattering in honour of Sir Dr Chandrasekhara V Raman, Nobel prize-winning scientist in physics. Properties of carbon nanomaterials such as electronic structure, phonon structure and defects are studied through the resonance Raman

spectrum. It is indeed an excellent technique to study carbon nanotubes and their characteristics[84].

There are Four Raman bands for SWNTs classified as the radial breathing modes (RBMs), the G band, the D band and the 2D band[85]. A unique signature phonon mode in the Raman spectra of carbon nanotubes is RBM mode, a sensitive mode to the diameter of the nanotubes. This low frequency mode (100-500 cm^{-1}) happens due to the stretching of the carbon atoms out of the plane and moving consistently in the radial direction[86]. Through the Kataura-Popov plot, if the RBM of the nanotube or its diameter is located on the excitation laser line, then the chirality and electronic transition energy can be acquired[87]. G band is the most substantial peak sensitive to any external mechanical deformation and its frequency ranges around 1500-1600 cm^{-1}. It is produced by the vibration of neighboring atoms along the nanotube axis in the opposite direction and around sits circumference[88]. The D band peak intensity represents defects in carbon nanotubes and is located in the range 1300-1400 cm^{-1}. The scattering processes of the D band consist of one elastic scattering process caused by defects such as impurities, disorder etc., and one inelastic scattering[89,90]. The intensity ratio of the D to G is a measure of the quality of the samples if the ratio increases when the number of SWNTs increases and the number of amorphous carbon decreases. The 2D band shows the crystallinity of carbon nanotubes and ranges in 2500-2800 cm^{-1}. This band is sensitive to sp^2 nanotube structure, which enables differencing between SWNTs and DWNTs or double layers of graphene due to the scattering of two inelastic processes[91]. Raman spectroscopy was carried out with a Horiba LabRam HR Evolution confocal Raman microscope, equipped with a 473 nm laser, a 600 lines/mm grating and a 100x long working distance objective. For all spectra, the laser power was kept at 0.5 mW.

2.5.4 Fluorescence Microscopy

Fluorescence microscopy is a commonly used wide-field microscopy technology that uses customized tagging of target structures to provide a unique, high contrast mechanism. Firstly, fluorescence is the emission of longer wavelength light from molecules excited by shorter wavelength light[92]. Removing the excitation wavelength(s) from the detection pathway allows us to detect only the emitted light from fluorescent molecules, resulting in extremely high contrast. Second, fluorescent molecules can be grafted explicitly to proteins or other molecules of interest, for example, through a fluorescent protein to a target molecule or through fluorescent-labeled antibodies that attach to specific proteins. The emitted light is collected with the same objective in epifluorescence microscopy. Because of Stokes shift, dichroic mirrors and filters may readily isolate the fluorescence signal from the excitation light before being observed. Because there is an almost little background, fluorescence detection is susceptible[93].

Another remarkable characteristic of fluorescence microscopy is the ability to label numerous proteins with spectrally different fluorophores simultaneously, allowing for independent detection, (co) localization, and the ratio of many molecules of interest. The resolution limit is typically on the order of 200 nm for state-of-the-art microscopes. Thus, it is not a problem to study the cellular behavior but to investigate individual molecules or image subcellular localization and organization; it quickly becomes a limiting factor.

Abbe's diffraction limit can be used to compute the best possible resolution, which is defined as the distance d between two structures necessary to distinguish them[94]:

$$\mathrm{d} = \frac{0.61.\ \lambda}{\mathrm{n}.\sin\alpha} \qquad 2.\ 10$$

The wavelength of light λ, the refractive index n of the medium through which the light travels, and half the opening angle of the objective all influence the distance d.

Even though standard fluorescence microscopy has shown to be a valuable tool in life science, there has been a growing need for imaging below the diffraction limit. Because this fundamental constraint cannot be broken, other super-resolution techniques have been developed. In this work, it is of great importance for the biomolecules such as fluorescent dyes (Chapter 4) and ss-DNA (Chapter 5) functionalized SWNTs to image them below the diffraction limit around a resolution under 20 nm. The diameter of the fluorescent dye functionalized SWNTs ranges in tens of nanometers. We opt for advanced microscopic techniques to image and localize the functionalized SWNTs discussed in the upcoming chapters.

2.5.5 Förster Resonance Energy Transfer (FRET)

Förster was the first to describe FRET, a radiationless energy transfer from an electronically excited donor fluorophore to an acceptor fluorophore in the electronic ground state through dipole-dipole coupling[94]. Resonance energy transfer measurements can be a valuable technique for exploring molecular interactions because the range of energy transfer is confined to around 10 nm. The efficiency of transmission is particularly sensitive to the separation distance between the donor fluorophore and acceptor molecule. Because resonance energy transfer is unaffected by a fluorophore's surrounding solvent shell, it yields molecular information distinct from that provided by solvent-dependent phenomena like fluorescence quenching, excited-state reactions, solvent relaxation, or anisotropic measurements. Fluorescence resonance energy transfer is not mediated by photon emission, and it does not even necessitate the presence of a fluorescent acceptor chromophore. The inverse sixth power of the distance between the donor and acceptor molecules determines the efficiency of the energy transfer mechanism. As a result, when

biomolecules labeled with the suitable donor and acceptor molecules are within 10 nanometers of each other, FRET measurements can be used as an effective molecular ruler for calculating distances. With increasing distance between the molecules, the capacity of the donor fluorophore to transfer its excitation energy to the acceptor by non-radiative interaction drips significantly. Several more forms of energy and/or electron transport are feasible at distances less than 1 nm. The resonance energy transfer process's distance dependence is the primary reason for its application in molecular interactions research[95].

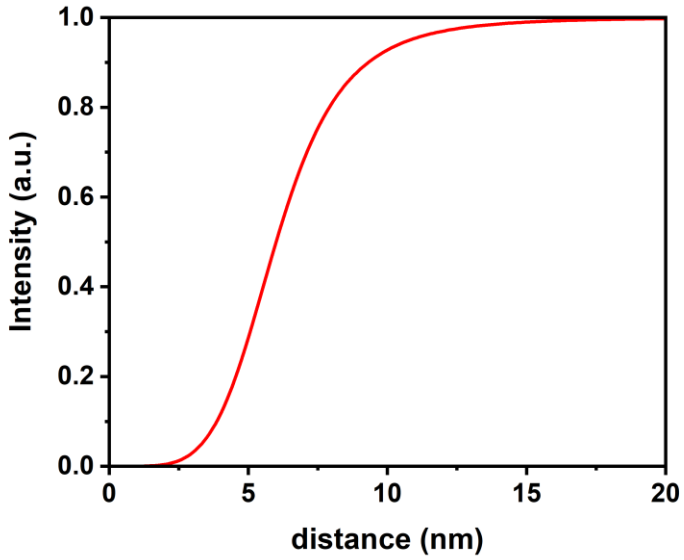

Figure 2.10 Expected plot of intensity as a function of the distance between the fluorophore and the carbon nanotube.

The rate of radiation-free energy transfer E is highly dependent on the separation distance r between the two molecules:

$$E = \frac{1}{1 + (\frac{r}{R_0})^6} \qquad 2.11$$

where R_0 is the Förster radius.

In this work, the representation of acceptor and donor represent carbon nanotube and ATTO655 fluorescent dye attached with single-stranded DNA imager strands, which will be discussed in Chapter 5. Single-stranded DNA molecules of different lengths (1 nm, 8 nm and 15 nm) are employed to investigate the fluorescence quenching behavior. Assuming the successful integration of DNA molecules with SWNTs and the fluorescent dyes are attached away with the known separation distance, it is expected to change the intensity as shown in Figure 2.10. Irrespective of the change in R_0 value, there is a change in intensity expected.

2.5.6 Fluorescence Lifetime Imaging Microscopy (FLIM)

Fluorescence Lifetime Imaging Microscopy is a robust approach for identifying fluorophores' unique molecular surroundings. FLIM detects molecular changes of fluorophores that are not visible with spectral approaches alone by measuring the time a fluorophore spends in an excited state before emitting a photon[95]. FLIM techniques have gained popularity because of their high sensitivity to the molecular environment and changes in molecular conformation. When FRET occurs with an acceptor molecule, the fluorescence lifetime of the donor fluorophore changes, FLIM can thus visualize changes in the proximity of FRET pairs. Specifically, the quenching of the donor emission by FRET leads to a decrease in its lifetime. FLIM requires only the donor's lifetime, so direct excitation for the acceptor is unnecessary, and acceptors with low quantum efficiencies can be used.

Furthermore, FLIM-FRET requires less excitation intensity because more comprehensive emissions filters can be used, allowing for FLIM-FRET pairs that are less photostable. At last, in FLIM-FRET, the quantification of the proportion between quenched and unquenched donors can be calculated using multi-exponential fitting. FLIM is essentially independent of fluorophore concentration, allowing it to evaluate whether a change in fluorescence intensity is due to changes

in quantum yield (e.g., fluorescence quenching), a difference in the fluorophore's overall concentration, or both. As a result, FLIM is highly suited for precise quenching dynamics observations. FLIM assists us in analyzing the fluorescently functionalized SWNTs (Chapter 4) and in surface grown CNTs (Chapter 6) to investigate the optical properties such as fluorescence lifetimes.

2.5.7 Stochastic Optical Reconstruction Microscopy (STORM)

STORM is a single molecule localization-based fluorescence imaging technique in which a super-resolution fluorescence image is constructed from the high accuracy localization of individual fluorescent molecules in three dimensions that are switched ON and OFF using different colors of light[95].

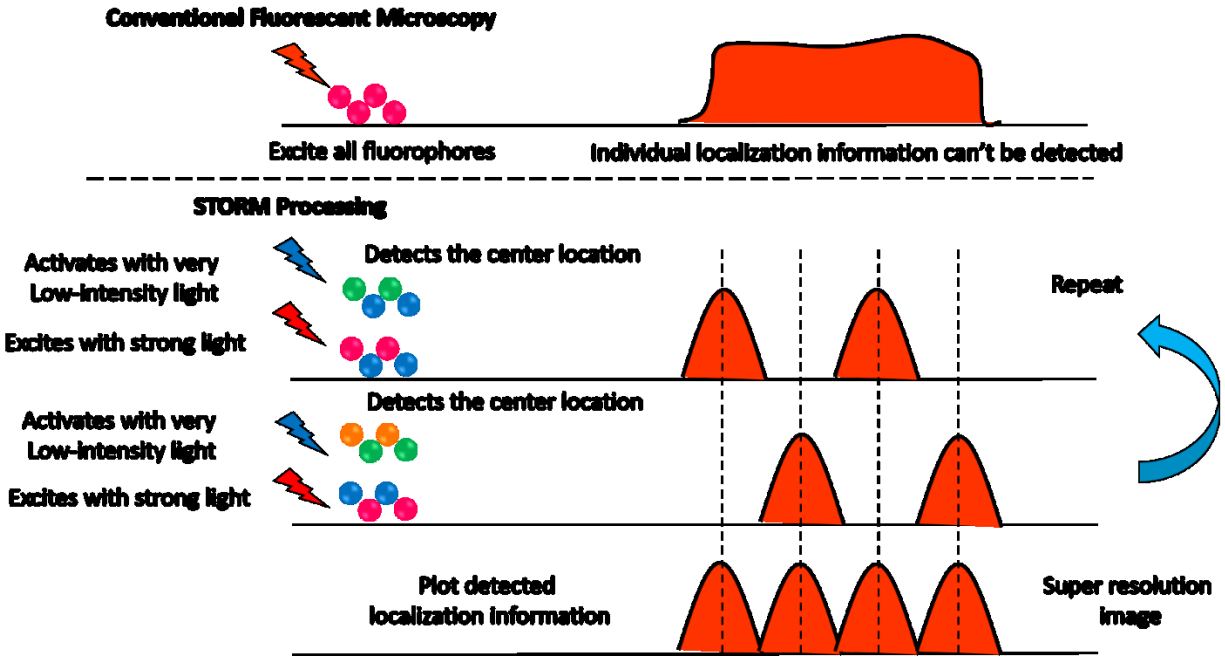

Figure 2.11 Working principle of STORM microscopy in comparison with conventional fluorescent microscopy.

With the combination of specific excitation parameters and specialized oxygen scavenging buffers, the technique is compatible with many fluorophores that can be switched between ON and OFF states[96,97].

The STORM imaging process comprises of series of imaging cycles. Only a fraction of the fluorophores in the field of view are turned on during each cycle so that each of the active fluorophores is optically distinguishable from the others, i.e., their images do not overlap. This permits the position of the fluorophores to be determined with high accuracy. The positions of numerous fluorophores can be identified, and hence an overall image reconstructed by repeating this procedure for multiple cycles, each causing a stochastically diverse collection of fluorophores to be switched on. Ideal fluorophores for STORM should be very bright, high rate of photoswitching property and exhibit minimal photobleaching in buffers.

In general, bright fluorophores such as Cyanine 5 and AF647 are the most commonly used fluorophores for STORM imaging. STORM microscopy can provide high-quality images of nano moieties resolved under 20 nm, helping to visualize the nanomolecular structures, interactions with biomolecules etc., The ability of STORM to localize a large number of switches within a diffraction-limited spot by cycling the switches on and off in a controlled manner, allowing it to be used as a general biological imaging technique, is a distinct advantage. In this work, AF647 functionalized SWNTs (Chapter 4) are resolved through STORM microscopy at the nanoscale level. However, this technique has two significant limitations: limited photon budget of fixed target labels and difficulty controlling photophysical fluorophore properties. These challenges open the gate to switch to the other advanced imaging technique where we employ single-stranded DNA molecules and explained below.

2.5.8 DNA Point Accumulation in Nanoscale Topography (DNA-PAINT)

Different single-molecule localization microscopy was introduced to overcome the limitations of other techniques called Point accumulation in Nanoscale topography (PAINT) [97]. Instead of labeling target molecules with fixed fluorophores, attaching freely diffusing dyes or dye-labeled ligands to target molecules of interest through permanent or transient binding. PAINT is simple to implement and does not require any distinct experimental conditions to achieve photoswitching, as long as probes can diffuse and reach their target molecules. It is challenging to implement PAINT specifically to label a broader range of biomolecules because interactions are primarily limited to hydrophobic interactions or electrostatic coupling and thus are complex to program[98,99].

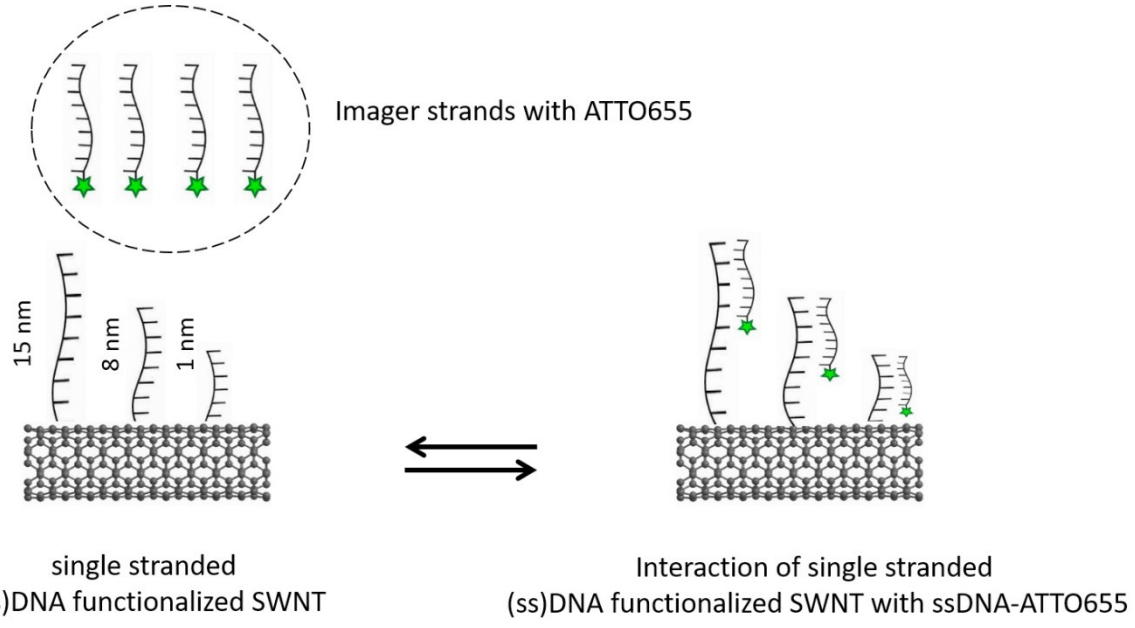

Figure 2.12 Schematic of DNA-PAINT: Representation of DNA-PAINT technique in which the SWNTs functionalized with ssDNA molecule to be imaged is shown as black strands. ssDNA attached with ATTO655 is shown as imager strands drawn with a green star.

DNA nanotechnology is a promising tool for leveraging the benefits of the PAINT concept while also establishing a programmable target–probe interaction system[100]. Specifically, DNA-based PAINT has been developed as a straightforward approach to overcoming restrictions of other localization-based super-resolution methods. DNA-PAINT decouples blinking from dye photophysics and adds the programmability and specificity of employing DNA molecules as imaging and labeling probes, similar to the original PAINT concept. A DNA-PAINT system comprises of following two components: a docking strand and an imager strand.

These are complementary single-stranded DNA oligomers, usually of different lengths. The docking strand is attached to the target molecule of interest (in our case through click functionalization), and the imager strand is conjugated to an organic dye and diffuses freely in the imaging buffer. Imager strands are usually undetected in the camera because they diffuse over many camera pixels throughout a single picture.

On the other hand, imager strands can transiently connect to docking strands due to their complementary sequence. During the bound state, imager strands are fixed at the same place for an extended amount of time, permitting the camera to accumulate enough photons from the dye to be detected. As a result, the user has complete control over the blinking kinetics, regardless of dye characteristics or illumination conditions[101]. For DNA functionalized SWNTs, this concept is the most suitable because it not only resolves structures at the nanoscale but also localizes the molecules (unlimited photon budget). In chapter 5, SWNTs are functionalized through single-stranded DNA molecules of different lengths and imaged through this technique.

2.6 References

(1) Zheng, L.X.; O'Connell, M.J.; Doorn, S.K.; Liao, X.Z.; Zhao, Y. H.; Akhado v, E.A.; Hoffbauer, M.A.; Roop, B.J.; Jia, Q. X.; Dye, R.C.; Peterson, D.E.; Huang, S.M.; Liu, J.; Zhu, Y.T. Ultralong Single Wall Carbon Nanotubes. *Na t. Mater.* **2004**, *3* (10), 673–676. https://doi.org/10.1038/nmat1216.

(2) Dresselhaus, M.S.; Dresselhaus, G.; Saito, R. Physics of Carbon Nanotubes. *Carbon N.Y.* **1995**, *33* (7), 883 – 891. https://doi.org/https://doi.org/10.1016/0 008-6223(95)00017-8.

(3) Proctor, J.E., Melendrez Armada, D., & Vijayaraghavan. *An Introduction to Graphene and Carbon Nanotubes (1st Ed.). CRC Press.*, 1st Edition.; 2017. https://doi.org/https://doi.org/10.1201/9781315368191.

(4) White, C.T.; Mintmire, J.W. Density of States Reflects Diameter in Nanotube s *Nature* **1998**, *394* (6688), 29 30. https://doi.org/10.1038/27801.

(5) Wallace, P. R. Erratum: The Band Theory of Graphite. *Phys.Rev.* **1947**, *72*(3) 258. https://doi.org/10.1103/PhysRev.72.258.

(6) Saito, R.; Dresselhaus, G.; Dresselhaus, M. S. *Physical Properties of Carbon Nanotubes*; Imperial College Press, 1998. https://doi.org/10.1142/p080.

(6a) Goss. K, (**2011**), *Interactions between parallel carbon nanotube quantu m dots,* Forschungszentrum Jülich*,* ISBN 978-3-89336-740-5.

(7) Ajiki, H.; Ando, T.Carbon Nanotubes: Optical Absorption in Aharonov-Bohm Flux. *Jpn. J. Appl. Phys.* **1995**, *34* (S1), 107. https://doi.org/10.7567/jjaps.34s 1.107.

(8) Damnjanović, M.; Milošević, I.; Vuković, T.; Sredanović, R. Full Symmetry, Optical Activity, and Potentials of Single-Wall and Multiwall Nanotubes.

Phys.Rev. B **1999**, *60* (4), 2728– 2739. https://doi.org/10.1103/PhysRevB.60.2728.

(9) Popov, V. N.; Henrard, L. Comparative Study of the Optical Properties of Sin gle Walled Carbon Nanotubes within Orthogonal and Nonorthogonal Tight B inding Models. *Phys. Rev. B* **2004**, *70* (11), 115407. https://doi.org/10.1103/PhysRevB.70.115407.

(10) Reich, S.; Maultzsch, J.; Thomsen, C.; Ordejón, P. Tight-Binding Description of Graphene. *Phys. Rev. B* **2002**, *66* (3), 35412. https://doi.org/10.1103/PhysRevB.66.035412.

(11) Bettinger, H. F. Carbon Nanotubes—Basic Concepts and Physical Properties. By S. Reich, C. Thomsen, J. Maultzsch. *Chem. Phys. Chem* **2004**, *5* (12), 1914–1915. https://doi.org/https://doi.org/10.1002/cphc.200400387.

(12) Maultzsch, J.; Reich, S.; Thomsen, C. Raman Scattering in Carbon Nanotubes Revisited. *Phys. Rev. B-Condens. Matter Mater. Phys.* **2002**, *65* (23), 1–4. https://doi.org/10.1103/PhysRevB.65.233402.

(13) Maultzsch, J.; Telg, H.; Reich, S.; Thomsen, C. Radial Breathing Mode of Single-Walled Carbon Nanotubes: Optical Transition Energies and Chiral-Index Assignment. *Phys. Rev. B* **2005**, *72* (20), 205438. https://doi.org/10.1103/PhysRevB.72.205438.

(14) Telg, H.; Maultzsch, J.; Reich, S.; Hennrich, F.; Thomsen, C. Chirality Distribution and Transition Energies of Carbon Nanotubes. *Phys. Rev. Lett.* **2004**, *93* (17), 1–4. https://doi.org/10.1103/PhysRevLett.93.177401.

(15) Girifalco, L. A.; Hodak, M.; Lee, R. S. Carbon Nanotubes, Buckyballs, Ropes, and a Universal Graphitic Potential. *Phys. Rev. B* **2000**, *62* (19), 13104–13110.

https://doi.org/10.1103/PhysRevB.62.13104.

(16) Chen, B.; Gao, M.; Zuo, J. M.; Qu, S.; Liu, B.; Huang, Y. Binding Energy of Parallel Carbon Nanotubes. *Appl. Phys. Lett.* **2003**, *83* (17), 3570– 3571. https://doi.org/10.1063/1.1623013.

(17) O'Connell, M.J.; Sivaram, S.; Doorn, S.K. Near-Infrared Resonance Raman Excitation Profile Studies of Single Walled Carbon Nanotube Intertube Interactions: A Direct Comparison of Bundled and Individually Dispersed Nanotubes. *Phys. Rev. B* **2004**, *69* (23) ,235415. https://doi.org/10.1103/PhysRevB.69.235415.

(18) Débarre, A.; Kobylko, M.; Bonnot, A. M.; Richard, A.; Popov, V. N.; Henrard, L.; Kociak, M. Electronic and Mechanical Coupling of Carbon Nanotubes: A Tunable Resonant Raman Study of Systems with Known Structures. *Phys. Rev. Lett.* **2008**, *101* (19), 197403. https://doi.org/10.1103/PhysRevLett.101.197403.

(19) Michel, T.; Paillet, M.; Nakabayashi, D.; Picher, M.; Jourdain, V.; Meyer, J. C.; Zahab, A. A.; Sauvajol, J.-L. Indexing of Individual Single-Walled Carbon Nanotubes from Raman Spectroscopy. *Phys. Rev. B* **2009**, *80* (24), 245416. https://doi.org/10.1103/PhysRevB.80.245416.

(20) Fouquet, M.; Telg, H.; Maultzsch, J.; Wu, Y.; Chandra, B.; Hone, J.; Heinz, T. F.; Thomsen, C. Longitudinal Optical Phonons in Metallic and Semiconducting Carbon Nanotubes. *Phys. Rev. Lett.* **2009**, *102* (7), 75501. https://doi.org/10.1103/PhysRevLett.102.075501.

(21) Ma, P.C.; Siddiqui, N.A.; Marom, G.; Kim, J. K. Dispersion and Functionalization of Carbon Nanotubes for Polymer-Based Nanocomposites: A Review. *Compos. Part A Appl. Sci. Manuf.* **2010**, *41* (10), 1345 – 1367. https://doi.org

/https://doi.org/10.1016/j.compositesa.2010.07.003.

(22) Sabet, S. M.; Mahfuz, H.; Terentis, A. C.; Nezakat, M.; Hashemi, J. Effects of POSS Functionalization of Carbon Nanotubes on Microstructure and Thermo mechanical Behavior of Carbon Nanotube/Polymer Nanocomposites. *J. Mate r. Sci.* **2018**, *53* (12), 8963–8977. https://doi.org/10.1007/s10853-018-2182-y.

(23) Maity, K. P.; Patra, A.; Prasad, V. Influence of the Chemical Functionalization of Carbon Nanotubes on Low Temperature Ac Conductivity with Polyaniline Composites. *J. Phys. D, Appl. Phys. 53* (12), 9. https://doi.org/DOI:101088/1 361-6463/ab5f18.

(24) Quintero- Jaime, A.F.; Cazorla- Amorós, D.; Morallon, E. Electrochemical F unctionalization of Single Wall Carbon Nanotubes with Phosphorus and Nitr ogen Species. *Electrochimica Acta*, 340, **2020**,135935. https://doi.org/10.101 6/j.electacta.2020.135935.

(25) Nakonechna O.I.; BelyavinaN.N.; DashevskyiM.M.; IvanenkoK.O.; RevoS.L. Novel Ti_2CuCx and Ti_3Cu_2Cx Carbides Obtained by Sintering of Products of Mechanochemical Synthesis of Ti, Cu and Carbon Nanotubes. *Phys. Chem. Solid State* **2019**, *19* (2), 179–185. https://doi.org/10.15330/pcss.19.2.179-185.

(26) Garzia Trulli, M.; Sardella, E.; Palumbo, F.; Palazzo, G.; Giannossa, L. C.; M angone, A.; Comparelli, R.; Musso, S.; Favia, P. Towards Highly Stable Aqu eous Dispersions of Multi Walled Carbon Nanotubes: The Effect of Oxygen Plasma Functionalization. *J. Colloid Interface Sci.* **2017**, *491*, 255–264. https://doi.org/https://doi.org/10.1016/j.jcis.2016.12.039.

(27) Singh, B.; Lohan, S.; Sandhu, P.S.; Jain, A.; Mehta, S. K. (Chapter 15). Func tionalized Carbon Nanotubes and Their Promising Applications in Therapeuti cs and Diagnostics. in *Nanobiomaterials in Medical Imaging*; Grumezescu, A

.M., Ed.; William Andrew Publishing, 2016; pp 455–478. https://doi.org/https://doi.org/10.1016/B978-0-323-41736-5.00015-7.

(28) Andrews, R.; Jacques, D.; Minot, M.; Rantell, T. Fabrication of Carbon Multi wall Nanotube/Polymer Composites by Shear Mixing. *Macromol. Mater. Eng.* **2002**, *287* (6), 395–403. https://doi.org/https://doi.org/10.1002/1439-2054(20020601)287:6<395::AID-MAME395>3.0.CO;2-S.

(29) Meng, L.; Fu, C.; Lu, Q. Advanced Technology for Functionalization of Carb on Nanotubes. *Prog. Nat. Sci.* **2009**, *19* (7), 801– 810. https://doi.org/10.1016 /j.pnsc.2008.08.011.

(30) Dang, Z.-M.; Wang, L.; Zhang, L.-P. Surface Functionalization of Multiwalled Carbon Nanotube with Trifluorophenyl. *J. Nanomater.* **2006**, *2006*, 83583. https://doi.org/10.1155/JNM/2006/83583.

(31) Fischer, J. E. Chemical Doping of Single-Wall Carbon Nanotubes. *Acc. Chem. Res.* **2002**, *35* (12), 1079–1086. https://doi.org/10.1021/ar0101638.

(32) Kim, W.-J.; Nair, N.; Lee, C. Y.; Strano, M. S. Covalent Functionalization of Single-Walled Carbon Nanotubes Alters Their Densities Allowing Electronic and Other Types of Separation. *J. Phys. Chem. C* **2008**, *112* (19), 7326–7331. https://doi.org/10.1021/jp710919b.

(33) Zhu, W.; Minami, N.; Kazaoui, S.; Kim, Y. Fluorescent Chromophore Functi onalized Single Wall Carbon Nanotubes with Minimal Alteration to Their Ch aracteristic One-Dimensional Electronic States. *J. Mater. Chem.* **2003**, *13* (9), 2196–2201. https://doi.org/10.1039/B303885H.

(34) Moniruzzaman, M.; Winey, K. I. Polymer Nanocomposites Containing Carbon Nanotubes. *Macromolecules* **2006**, *39* (16), 5194 - 5205. https://doi.org/10.10

21/ma060733p.

(35) Vogel, S.R.; Müller, K.; Plutowski, U.; Kappes, M.M.; Richert, C. DNA–Carbon Nanotube Interactions and Nanostructuring Based on DNA. *Phys. status solidi* **2007**, *244* (11), 4026 - 4029. https://doi.org/https://doi.org/10.1002/pssb.200776108.

(36) Shin, S.R.; Lee, C.K.; So, I.S.; Jeon, J.H.; Kang, T.M.; Kee, C.W.; Kim, S.I.; Spinks, G.M.; Wallace, G.G.; Kim, S.J. DNA Wrapped Single Walled Carbo n Nanotube Hybrid Fibers for Supercapacitors and Artificial Muscles. *Adv.M ater.***2008**, *20*(3),466– 470. https://doi.org/https://doi.org/10.1002/adma.200701102.

(37) Mu, Q.; Liu, W.; Xing, Y.; Zhou, H.; Li, Z.; Zhang, Y.; Ji, L.; Wang, F.; Si, Z.; Zhang, B.; Yan, B. Protein Binding by Functionalized Multiwalled Carbon Nanotubes Is Governed by the Surface Chemistry of Both Parties and the Nanotube Diameter. *J. Phys. Chem. C* **2008**, *112* (9), 3300– 3307. https://doi.org/10.1021/jp710541j.

(38) Yu, J.G.; Hunag, K.L.; Liu, S.Q.; Tang, J.C. Preparation and Characterization of Polycarbonate Modified Multiple-Walled Carbon Nanotubes. *Chinese J. Chem.* **2008**, *26* (3), 560– 563. https://doi.org/https://doi.org/10.1002/cjoc.200890105.

(39) Nakayama - Ratchford, N.; Bangsaruntip, S.; Sun, X.; Welsher, K.; Dai, H. N oncovalent Functionalization of Carbon Nanotubes by Fluorescein - Polyethy lene Glycol: Supramolecular Conjugates with pH-Dependent Absorbance and Fluorescence. *J. Am. Chem. Soc.* **2007**, *129* (9), 2448– 2449. https://doi.org/10.1021/ja068684j.

(40) Star, A.; Stoddart, J.F.; Steuerman, D.; Diehl, M.; Boukai, A.; Wong, E.W.;

Yang, X.; Chung, S.-W.; Choi, H.; Heath, J. R. Preparation and Properties of Polymer-Wrapped Single-Walled Carbon Nanotubes. *Angew. Chemie Int. Ed.* **2001**, *40* (9), 1721 – 1725. https://doi.org/https://doi.org/10.1002/1521- 3773(20010504)40:9<1721::AID-ANIE17210>3.0.CO;2-F.

(41) Star, A.; Stoddart, J. F. Dispersion and Solubilization of Single-Walled Carbon Nanotubes with a Hyperbranched Polymer. *Macromolecules* **2002**, *35* (19), 7 516–7520. https://doi.org/10.1021/ma0204150.

(42) Star, A.; Liu, Y.; Grant, K.; Ridvan, L.; Stoddart, J.F.; Steuerman, D.W.; Die hl, M.R.; Boukai, A.; Heath, J.R. Noncovalent Side Wall Functionalization of SingleWalled Carbon Nanotubes. *Macromolecules* **2003**, *36* (3), 553–560. https://doi.org/10.1021/ma021417n.

(43) Liu, P. Modifications of Carbon Nanotubes with Polymers. *Eur. Polym. J.* **20 05**, *41* (11), 2693– 2703. https://doi.org/https://doi.org/10.1016/j.eurpolymj.2 005.05.017.

(44) Velasco-Santos, C.; Martínez-Hernández, A. L.; Lozada-Cassou, M.; Alvarez-Castillo, A.; Castaño, V. M. Chemical Functionalization of Carbon Nanotubes through an Organosilane. *Nanotechnology* **2002**, *13* (4), 495– 498. https://doi .org/10.1088/0957-4484/13/4/311.

(45) Aizawa, M.; Shaffer, M. S. P. Silylation of Multi-Walled Carbon Nanotubes. *Chem. Phys. Lett.* **2003**, *368*(1), 121– 124. https://doi.org/https://doi.org/10.1 016/S0009-2614(02)01767-0.

(46) Fadeev, A.Y.; McCarthy, T.J. Self-Assembly is not the only reaction possible between alkyltrichlorosilanes and surfaces: Monomolecular and oligomeric covalently attached layers of dichloro and trichloroalkylsilanes on silicon. *Langmuir* **2000**, *16* (18), 7268–7274. https://doi.org/10.1021/la000471z.

(47) Velasco-Santos, C. Silanization of Carbon Nanotubes: Surface Modification and Polymer Nanocomposites; Martínez-Hernández, A.L., Ed.; IntechOpen: Rijeka, 2011; p Ch. 13. https://doi.org/10.5772/17274.

(48) Kolb, H. C.; Finn, M. G.; Sharpless, K. B. Click Chemistry: Diverse Chemical Function from a Few Good Reactions. *Angew. Chem. Int. Ed. Engl.* **2001**, *40* (11), 2004– 2021. https://doi.org/10.1002/1521- 3773(20010601)40:11<2004 ::aid-anie2004>3.3.co;2-x.

(49) Fort, E. H.; Donovan, P. M.; Scott, L. T. Diels-Alder Reactivity of Polycyclic Aromatic Hydrocarbon Bay Regions: Implications for Metal-Free Growth of Single-Chirality Carbon Nanotubes. *J. Am. Chem. Soc.* **2009**, *131* (44), 16006–16007. https://doi.org/10.1021/ja907802g.

(50) Song, W.; Wang, Y.; Qu, J.; Lin, Q. Selective Functionalization of a genetical ly encoded alkene-containing protein via "Photoclick Chemistry" in Bacterial Cells. *J. Am. Chem. Soc.* **2008**, *130* (30), 9654– 9655. https://doi.org/10.1021 /ja803598e.

(51) Blackman, M.L.; Royzen, M.; Fox, J.M. Tetrazine Ligation: Fast Bioconjugat ion Based on Inverse-Electron-Demand Diels-Alder Reactivity. *J. Am. Chem. Soc.* **2008**, *130* (41), 13518–13519. https://doi.org/10.1021/ja8053805.

(52) Meldal, M.; Tornøe, C. W. Cu-Catalyzed Azide-Alkyne Cycloaddition. *Chem. Rev.* **2008**, *108* (8), 2952–3015. https://doi.org/10.1021/cr0783479.

(53) Li, H.; Cheng, F.; Duft, A.M.; Adronov, A. Functionalization of Single Walle d Carbon Nanotubes with Well Defined Polystyrene by "Click" Coupling. *J. Am. Chem. Soc.* **2005**, *127* (41), 14518– 14524. https://doi.org/10.1021/ja054 958b.

(54) Bahr, J.L.; Tour, J.M. Highly Functionalized Carbon Nanotubes Using in Situ Generated Diazonium Compounds. *Chem. Mater.* **2001**, *13* (11), 3823–3824. https://doi.org/10.1021/cm0109903.

(55) Teschner, D.; Borsodi, J.; Wootsch, A.; Révay, Z.; Hävecker, M.; Knop-Gericke, A.; Jackson, S. D.; Schlögl, R. The Roles of Subsurface Carbon and Hydrogen in Palladium-Catalyzed Alkyne Hydrogenation. *Science.* **2008**, *320* (5872), 86–89. https://doi.org/10.1126/science.1155200.

(56) Lutz, J.F. 1,3-Dipolar Cycloadditions of Azides and Alkynes: A Universal Ligation Tool in Polymer and Materials Science. *Angew. Chemie Int. Ed.* **2007**, *46* (7), 1018–1025. https://doi.org/https://doi.org/10.1002/anie.200604050.

(57) Antoni, P.; Nyström, D.; Hawker, C.J.; Hult, A.; Malkoch, M.A Chemoselecti ve Approach for the accelerated synthesis of well- defined dendritic architect ures. *Chem.Commun.***2007**, *22*, 2249– 2251.https://doi.org/10.1039/B703547 K.

(58) Nandivada, H.; Jiang, X.; Lahann, J. Click Chemistry: Versatility and Control in the Hands of Materials Scientists. *Adv. Mater.* **2007**, *19* (17), 2197–2208. https://doi.org/https://doi.org/10.1002/adma.200602739.

(59) Voggu, R.; Suguna, P.; Chandrasekaran, S.; Rao, C.N.R. Assembling Covale ntly Linked Nanocrystals and Nanotubes through Click Chemistry. *Chem. Ph ys. Lett.* **2007**, *443* (1– 3), 118– 121. https://doi.org/10.1016/j.cplett.2007.06. 050.

(60) Kumar, I.; Rana, S.; Rode, C. V; Cho, J. W. Functionalization of Single-Walled Carbon Nanotubes with Azides Derived from Amino Acids Using Click Chemistry. *J. Nanosci. Nanotechnol.* **2008**, *8* (7), 3351–3356. https://doi.org/10.1166/jnn.2008.109.

(61) de la Torre, G.; Blau, W.; Torres, T. A Survey on the Functionalization of Single Walled Nanotubes. The Chemical Attachment of Phthalocyanine Moie ties. *Nanotechnology,* **2003**, *14* (7), 765–771. https://doi.org/10.1088/0957-4484/14/7/312.

(62) Ballesteros, B.; Campidelli, S.; de la Torre, G.; Ehli, C.; Guldi, D. M.; Prato, M.; Torres, T. Synthesis, Characterization and Photophysical Properties of a SWNT-Phthalocyanine Hybrid. *Chem. Commun.* **2007**, *28*,2950–2952. https://doi.org/10.1039/B702819A.

(63) Campidelli, S.; Ballesteros, B.; Filoramo, A.; Díaz, D.D.; De La Torre, G.; Torres, T.; Rahman, G. M. A.; Ehli, C.; Kiessling, D.; Werner, F.; Sgobba, V.; Guldi, D.M.; Cioffi, C.; Prato, M.; Bourgoin, J.P. Facile Decoration of Functi onalized single wall Carbon Nanotubes with Phthalocyanines via "Click Che mistry." *J. Am. Chem. Soc.* **2008**, *130* (34), 11503– 11509. https://doi.org/10. 1021/ja8033262.

(64) Agard, N. J.; Prescher, J. A.; Bertozzi, C. R. A Strain-Promoted [3 + 2] Azide-Alkyne Cycloaddition for Covalent Modification of Biomolecules in Living Systems. *J. Am. Chem. Soc.* **2004**, *126* (46),15046 – 15047. https://doi.org/10 .1021/ja044996f.

(65) Tajmir-Riahi, H. A.; Langlais, M.; Savoie, R. A Laser Raman Spectroscopic Study of the Interaction of Calf-Thymus DNA with Cu(II) and Pb(II) Ions: Metal Ion Binding and DNA Conformational Changes. *Nucleic Acids Res.* **1988**, *16* (2), 751–762. https://doi.org/10.1093/nar/16.2.751.

(66) Shey, M. S.; Hughes, E. J.; de Kock, M.; Barnard, C.; Stone, L.; Kollmann, T. R.; Hanekom, W. A.; Scriba, T. J. Optimization of a Whole Blood Intracellular Cytokine Assay for Measuring Innate Cell Responses to Mycobacteria. *J.*

Immunol. Methods **2012**, *376* (1– 2), 79– 88. https://doi.org/10.1016/j.jim.2011.11.011.

(67) Jewett, J.C.; Bertozzi, C.R. Cu- Free Click Cycloaddition Reactions in Chemical Biology. *Chem. Soc. Rev.* **2010**, *39* (4), 1272– 1279. https://doi.org/10.1039/b901970g.

(68) Escorihuela, J.; Marcelis, A. T. M.; Zuilhof, H. Metal-Free Click Chemistry Reactions on Surfaces. *Adv. Mater. Interfaces* **2015**, *2* (13),1–42. https://doi.org/10.1002/admi.201500135.

(69) Agard, N.J.; Baskin, J.M.; Prescher, J.A.; Lo, A.; Bertozzi, C.R. A Comparative Study of Bioorthogonal Reactions with Azides. *ACS Chem. Biol.* **2006**, *1* (10), 644–648. https://doi.org/10.1021/cb6003228.

(70) Ning, X.; Guo, J.; Wolfert, M. A.; Boons, G.J. Visualizing Metabolically Labeled Glycoconjugates of Living Cells by Copper-Free and Fast Huisgen Cycloadditions. *Angew. Chemie - Int. Ed.* **2008**, *47* (12), 2253–2255. https://doi.org/10.1002/anie.200705456.

(71) Debets, M. F.; van Berkel, S. S.; Dommerholt, J.; Dirks, A. T. J.; Rutjes, F. P. J. T.; van Delft, F. L. Bioconjugation with Strained Alkenes and Alkynes. *Acc. Chem. Res.* **2011**, *44* (9), 805–815. https://doi.org/10.1021/ar200059z.

(72) Kuzmin, A.; Poloukhtine, A.; Wolfert, M.A.; Popik, V.V. Surface Functionalization Using Catalyst- Free Azide−Alkyne Cycloaddition. *Bioconjug. Chem.* **2010**, *21* (11), 2076–2085. https://doi.org/10.1021/bc100306u.

(73) Debets, M. F.; van Berkel, S. S.; Schoffelen, S.; Rutjes, F. P. J. T.; van Hest, J. C. M.; van Delft, F. L. Aza-Dibenzocyclooctynes for Fast and Efficient Enzyme PEGylation via Copper-Free (3+2) Cycloaddition. *Chem. Commun.*

2010, *46* (1), 97–99. https://doi.org/10.1039/B917797C.

(74) Marks, I.S.; Kang, J.S.; Jones, B.T.; Landmark, K.J.; Cleland, A.J.; Taton, T. A. Strain-Promoted "Click" Chemistry for Terminal Labeling of DNA. *Bioconjug.Chem.***2011**, *22* (7), 1259— 1263. https://doi.org/10.1021/bc10036 68.

(75) Gobbo, P.; Mossman, Z.; Nazemi, A.; Niaux, A.; Biesinger, M. C.; Gillies, E. R.; Workentin, M. S. Versatile Strained Alkyne Modified Water-Soluble AuNPs for Interfacial Strain Promoted Azide Alkyne Cycloaddition (I- SPA AC). *J. Mater. Chem. B* **2014**, *2* (13), 1764– 1769. https://doi.org/10.1039/c3 tb21799j.

(76) Gobbo, P.; Novoa, S.; Biesinger, M. C.; Workentin, M. S. Interfacial Strain-Promoted Alkyne-Azide Cycloaddition (I-SPAAC) for the Synthesis of Nanomaterial Hybrids. *Chem. Commun.* **2013**, *49* (38), 3982–3984. https://doi.org/10.1039/c3cc41634h.

(77) Heuer-Jungemann, A.; Kirkwood, R.; El-Sagheer, A. H.; Brown, T.; Kanaras, A. G. Copper-Free Click Chemistry as an Emerging Tool for the Programmed Ligation of DNA-Functionalised Gold Nanoparticles. *Nanoscale* **2013**, *5* (16), 7209–7212. https://doi.org/10.1039/c3nr02362a.

(78) Fong, D.; Andrews, G.M.; McNelles, S.A.; Adronov, A. Decoration of Polyfluorene-Wrapped Carbon Nanotube Thin Films via Strain-Promoted Azide–Alkyne Cycloaddition. *Polym. Chem.* **2018**, *9* (35), 4460–4467. https://doi.org/10.1039/C8PY01003J.

(79) Frielinghaus, R.; Besson, C.; Houben, L.; Saelhoff, A. K.; Schneider, C. M.; Meyer, C. Controlled Covalent Binding of Antiferromagnetic Tetramanganese Complexes to Carbon Nanotubes. *RSC Adv.* **2015**, *5* (102), 84119–84124.

https://doi.org/10.1039/c5ra14983e.

(80) Schnee, M.; Besson, C.; Frielinghaus, R.; Lurz, C.; Kögerler, P.; Schneider, C. M.; Meyer, C. Quantum Transport in Carbon Nanotubes Covalently Functionalized with Magnetic Molecules. *Phys. Status Solidi Basic Res.* **2016**, *253* (12), 2424–2427. https://doi.org/10.1002/pssb.201600292.

(81) Kong, J.; Dai, H. Synthesis of Individual SWCNTs on Patterned Silicon Wafers. *Nature* **1998**, *395* (3), 1–4.

(82) Susi, T.; Pichler, T.; Ayala, P. X-Ray Photoelectron Spectroscopy of Graphitic Carbon Nanomaterials Doped with Heteroatoms. *Beilstein J. Nanotechnol.* **2015**, *6* (1), 177–192. https://doi.org/10.3762/bjnano.6.17.

(83) Dresselhaus, M. S.; Jorio, A.; Saito, R. Characterizing Graphene, Graphite, and Carbon Nanotubes by Raman Spectroscopy. *Annu. Rev. Condens. Matter Phys.* **2010**, *1* (1), 89–108. https://doi.org/10.1146/annurev-conmatphys-070909-103919.

(84) Jorio, A.; Fantini, C.; Pimenta, M. A.; Capaz, R. B.; Samsonidze, G. G.; Dresselhaus, G.; Dresselhaus, M. S.; Jiang, J.; Kobayashi, N.; Grüneis, A.; Saito, R. Resonance Raman Spectroscopy (n,m)-Dependent Effects in Small-Diameter Single-Wall Carbon Nanotubes. *Phys. Rev. B - Condens. Matter Mater.Phys.***2005**, *71* (7), 1–11. https://doi.org/10.1103/PhysRevB.71.075401.

(85) Graupner, R. Raman Spectroscopy of Covalently Functionalized Single-Wall Carbon Nanotubes. *J.Raman Spectrosc.* **2007**, *38* (6), 673–683. https://doi.org/https://doi.org/10.1002/jrs.1694.

(86) Fantini, C.; Jorio, A.; Souza, M.; Strano, M. S.; Dresselhaus, M. S.; Pimenta, M. A. Optical Transition Energies for Carbon Nanotubes from Resonant

Raman Spectroscopy : Environment and Temperature Effects. **2004**, No. October, 1–4. https://doi.org/10.1103/PhysRevLett.93.147406.

(87) Dresselhaus, M. S.; Dresselhaus, G.; Jorio, A.; Souza Filho, A. G.; Saito, R. Raman Spectroscopy on Isolated Single Wall Carbon Nanotubes. *Carbon N. Y.* **2002**, *40* (12), 2043–2061. https://doi.org/https://doi.org/10.1016/S0008-6223(02)00066-0.

(88) Prithu Mukhopadhyay, R. K. G. *Graphite, Graphene, and Their Polymer Nanocomposites*, 1st Edition.; Taylor and Francis Group, **2012**, 631. https://doi.org/10.1201/b13051.

(89) Filho, A.G.S.; Jorio, A.; Samsonidze, G.G.; Dresselhaus, G.; Saito, R.; Dresse lhaus, M. S. Raman Spectroscopy for Probing Chemically/Physically Induced Phenomena in Carbon Nanotubes. *Nanotechnology* **2003**, *14* (10), 1130–1139. https://doi.org/10.1088/0957-4484/14/10/311.

(90) Maultzsch, J.; Reich, S.; Thomsen, C. Chirality-Selective Raman Scattering of the D Mode in Carbon Nanotubes. *Phys. Rev. B* **2001**, *64* (12), 121407. https://doi.org/10.1103/PhysRevB.64.121407.

(91) Dresselhaus, M.S.; Jorio, A.; Hofmann, M.; Dresselhaus, G.; Saito, R. Perspectives on Carbon Nanotubes and Graphene Raman Spectroscopy. *Nano Lett.* **2010**, *10* (3), 751–758. https://doi.org/10.1021/nl904286r.

(92) Joseph R. Lakowicz. *Principles of Fluorescence Spectroscopy*; Springer US, **2006**. https://doi.org/10.1007/978-0-387-46312-4.

(93) Jablonski, A. Efficiency of Anti-Stokes Fluorescence in Dyes. *Nature* **1933**, *131* (3319), 839–840. https://doi.org/10.1038/131839b0.

(94) Abbe, E. Beiträge Zur Theorie Des Mikroskops Und Der Mikroskopischen

Wahrnehmung. *Arch. für Mikroskopische Anat.* **1873**, *9* (1), 413–468. https://doi.org/10.1007/BF02956173.

(95) Datta, R.; Heaster, T. M.; Sharick, J. T.; Gillette, A. A.; Skala, M. C. Fluorescence Lifetime Imaging Microscopy: Fundamentals and Advances in Instrumentation, Analysis, and Applications. *J. Biomed. Opt.* **2020**, *25* (7), 1–43. https://doi.org/10.1117/1.JBO.25.7.071203.

(96) Rust, M. J.; Bates, M.; Zhuang, X. Sub-Diffraction-Limit Imaging by Stochastic Optical Reconstruction Microscopy (STORM). *Nat. Methods* **2006**, *3* (10), 793–796. https://doi.org/10.1038/nmeth929.

(97) Heilemann, M.; van de Linde, S.; Schüttpelz, M.; Kasper, R.; Seefeldt, B.; Mukherjee, A.; Tinnefeld, P.; Sauer, M. Subdiffraction Resolution Fluoresce nce Imaging with Conventional Fluorescent Probes. *Angew. Chemie Int. Ed.* **2008**, *47* (33), 6172– 6176. https://doi.org/https://doi.org/10.1002/anie.20080 2376.

(98) Schnitzbauer, J.; Strauss, M. T.; Schlichthaerle, T.; Schueder, F.; Jungmann, R. Super-Resolution Microscopy with DNA-PAINT. *Nat. Protoc.* **2017**, *12* (6), 1198–1228. https://doi.org/10.1038/nprot.2017.024.

(99) Agasti, S.S.; Wang, Y.; Schueder, F.; Sukumar, A.; Jungmann, R.; Yin, P. DNA-Barcoded Labeling Probes for Highly Multiplexed Exchange-PAINT Imaging. *Chem. Sci.* **2017**, *8* (4), 3080– 3091. https://doi.org/10.1039/C6SC0 5420J.

(100) Oi, C.; Mochrie, S. G. J.; Horrocks, M. H.; Regan, L. PAINT Using Proteins: A New Brush for Super-Resolution Artists. *Protein Sci.* **2020**, *29* (11), 2142–2149. https://doi.org/https://doi.org/10.1002/pro.3953.

(101) Nieves, D.J.; Gaus, K.; Baker, M.A.B. DNA- Based Super Resolution Micro scopy: DNA- PAINT. *Genes (Basel).* **2018**, *9* (12). https://doi.org/10.3390/ge nes9120621.

Chapter 3

Click functionalization of single-walled carbon nanotubes with gold nanoparticles

3.1 Introduction

Single-walled carbon nanotubes (SWNTs) are extremely promising and have unique structural, chemical and physical properties[1] and thus make them a suitable candidate for exceptional innovations of different applications such as molecular electronics[2,3], advanced composite materials[4] and biomedical applications[5–7]. Owing to their hydrophobic nature, SWNTs have the tendency to agglomerate, which limits the materials design[8,9]. They can be chemically modified by attaching various functionalities to the surfaces of the nanotubes widens the scope to utilize them in various applications. Click chemistry offers us to tailor a wide range of molecules in a simple way and with high efficiency. Most of the functionalization routes disturb the structural integrity of the nanotubes and thus fail to achieve a high degree of functionalization. The functionalization route, which comprises cycloaddition reactions, is a controlled approach with very high selectivity and efficiency[10,11]. There are different click reactions, including Diels Alder reaction[12], photo click reaction[13], tetrazine cycloaddition[14] and the most famous Huisgen azide-alkyne 1,3 cycloaddition[15].

Among the collection of these reactions, Cu(I) catalyzed azide-alkyne 3+2 cycloaddition (CuAAC) is the most studied and effective reaction of all[15–20]. Click chemistry has been reported with carbon nanotubes via various functional materials such as zinc or cobalt phthalocyanine[21,22], polystyrene polymers[23], amphiphilic polymer brushes[24] and magnetic nanoparticles[25]. In general, click functionalized carbon nanotubes were investigated through various methodologies, including the copper-catalyzed route, to understand characteristics such as hydrophobicity,

conductivity, optical property, biocompatibility, etc[20]. Qi et al. reported that the azide attached SWNTs were click coupled through CuAAC route with alkyne modified protein, used as a sensing platform with good sensitivity and stability for the immunoassay[26]. Covalently attached SWNTs and DWNTs TFTs (Double-walled carbon nanotube Thin Film Transistors) were also reported and used as chemical sensors with ultrahigh sensitivity and selectivity[27].

However, there has been an interest in developing novel click reactions involving living systems or biomolecules without metal catalysis as it could be cytotoxic[28–30]. One of the effective reactions yet biocompatible is the copper-free [3+2] Huisgen cycloaddition, also known as strain-promoted alkyne-azide cycloaddition (SPAAC). This reaction was based on cyclic alkynes and azides introduced by C.R. Betrozzi[31]. Though the SPAAC reaction is slower when compared to the CuAAC reaction, it is not compromising in many cases such as high selectivity and efficiency and, most significantly, the feasibility in biorthogonal labeling and imaging[32].

Hence, we employ a route involving silanization and strain-promoted azide-alkyne cycloaddition (SPAAC) or copper-free "click chemistry" to functionalize SWNTs with gold nanoparticles that yield dense and homogeneous results coverage. We present that this novel route can be transferred to the nanotubes grown on substrates as well. At the same time, it is specific and selective and thus enables click functionalization after the CNTs have been integrated into the devices. Gold nanoparticles functionalized carbon nanotubes are of interest in material chemistry because of their various applications in sensing, nanomedicine and catalysis[33–36]. This work lays the foundation for functionalizing different functional molecules such as fluorescent dyes and other molecules with SWNTs and studying its post

functionalization properties such as fluorescence quenching and conductivity on nanoelectronic devices.

3.2 Results and Discussion

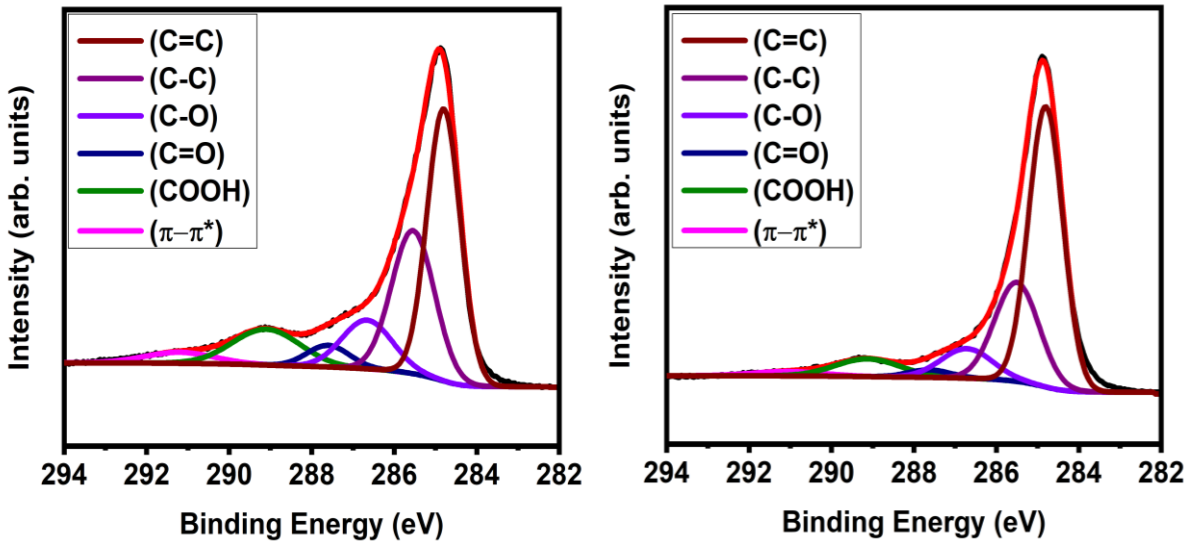

Figure 3.1 XPS of the carbon C 1s peak of carboxylated SWNTs (a) before (b) after silanization.

In the following, we characterize and discuss every step of the functionalization scheme. Figure 3.1 shows the high-resolution C 1s XPS spectra for the carboxylated SWNTs before (Figure 3.1 (a)) and after (Figure 3.1 (b)) silanization. The spectra for the carboxylated SWNTs deconvoluted into six components: the peak at 284.8 eV (C=C) is attributed to graphitic structure, the peak at 285.5 eV is attributed to sp^3 hybridized carbon atoms (C-C), and the remaining peaks are 286.6 eV (ether/alcohol C-O), 287.6 eV (carbonyl groups C=O) and 289.1 eV (carboxyl groups COOH). The last peak at 291.2 eV is assigned to the π - π* transition peak[37–40]. All binding energies are calibrated to the sp^2 hybridized carbon at 284.8 eV.

The relative intensity of the COOH peak is large compared to previous reports, while the sp^3 carbon content is slightly increased[37,39]. We attribute this to carboxylic groups' high contribution, leading to an increase of sp^3 carbon content as reported in Lee et al.[38]. The COOH peak shows a drastic decrease from 11% to 6.6% after silanization. We attribute this to the successful silanization reaction where the silane molecules are attached to the functional groups present in the nanotubes. A similar reduction of the COOH peak is reported by Ma et al. after reduction and silanization of MWNTs[41].

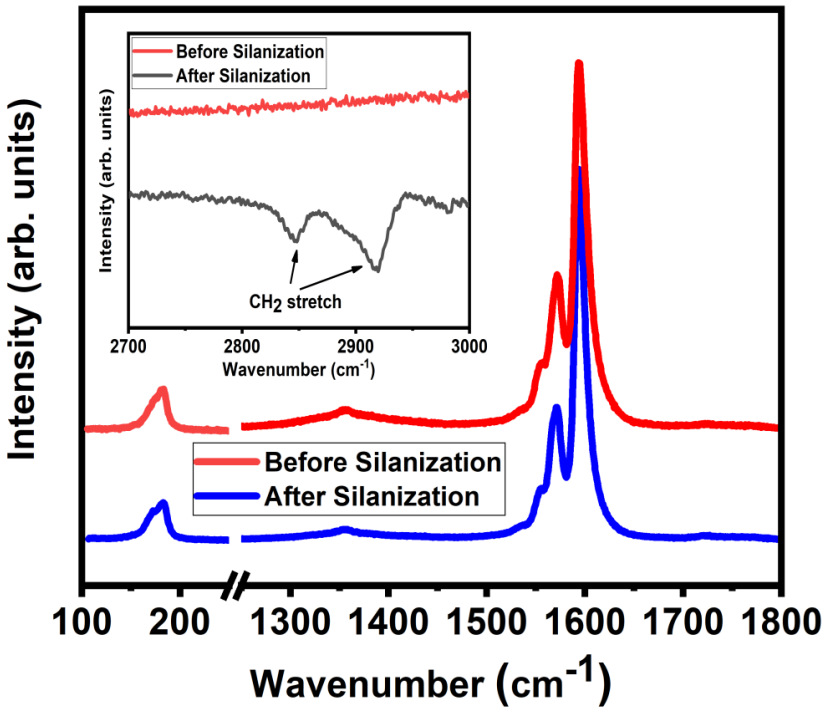

Figure 3.2 Raman shifts of Radial Breathing Mode, the D mode, and the G mode before and after silanization. Measured Laser Wavelength: 473 nm. Spectra are normalized with respect to G-mode intensity. Inset: FT-IR before and after silanization.

Figure 3.2 shows the Raman spectra of both carboxylated SWNTs and silanized SWNTs. There is no significant change of the defect mode at approx. 1350 cm^{-1} after

silanization[23]. The silane attachment to the carboxylated SWNTs thus does not lead to additional defects. Previous studies reported a vanishing radial breathing mode (RBM) after functionalization for small diameter nanotubes[21,42]. In contrast, we do observe RBMs in the Raman spectra before as well as after the silanization. We attribute this to the large diameter (on average of 1.55 nm) of our SWNTs, where the RBM intensity decreases only gradually with layer by layer functionalization[38]. The FT-IR spectra in the inset of figure 3.2 show clear absorption peaks at 2918 and 2848 cm^{-1} for the silanized SWNTs. They are caused by the symmetric and the asymmetric stretching mode of methylene groups from the silane absent in the carboxylated SWNTs[39,41]. These modes are absent in the carboxylated SWNTs before the silanization and thus are not caused by aliphatic defects of the tubes as in reference[43].

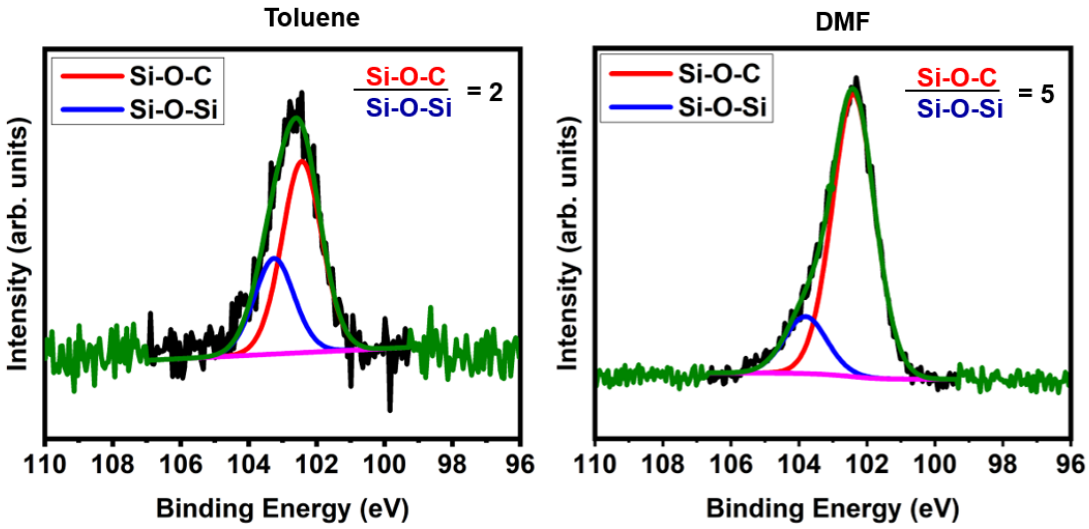

Figure 3.3 XPS of the Si 2p peak of carboxylated SWNTs after silanization using (a) toluene and (b) DMF as the solvent.

They deconvoluted into two peaks that correspond to two chemical states of Si: The peak at 102.4 eV is caused by (Si-O-C) links while the peak at 103.2 eV shows (Si-O-Si) connections[43]. The former represents the bond of the silane to the SWNT, and

the latter indicates a cross-linking between silane molecules. Cross-linking is likely between trichlorosilane molecules and is similar as in trimethoxy silanes bound to MWNTs[44]. The ratio between the peaks is thus an indicator of the binding efficiency of the silane to the SWNTs. We find a ratio of 0.5 (0.1 error range) for (Si-O-Si)/(Si-O-C) when toluene is used as the solvent (Figure 3.3 (a)). This indicates that about 50% of the silane molecules are not attached to the nanotube but another silane. This ratio changes significantly when DMF is used as the solvent (Figure 3.3 (b)), where only about 20% of the silane molecules are not grafted to an SWNT.

The different binding efficiency is reflected in the dispersibility of the SWNTs presented in image 3.4. It shows the four vials containing equal volumes and masses of carboxylated SWNTs and silanized SWNTs dispersed by different solvents (Toluene: C1, S1 and DMF (extra dry): C2, S2) after ultra-sonication for 30 minutes. The nanotubes dispersed in toluene quickly settle down, though the fraction appears to be lower for the silanized CNTs. On the other hand, the carboxylated and the silanized SWNTs form a very clear, dark black solution in DMF that remains stable even for several weeks. In summary, the results of the different characterization techniques lead to the conclusion that the silane molecules are grafted to the SWNTs via the carboxyl groups.

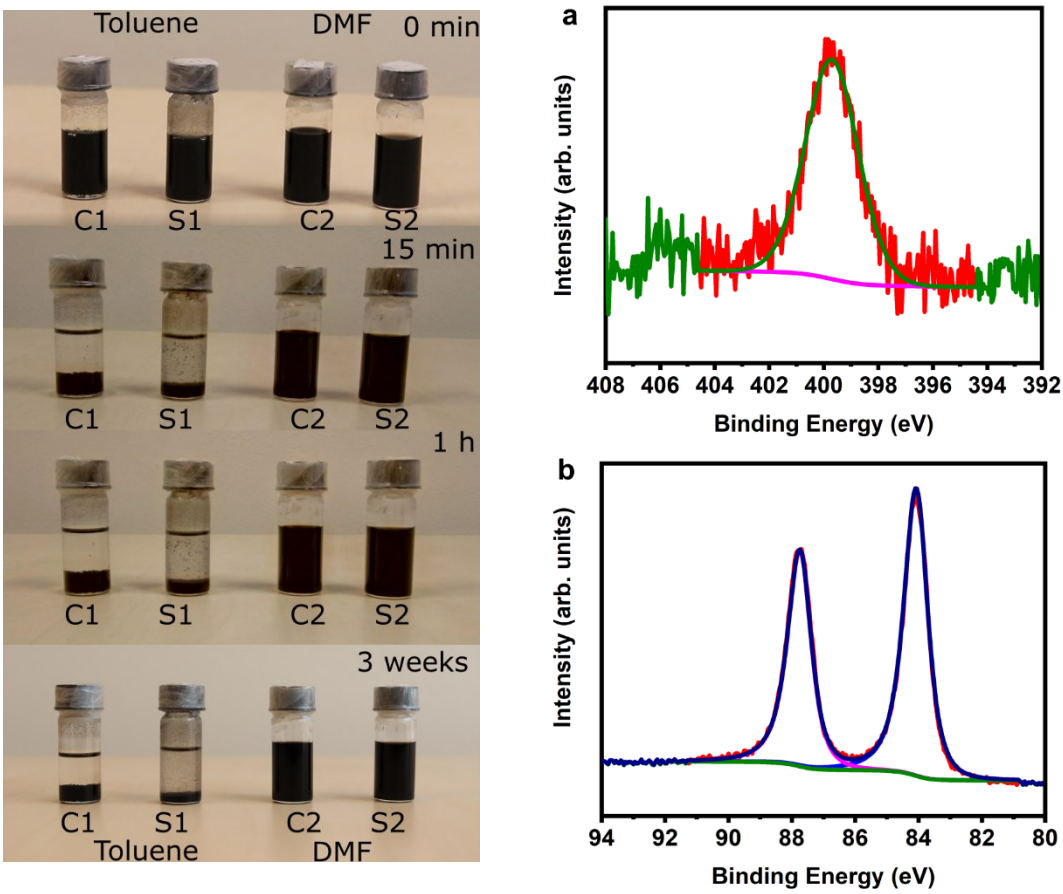

Figure 3.4 Dispersibility experiment of carboxylated and silanized SWNTs with different solvents Toluene and DMF (Toluene: C1, S1 and DMF (extra dry): C2, S2). High resolution XPS spectra of N 1s after Azidization. (b) High resolution XPS spectra of Au $4f_{7/2}$ and Au $4f_{5/2}$ after click reaction.

In the following, we first discuss the last steps of the functionalization route - azidization and click-reaction with AuNPs - before presenting the structural characterization by TEM. Figure 3.4 (a) shows the high resolution N 1s peak of SWNTs after azidization; it is consigned around 400 eV assures the nitrogen presence, which matches with the previous studies[45,46]. The high resolution C 1s spectra after azidization and click reaction are shown in figure 3.5. They show a

small shift of the peak formerly attributed to carbonyl groups from 287.6 to 288 eV. We attribute this to the presence of C-N bonds after the azidization[47].

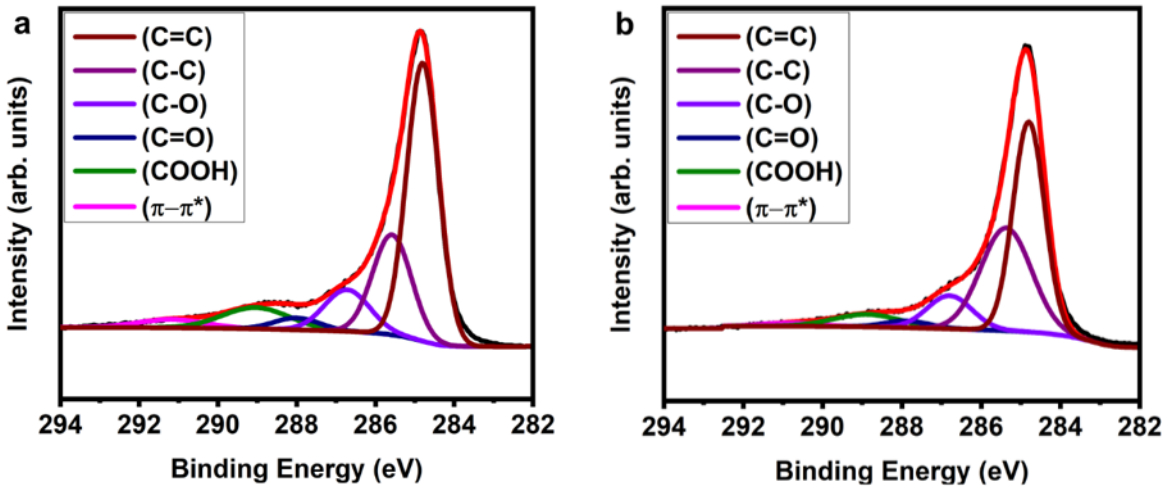

Figure 3.5 XPS C1s spectra after azidization and click reaction of functionalized SWNTs.

The successful click-reaction with AuNPs-DBCO is shown by the high resolution XPS Au 4f spectra in Figure 3.4 (b). The Au $4f_{7/2}$ and Au $4f_{5/2}$ peaks are assigned at 84.3 eV and 87.9 eV, respectively[48–50]. TEM is used for the structural characterization of the gold functionalized SWNTs. Figure 3.6 shows images of SWNTs after functionalization using different solvents. Gold nanoparticles are clearly identified on the surface of the functionalized SWNTs. The functionalization appears to be rather inhomogeneous when toluene is used as the solvent (Figure 3.6 (a)), comparable to previous studies on MWNTs functionalized with AuNPs[49,50]. We attribute this to the agglomeration of SWNT bundles during the series of reaction causes due to the solvent (in this case, toluene). As a result, the components we attach do not react with their corresponding functional groups. The whole synthesis procedure is followed as a control experiment without involving any main constituents such as silane or azide.

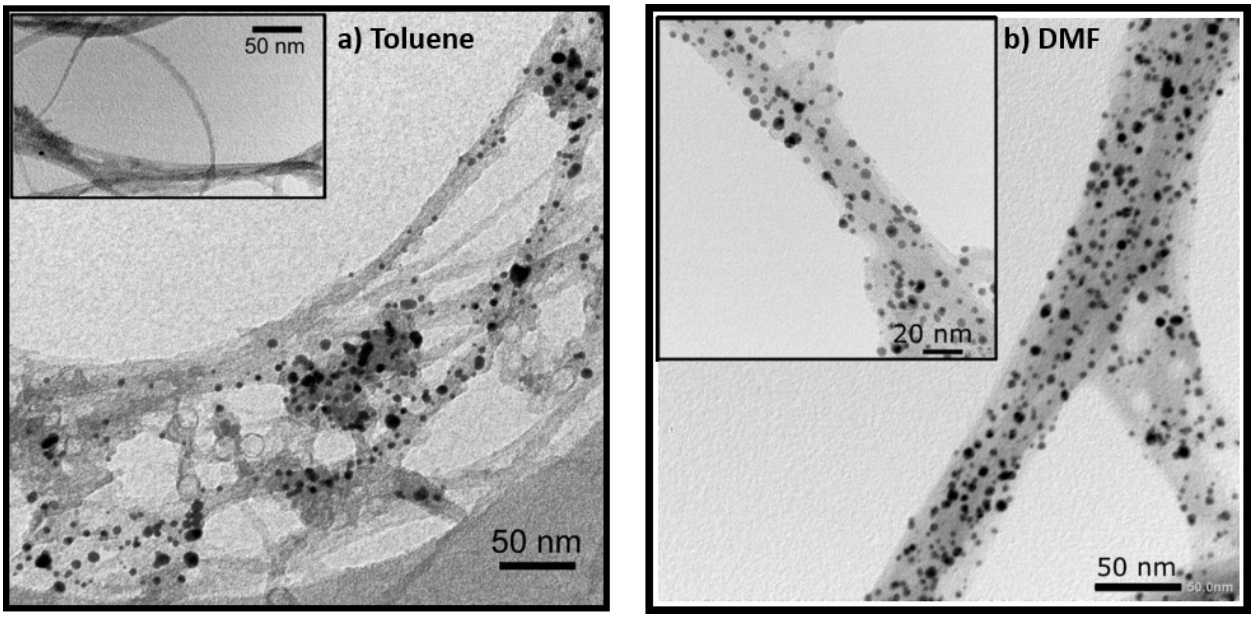

Figure 3.6 TEM images of gold nanoparticles functionalized SWNTs after silanization with a) Toluene and b) DMF. Inset: a) Negative control experiment b) High magnification TEM image.

As a final step, the DBCO functionalized AuNPs are added to the solution, followed by the washing procedure. We did not find any trace of gold nanoparticles on the CNTs in the subsequent TEM characterization, as shown in the inset of figure 3.6 (a). This implies the specific bonding between azide and DBCO in the actual functionalization. The distribution of gold nanoparticles is much more homogeneous compared to toluene treatment when DMF is used as the solvent, as shown in figure 3.6 (b). Mostly, individual AuNPs are attached, though sometimes two of them appear close together. Larger agglomerations appear very rarely. Together with the XPS data of the Si 2p peak, this supports the interpretation that cross-linking between the silanes is the primary reason for the strong agglomeration of the silanized CNTs. The functionalization density is similar to the one achieved by Gobbo et al., who functionalized SWNTs with gold nanoparticles through SPAAC, however, with the DBCO attached to the CNT[48].

3.3 Conclusion

In summary, this chapter shows an efficient and mild functionalization of SWNTs by using a unique synthesis route involving both silanization and click reaction (SPAAC) in a non-toxic way. Gold nanoparticles (5 nm) were used to functionalize the surface of the nanotubes after silanization and azidization reactions. Surface characterization (XPS) after every reaction shows the respective molecules' presence onto the nanotube surface. The solvent (DMF or Toluene) used during the initial process and silanization reaction affects the homogeneity and the density of the functionalization. This click functionalization route demonstrated that the single-walled carbon nanotubes can be surface modified covalently with versatile, functional molecules and can be utilized in different applications. DBCO is an abundant functionalization of commercially available molecules and nanoparticles. Thus, our route can be easily employed to graft a variety of nano-materials to SWNTs.

3.4 References

(1) Iijima, S.; Ichihashi, T. Single-Shell Carbon Nanotubes of 1-nm Diameter. *Nature* **1993**, *363* (6430), 603–605. https://doi.org/10.1038/363603a0.

(2) Avouris, P. Molecular Electronics with Carbon Nanotubes. *Acc. Chem. Res.* **2002**, *35* (12), 1026–1034. https://doi.org/10.1021/ar010152e.

(3) Collins, P. G.; Avouris, P. Nanotubes for Electronics. *Sci. Am.* **2000**, *283* (6), 62–69. https://doi.org/10.1038/scientificamerican1200-62.

(4) Ajayan, P. M. Nanotubes from Carbon. *Chem. Rev.* **1999**, *99* (7), 1787–1800. https://doi.org/10.1021/cr970102g.

(5) Katz, E.; Willner, I. Biomolecule-Functionalized Carbon Nanotubes: Applications in Nanobioelectronics. *ChemPhysChem* **2004**, *5* (8), 1084–1104. https://doi.org/10.1002/cphc.200400193.

(6) Kotov, N. A.; Winter, J. O.; Clements, I. P.; Jan, E.; Timko, B. P.; Campidelli, S.; Pathak, S.; Mazzatenta, A.; Lieber, C. M.; Prato, M.; Bellamkonda, R. V.; Silva, G. A.; Kam, N. W. S.; Patolsky, F.; Ballerini, L. Nanomaterials for Neural Interfaces. *Adv. Mater.* **2009**, *21* (40), 3970–4004. https://doi.org/10.1002/adma.200801984.

(7) Ménard-Moyon, C.; Kostarelos, K.; Prato, M.; Bianco, A. Functionalized Carbon Nanotubes for Probing and Modulating Molecular Functions. *Chem. Biol.* **2010**, *17* (2), 107–115. https://doi.org/10.1016/j.chembiol.2010.01.009.

(8) Campidelli, S. Click Chemistry for Carbon Nanotubes Functionalization. *Curr. Org. Chem.* **2012**, *15* (8), 1151–1159. https://doi.org/10.2174/138527211795203004.

(9) Salavagione, H. J.; Fatou, M. A. G.; Martínez, G.; Marco, C.; Ellis, G. J. Click

Functionalization of Carbon Nanotubes and Graphene with Polymers. *Chemical Functionalization of Carbon Nanomaterials: Chemistry and Applications*. **2015**, 398–429. https://doi.org/10.1201/b18724-18.

(10) Cabana, J.; Martel, R. Probing the Reversibility of Sidewall Functionalization Using Carbon Nanotube Transistors. *J. Am. Chem. Soc.* **2007**, *129* (8), 2244–2245. https://doi.org/10.1021/ja068320r.

(11) Cognet, L.; Tsyboulski, D.A.; Rocha, J.-D. R.; Doyle, C.D.; Tour, J.M.; Weisman, R.B. Stepwise Quenching of Exciton Fluorescence in Carbon Nanotubes by Single-Molecule Reactions. *Science* **2007**, *316* (5830), 1465–1468. https://doi.org/10.1126/science.1141316.

(12) Fort, E.H.; Donovan, P.M.; Scott, L.T. Diels−Alder Reactivity of Polycyclic Aromatic Hydrocarbon Bay Regions: Implications for Metal-Free Growth of Single-Chirality Carbon Nanotubes. *J. Am. Chem. Soc.* **2009**, *131* (44), 16006–16007. https://doi.org/10.1021/ja907802g.

(13) Song, W.; Wang, Y.; Qu, J.; Lin, Q. Selective Functionalization of a Genetica lly Encoded Alkene-Containing Protein via "Photoclick Chemistry" in Bacterial Cells. *J. Am. Chem. Soc.* **2008**, *130* (30), 9654– 9655. https://doi.or g/10.1021/ja803598e.

(14) Blackman, M.L.; Royzen, M.; Fox, J.M. Tetrazine Ligation: Fast Bioconjugat ion Based on Inverse-Electron-Demand Diels−Alder Reactivity. *J. Am. Chem. Soc.* **2008**, *130* (41), 13518–13519. https://doi.org/10.1021/ja8053805.

(15) Huisgen, R. Cycloadditions - Definition, Classification, and Characterization . *Angew. Chemie Int. Ed. English* **1968**, *7* (5), 321– 328. https://doi.org/https:/ /doi.org/10.1002/anie.196803211.

(16) Hein, J.E.; Fokin, V.V. Copper-Catalyzed Azide–Alkyne Cycloaddition (CuAAC) and beyond: New Reactivity of Copper(i) Acetylides. *Chem. Soc. Rev.* **2010**, *39* (4), 1302–1315. https://doi.org/10.1039/B904091A.

(17) Meldal, M.; Tornøe, C. W. Cu-Catalyzed Azide−Alkyne Cycloaddition. *Chem. Rev.* **2008**, *108* (8), 2952–3015. https://doi.org/10.1021/cr0783479.

(18) 1,3-Dipolar Cycloaddition Chemistry. Volumes 1 and 2. Edited by Albert Padwa. John Wiley and Sons. New York, 1984. *J. Heterocycl. Chem.* **1986**, *23* (6), 1899. https://doi.org/https://doi.org/10.1002/jhet.5570230658.

(19) Tiwari, V.K.; Mishra, B.B.; Mishra, K.B.; Mishra, N.; Singh, A.S.; Chen, X. Cu-Catalyzed Click Reaction in Carbohydrate Chemistry. *Chem. Rev.* **2016**, *116* (5), 3086–3240. https://doi.org/10.1021/acs.chemrev.5b00408.

(20) Han, J.; Gao, C. Functionalization of Carbon Nanotubes and Other Nanocarb ons by Azide Chemistry. *Nano- Micro Lett.* **2010**, *2* (3), 213– 226. https://doi .org/10.1007/BF03353643.

(21) Jubete, E.; Żelechowska, K.; Loaiza, O. A.; Lamas, P. J.; Ochoteco, E.; Farmer, K. D.; Roberts, K. P.; Biernat, J. F. Derivatization of SWCNTs with Cobalt Phthalocyanine Residues and Applications in Screen Printed Electrodes for Electrochemical Detection of Thiocholine. *Electrochim. Acta* **2011**, *56* (11),3988– 3995. https://doi.org/https://doi.org/10.1016/j.electacta.2011.01.1 23.

(22) Campidelli, S.; Ballesteros, B.; Filoramo, A.; Díaz, D.D.; De La Torre, G.; Torres, T.; Rahman, G.M. A.; Ehli, C.; Kiessling, D.; Werner, F.; Sgobba, V.; Guldi, D.M.; Cioffi, C.; Prato, M.; Bourgoin, J.P. Facile Decoration of Functi onalized Single Wall Carbon Nanotubes with Phthalocyanines via “Click Che mistry.” *J. Am. Chem. Soc.* **2008**, *130* (34), 11503– 11509. https://doi.org/10.

1021/ja8033262.

(23) Li, H.; Cheng, F.; Duft, A.M.; Adronov, A. Functionalization of Single Walle d Carbon Nanotubes with Well-Defined Polystyrene by “Click” Coupling. *J. Am. Chem. Soc.* **2005**, *127* (41), 14518– 14524. https://doi.org/10.1021/ja054 958b.

(24) Zhang, Y.; He, H.; Gao, C.; Wu, J. Covalent Layer-by-Layer Functionalization of Multiwalled Carbon Nanotubes by Click Chemistry. *Langmuir* **2009**, *25* (10), 5814–5824. https://doi.org/10.1021/la803906s.

(25) He, H.; Zhang, Y.; Gao, C.; Wu, J. ‘Clicked’ Magnetic Nanohybrids with a Soft Polymer Interlayer. *Chem. Commun.* **2009**, *13*, 1655– 1657. https://doi.o rg/10.1039/B821280E.

(26) Qi, H.; Ling, C.; Huang, R.; Qiu, X.; Shangguan, L.; Gao, Q.; Zhang, C. Functionalization of Single-Walled Carbon Nanotubes with Protein by Click Chemistry as Sensing Platform for Sensitized Electrochemical Immunoassay. *Electrochim. Acta* **2012**, *63*, 76– 82. https://doi.org/https://doi.org/10.1016/j.e lectacta.2011.12.084.

(27) Huang, J.; Ng, A. L.; Piao, Y.; Chen, C.-F.; Green, A. A.; Sun, C.-F.; Hersam, M. C.; Lee, C. S.; Wang, Y. Covalently Functionalized Double-Walled Carbon Nanotubes Combine High Sensitivity and Selectivity in the Electrical Detection of Small Molecules. *J. Am. Chem. Soc.* **2013**, *135* (6), 2306–2312. https://doi.org/10.1021/ja310844u.

(28) Gierlich, J.; Burley, G. A.; Gramlich, P. M. E.; Hammond, D. M.; Carell, T. Click Chemistry as a Reliable Method for the High-Density Postsynthetic Functionalization of Alkyne-Modified DNA. *Org. Lett.* **2006**, *8* (17), 3639–3642. https://doi.org/10.1021/ol0610946.

(29) Wang, Q.; Chan, T. R.; Hilgraf, R.; Fokin, V. V; Sharpless, K. B.; Finn, M. G. Bioconjugation by Copper(I)-Catalyzed Azide-Alkyne [3 + 2] Cycloaddition. *J. Am. Chem. Soc.* **2003**, *125* (11), 3192– 3193. https://doi.org/10.1021/ja021381e.

(30) Manova, R.; van Beek, T. A.; Zuilhof, H. Surface Functionalization by Strain-Promoted Alkyne–Azide Click Reactions. *Angew. Chemie Int. Ed.* **2011**, *50* (24), 5428–5430. https://doi.org/https://doi.org/10.1002/anie.201100835.

(31) Agard, N.J.; Prescher, J.A.; Bertozzi, C.R. A Strain-Promoted [3+2] Azide−Alkyne Cycloaddition for Covalent Modification of Biomolecules in Living Systems. *J. Am. Chem. Soc.* **2004**, *126* (46), 15046–15047. https://doi.org/10.1021/ja044996f.

(32) Li, L.; Zhang, Z. Development and Applications of the Copper-Catalyzed Azide-Alkyne Cycloaddition (CuAAC) as a Bioorthogonal Reaction. *Molecules* **2016**, *21* (10). https://doi.org/10.3390/molecules21101393.

(33) Chauhan, N.; Singh, A.; Narang, J.; Dahiya, S.; Pundir, C. S. Development of Amperometric Lysine Biosensors Based on Au Nanoparticles/Multiwalled Carbon Nanotubes/Polymers Modified Au Electrodes. *Analyst* **2012**, *137* (21), 5113–5122. https://doi.org/10.1039/C2AN35629E.

(34) Huang, J.; Xing, X.; Zhang, X.; He, X.; Qing, L.; Lian, W.; Zhu, H. A Molecularly Imprinted Electrochemical Sensor Based on Multiwalled Carbon Nanotube-Gold Nanoparticle Composites and Chitosan for the Detection of Tyramine. *Food Res. Int.* **2011**, *44* (1), 276— 281. https://doi.org/10.1016/j.foodres.2010.10.020.

(35) Cai, D.; Yu, Y.; Lan, Y.; Dufort, F. J.; Xiong, G.; Paudel, T.; Ren, Z.; Wagner, D. J.; Chiles, T. C. Glucose Sensors Made of Novel Carbon Nanotube-Gold

Nanoparticle Composites. *Biofactors* **2007**, *30* (4), 271–277. https://doi.org/10.1002/biof.5520300409.

(36) Guo, Y.; Guo, S.; Fang, Y.; Dong, S. Gold Nanoparticle/Carbon Nanotube Hybrids as an Enhanced Material for Sensitive Amperometric Determination of Tryptophan. *Electrochim. Acta* **2010**, *55* (12), 3927– 3931. https://doi.org/ https://doi.org/10.1016/j.electacta.2010.02.024.

(37) Roy, S.; Das, T.; Ming, Y.; Chen, X.; Yue, C. Y.; Hu, X. Specific Functionalization and Polymer Grafting on Multiwalled Carbon Nanotubes to Fabricate Advanced Nylon 12 Composites. *J. Mater. Chem. A* **2014**, *2* (11), 3961–3970. https://doi.org/10.1039/c3ta14528j.

(38) Lee, Y. J.; Ham, S. R.; Kim, J. H.; Yoo, T. H.; Kim, S. R.; Lee, Y. T.; Hwang, D. K.; Angadi, B.; Seo, W. S.; Ju, B. K.; Choi, W. K. Highly Dispersible Buckled Nanospring Carbon Nanotubes for Polymer Nano Composites. *Sci. Rep.* **2018**, *8* (1), 1–10. https://doi.org/10.1038/s41598-018-23172-1.

(39) Wang, W.-H.; Huang, B.-C.; Wang, L.-S.; Ye, D.-Q. Oxidative Treatment of Multi-Wall Carbon Nanotubes with Oxygen Dielectric Barrier Discharge Plasma. *Surf. Coatings Technol.* **2011**, *205* (21), 4896– 4901. https://doi.org/ https://doi.org/10.1016/j.surfcoat.2011.04.100.

(40) Datsyuk, V.; Kalyva, M.; Papagelis, K.; Parthenios, J.; Tasis, D.; Siokou, A.; Kallitsis, I.; Galiotis, C. Chemical Oxidation of Multiwalled Carbon Nanotubes. *Carbon N.Y.* **2008**, *46* (6), 833– 840. https://doi.org/https://doi.org/10.1016/j.carbon.2008.02.012.

(41) Ma, P. C.; Kim, J.-K.; Tang, B. Z. Functionalization of Carbon Nanotubes Using a Silane Coupling Agent. *Carbon N. Y.* **2006**, *44* (15), 3232–3238. https://doi.org/https://doi.org/10.1016/j.carbon.2006.06.032.

(42) Fantini, C.; Usrey, M.L.; Strano, M.S. Investigation of Electronic and Vibrational Properties of Single-Walled Carbon Nanotubes Functionalized with Diazonium Salts. *J. Phys. Chem. C* **2007**, *111* (48), 17941–17946. https://doi.org/10.1021/jp071841w.

(43) Vennerberg, D.; Rueger, Z.; Kessler, M. R. Effect of Silane Structure on the Properties of Silanized Multiwalled Carbon Nanotube - Epoxy nanocomposit es. *Polymer (Guildf).* **2014**, *55* (7), 1854– 1865. https://doi.org/10.1016/j.poly mer.2014.02.018.

(44) Velasco-Santos, C.; Martínez-Hernández, A. L.; Lozada-Cassou, M.; Alvarez-Castillo, A.; Castaño, V. M. Chemical Functionalization of Carbon Nanotubes through an Organosilane. *Nanotechnology* **2002**, *13* (4), 495–498. https://doi.org/10.1088/0957-4484/13/4/311.

(45) Yan, Y. H.; Cui, J.; Chan-Park, M. B.; Wang, X.; Wu, Q. Y. Systematic Studies of Covalent Functionalization of Carbon Nanotubes via Argon Plasma-Assisted UV Grafting. *Nanotechnology* **2007**, *18* (11), 115712. https://doi.org/10.1088/0957-4484/18/11/115712.

(46) Gobbo, P.; Mossman, Z.; Nazemi, A.; Niaux, A.; Biesinger, M.C.; Gillies, E. R.; Workentin, M.S. Versatile Strained Alkyne Modified Water-Soluble AuNPs for Interfacial Strain Promoted Azide-Alkyne Cycloaddition (I-SPAAC). *J. Mater. Chem. B* **2014**, *2* (13), 1764 – 1769. https://doi.org/10.10 39/c3tb21799j.

(47) Dementjev, A. P.; de Graaf, A.; van de Sanden, M. C. M.; Maslakov, K. I.; Naumkin, A.V; Serov, A.A. X-Ray Photoelectron Spectroscopy Reference Data for Identification of the C_3N_4 Phase in Carbon–Nitrogen Films. *Diam. Relat.Mater.***2000**, *9*(11), 1904 – 1907. https://doi.org/https://doi.org/10.1016

/S0925-9635(00)00345-9.

(48) Gobbo, P.; Novoa, S.; Biesinger, M. C.; Workentin, M. S. Interfacial Strain-Promoted Alkyne-Azide Cycloaddition (I-SPAAC) for the Synthesis of Nanomaterial Hybrids. *Chem. Commun.* **2013**, *49* (38), 3982–3984. https://doi.org/10.1039/c3cc41634h.

(49) Islam, M. R.; Bach, L. G.; Nga, T. T.; Lim, K. T. Covalent Ligation of Gold Coated Iron Nanoparticles to the Multi-Walled Carbon Nanotubes Employing Click Chemistry. *J. Alloys Compd.* **2013**, *561*, 201– 205. https://doi.org/https ://doi.org/10.1016/j.jallcom.2013.01.176.

(50) Duc Chinh, V.; Speranza, G.; Migliaresi, C.; Van Chuc, N.; Minh Tan, V.; Phuong, N.-T. Synthesis of Gold Nanoparticles Decorated with Multiwalled Carbon Nanotubes (Au - MWCNTs) via Cysteaminium Chloride Functionali zation. *Sci. Rep.* **2019**, *9* (1), 5667. https://doi.org/10.1038/s41598-019-42055-7.

Chapter 4

Click functionalization of single-walled carbon nanotubes with fluorescent dyes

4.1 Introduction

This chapter discusses the functionalization and characterization of single-walled carbon nanotubes with fluorescent dyes such as Cyanine 3 and AF647. Carbon nanotubes are widely used in biomedical applications like cell tracking and labeling, nanosensors, controlled drug delivery, and bioactive reagents[1]. It is significant to visualize the carbon nanotubes functionalized with biomolecules to apply nanotubes in biological systems. The fluorescence labeling of nanotubes will open up a more extensive range of applications, particularly in single-molecule devices based on optics. Despite promising properties, single-walled carbon nanotubes are limited for bio applications due to their low biocompatibility.

As discussed in Chapter 3, pristine carbon nanotubes are highly hydrophobic and thus have poor dispersibility making them unsuitable for bio applications. Moreover, some investigations have reported toxic effects after exposing SWNTs and MWNTs to biological systems due to factors such as metal impurities, surface charge, shape, length, agglomeration etc.,[2,3] Surface grafting is essential to solubilize the nanotubes in aqueous solutions and should enhance the biocompatibility of the carbon nanotubes. Non-toxic way of functionalization is significant to employ the carbon nanotubes in biosystems. Functionalization via *"grafting to"* or *"grafting from"* routes are the techniques used to alter the surface characteristics of the nanotubes in order to create a platform for further interactions with molecules[4,5].

As established in Chapter 3, SPAAC is one of the most versatile and suitable methods for efficiently functionalizing the surface of nanomaterials with biomolecules such as fluorescent dyes because the route is nontoxic. Investigations

of photophysical properties of photosensitive molecules attached to SWNTs are interesting as they make hybrid materials and sensing and light-harvesting devices.

Chiu et al. reported that fluorescent quenching of covalently functionalized SWNTs through factors such as direct charge transfers and from metal impurities[6]. In contrast, the covalent attachment of fluorophores to carbon nanotubes did not affect the fluorescence signal in different conditions under the fluorescence microscope reported in reference[7]. It is important to understand the interaction of fluorescent molecules with carbon nanotubes functionalized covalently to open the application window, especially in biosystems.

Long-wavelength dyes are widely used in fluorescence microscopy because they are optimally excited by light sources and fluoresce at wavelengths longer than usual sources of cell autofluorescence and the background fluorescence of the dyes is generally low[8]. Hence, we employ Cyanine 3 fluorescent dye to evaluate the photophysical properties of the functionalized SWNTs. In addition to this, a fluorescent dye similar to that of Cyanine 3 is also attached to SWNTs, known as Alexa Fluor 647, as they are more resistant to photobleaching than cyanine counterparts due to their photo stability. AF647 dye has similar qualities as Cyanine 3 like absorption maxima, emission maxima, stokes shift and extinction coefficient. However, there is a drastic difference in their lifetimes noted as 0.3 ns and 1 ns for Cyanine 3 and AF647, respectively.

The visualization of fluorescent dye functionalized nanotubes using a conventional microscope is extremely difficult because of their diameters. This study aims to utilize the synthetic route we established into fluorescent dyes and characterize the functionalized SWNTs localization, dynamics, fluorescence quenching and grafting efficiency under advanced microscopic setups.

4.2 Results and Discussion

We employ fluorescent dyes such as Cyanine 3 and AF647 to graft nanotubes through the established synthetic route in Chapter 2. To begin with, Cyanine 3 (Cy3) DBCO molecules are clicked with SWNTs. Cy3 DBCO is a bright, red-fluorescent probe routinely used to imaging azide-containing biomolecules without the need for copper catalyst with an excitation maximum of 555 nm and an emission maximum of 570 nm[9]. It is indeed significant to correlate at the same region of interest to study the structural information and fluorescence property of the functionalized SWNTs. We characterize the Cy3 functionalized SWNTS through AFM-EFM, a hybrid instrument specifically designed to extract the correlative information at the particular region of interest.

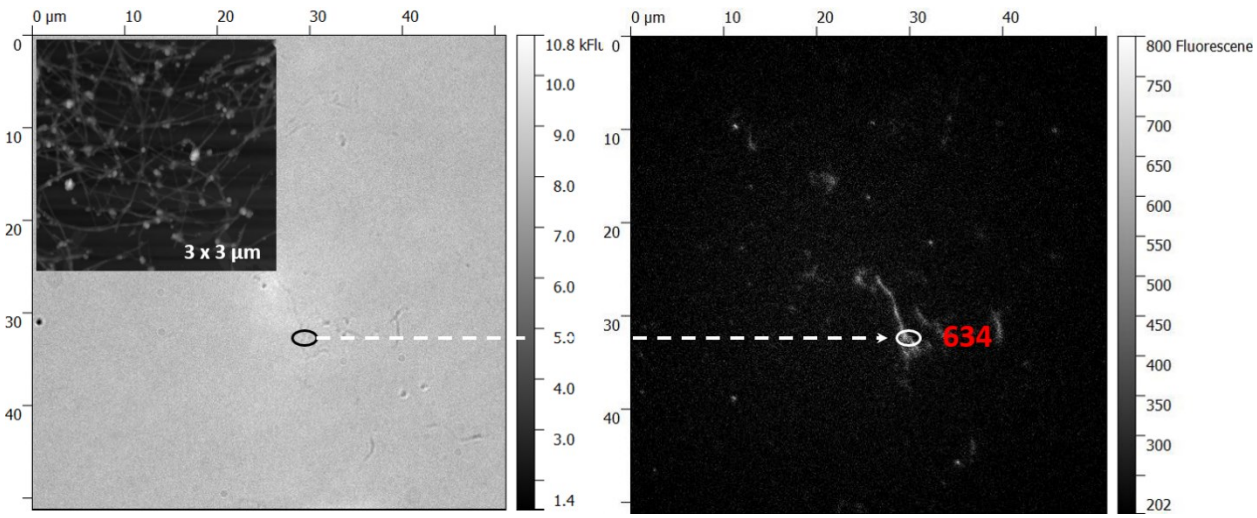

Figure 4.1 Bright Field and Fluorescence images of Cyanine 3 Dye functionalized SWNTs. EM Gain: 262. Laser wavelength 561 nm and Laser Power: 3 mW (Inset: AFM image: Diameter ranges in 10 nm). The fluorescence intensity of the elliptically marked area is noted as 634 in the fluorescence image.

Figure 4.1 shows the epifluorescence microscopic images of Cy3 functionalized SWNTs drop cast in a glass coverslip in a bright field and fluorescence images. Some of the nanotube bundles are visible in the bright field image, and their corresponding AFM image displays that the diameter lies in the range of 10 nm. AFM and fluorescence images are measured in different regions of the same sample. Thus, we observe dense bundles in the AFM image and single individual rope in the fluorescence image. Moreover, we managed to see the same nanotube bundle fluoresce in fluorescence imaging with the laser wavelength excitation of 561 nm with 3 mW laser power. However, it is difficult to resolve the functionalized nanotube bundle through epifluorescence microscopy due to the photobleaching effect and complex high resolution imaging at the nanoscale level.

We attribute this to the fact that the Cy3 dye has a high photobleaching effect and low resistance towards fluorescence quenching, especially at the high degree of labeling. So, the functionalization of Cy3 with SWNTs is successfully demonstrated through epifluorescence microscopy. We can comprehend the fluorescence but could not resolve the structural and photophysical properties because the structures are in the nanometer range, which makes conventional microscopy challenging to go beyond the diffraction limit. To overcome these challenges, it is necessary to find an alternative clickable fluorescent dye with upper resistance to fluorescence quenching with a higher degree of labeling and a more negligible photobleaching effect due to their better photo stability after conjugation[8].

Alex Fluor 647 (AF647) is the most commonly used clickable fluorescent dye used in advanced microscopic setups as they are very bright, long-wavelength and less self-quenching under imaging conditions. Alexa Fluor dyes are spectrally similar to the cyanine dyes but have more advantages relatively such as higher FRET

efficiencies, higher quantum efficiency and capable of retaining their fluorescence after functionalization[8].

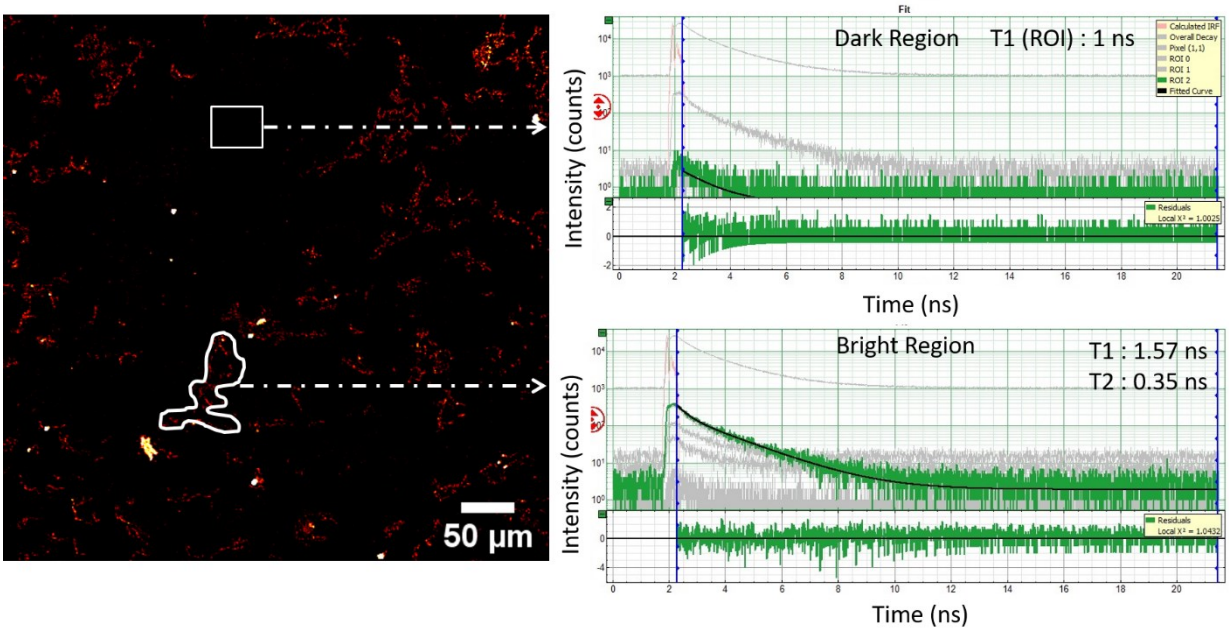

Figure 4.2 LSM image of AF647 functionalized SWNTs drop cast on a glass coverslip. FRET-FLIM analysis at two regions of interest. The dark region represents the glass coverslip surface and the bright region shows AF647 functionalized nanotube bundles.

Using the same synthetic route, SWNTs are functionalized with AF647 fluorescent dyes attached with DBCO. AF647 functionalized nanotubes are dispersed in isopropanol for characterizing further after ultra-sonication and centrifugation. FLIM analysis is carried out on this sample drop cast on a standard glass coverslip. Figure 4.2 shows the LSM image of the AF647 functionalized SWNTs and their corresponding lifetimes at a particular area of interest (ROI). We attribute two ROIs to functionalized nanotube bundles (Bright Region) and the surface of the glass coverslip (Dark Region). The bright region appears to have two different lifetimes noted as T_1=1.57 ns and T_2=0.35 ns. The reference measurement is carried out by

drop casting only AF647 dye on quartz substrate and the observed lifetime is 1.1 ns. The lifetime of T_2=0.35 ns represents the fluorescent dye attachment towards the nanotube and we attribute this to the fluorescence quenching effect of the nanotubes. Another lifetime shows around T_1=1.57 ns and this is undoubtedly not from either the free dye or the functionalized SWNTs as the lifetime exceeds more than 1 ns. Another reference measurement for a dirt area at standard coverslip was noted as 1.5 ns and this lifetime might be due to the same phenomenon. However, the correlation at the same area of interest is challenging with the standard glass coverslip.

Structural characterization is impossible without knowing the measurement region. Functionalized SWNTs are a mixed combination of nanotubes with different chirality. Furthermore, it is of great interest to assign the chirality of nanotubes by employing different laser wavelengths. Photo-etched coverslips are employed to correlate at the same region of interest with the assistance of Raman spectroscopy, fluorescence lifetime microscopy and scanning electron microscopy. Photoetched coverslips are nothing but the standard glass coverslip with a numbered marker system engraved with laser. Figure 4.3 (d) shows the photoetched coverslip schematic diagram in the inset. Raman spectroscopy is carried out at specific areas with the help of photoetched coverslips to detect the chirality of nanotubes using different laser wavelengths such as 473 nm, 633 nm and 532 nm.

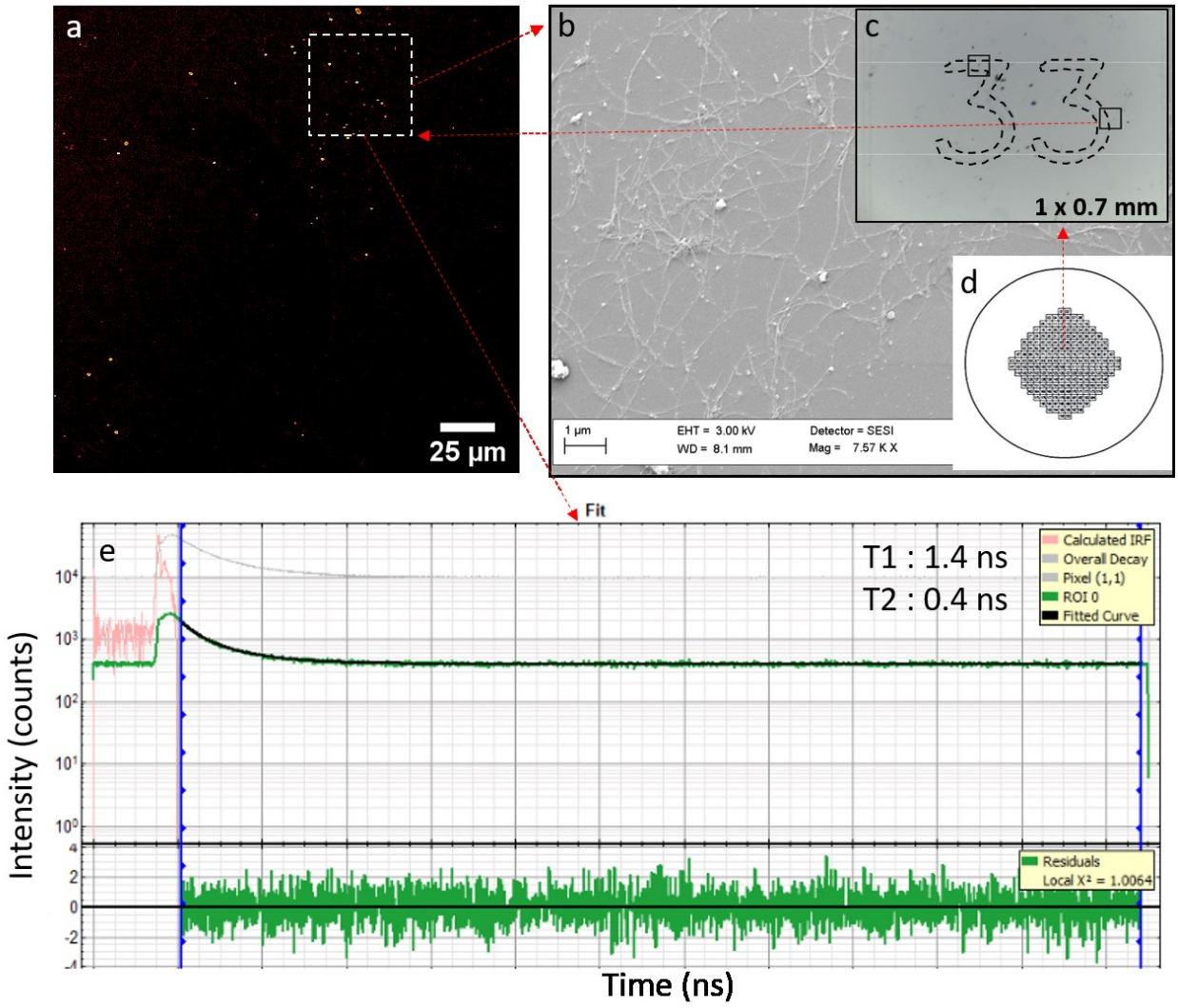

Figure 4.3 AF647 functionalized SWNTs drop cast on a photo-etched coverslip. a) LSM image of AF647-SWNTs bundles near Marker 33 b) SEM image at the same area of interest c) Inset: Camera Image (Marker 33) d) Inset: Overview image of a photo-etched glass coverslip. e) FLIM analysis at the same ROI.

The chirality assignment of AF647 functionalized nanotubes at different wavelengths at various spots is shown in Table 4.1. Figure 4.3 shows the LSM image of AF647 functionalized SWNTs and their corresponding FLIM spectra at the same areas as Raman measurements. We manage to fit data bi exponentially as they tend

to have two lifetimes. The mean values of the two lifetimes are T_1=1.4 ns and T_2=0.4 ns approximately. We attribute these phenomena to two factors: (i) lifetime due to the dirt agglomeration (T_1=1.4 ns) and (ii) covalently functionalized SWNTs (T_2=0.4 ns). Knowing that the fluorescent lifetime of AF647 dye is around one ns, we consider that the T_1=1.4 ns corresponds to the dirt on the coverslip supported with a reference measurement and the other T_2=0.4 ns represents covalently functionalized SWNTs as the nanotubes tend to quench the fluorescence.

Figure 4.3 (a) shows the LSM image of the AF647 SWNTs on a photoetched coverslip and bright white spots inside the marked area might be the dirt agglomeration. In addition to this, figure 4.3 (b) shows the overview SEM image of the AF647 functionalized SWNTs at the same region of interest as the image reveals that the spots where we performed Raman spectroscopy and FLIM analysis are distributed with the network of nanotubes.

Laser	wRBM (cm^{-1})	(n,m) assignment	Branch
473 nm	171.24	SC (14,6)	SC (12,10)
	184.63	SC (12,7) or (13,5)	SC (12,10)
633 nm	155.19	SC (16,6) or (15,8)	SC (12,10)
	173.07	M (13,7)	M (11,11)
	196.34	M (13,4)	M (10,10)
532 nm	160.14	SC (16,5) or (15,7)	SC (13,11)
	173.80	SC (12,8)	SC (11,10)
	180.03	SC (13,6)	SC (11,10)
	187.85	SC (15,2)	SC (11,10)

Table 4.1 Chirality assignment of the AF647 functionalized SWNTs measured at the same region of interest.

The nanotube bundles are in the range of 10-60 nm after the grafting procedure. It is indeed a complex task to quantify the properties of the functionalized nanotubes unless we localize the individual nanotube in high resolution. To localize the fluorophores covalently attached with SWNTs with high accuracy, we employ the STORM imaging technique referred to in chapter 1. It can identify the numerous fluorophores and resolve the ultra-structures under 20 nm after the reconstruction of many iterations. Figure 4.4 (a) shows the STORM images of AF647 functionalized SWNTs drop cast on the coverslip. The experiment is performed with the oxygen scavenging buffer to control the photobleaching of the fluorescent dyes. 20 K frames are reconstructed to form a super-resolved image.

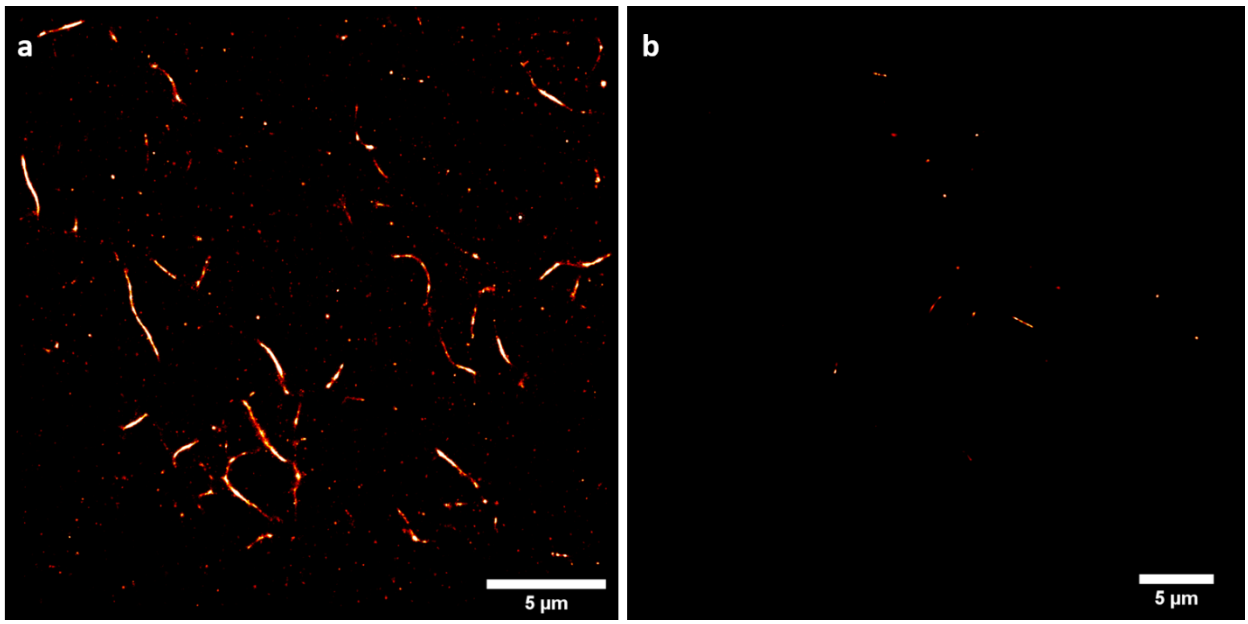

Figure 4.4 a) d-STORM image of AF647 functionalized SWNTs. b) Control experiment of nanotubes with AF647 (not functionalized). 20 K frames recorded. Activation laser wavelength: 405 nm. Excitation laser wavelength: 642 nm.

We managed to resolve the individual nanotube bundle of diameter less than 100 nm and length of around 5 μm, which we could not achieve through other microscopic techniques. The grafting efficiency of fluorophores looks homogeneous with the nanotubes. However, the d-STORM requires a high degree of efficient labeling to resolve the structure of diameters in the nanometer range, which could not be accomplished from the experiment as the nanotubes tend to quench strongly and provide low signal intensities. This further reduces the precision of each localization which is very few, and thus lowers the image's resolution. Later, the AF647 fluorescent dyes' concentration increases, and the functionalization is carried out for better imaging. Similarly, D Joshi et al. reported that the SWNTs and graphene nano ribbons are functionalized with cyanine 5 dye (similar to AF647) through the CuAAC route and imaged the fluorescent dye attached SWNTs via STORM technique. Super resolved images of functionalized SWNTs show the individual bundle length in the range between 50 – 80 nm[10].

A high concentration of functionalized SWNTs and free dyes on the surface are imaged, and the residues can be reduced after further dilution. A control experiment is carried out to demonstrate the covalent attachment of fluorescent dyes towards the nanotubes and not just free dyes covering the nanotubes. Figure 4.4 (b) shows the STORM image of the control experiment with AF647 dyes added to the nanotubes without following the functionalization procedure. As expected, there are slight traces of free dyes on the surface of the coverslip but not from the nanotubes. It is significant to enhance the functionalization density of SWNTs and keep the fluorophore away by increasing the distance with the surface of the SWNTs.

4.3 Conclusion

In this chapter, we successfully functionalized SWNTs with fluorescent dyes by following the SPAAC route, a non-toxic way of functionalizing SWNTs. Long-wavelength, bright dyes like Cyanine 3 and AF647 are used to click with nanotubes to study the photophysical properties through different microscopic techniques. Correlation among lifetime analysis, Raman spectroscopy and structural characteristics are carried out at the same region of interest for AF647 functionalized SWNTs. Two fluorescent lifetimes are detected for the AF647 SWNTs, representing the covalently attached SWNTs and free dyes on the coverslip. STORM technique is performed on AF647 SWNTs managed to resolve nanotubes bundles but lacked to investigate fluorescence quenching due to low degree of labeling and high fluorescence quenching. However, with the increase in fluorescent dye concentration, we managed to resolve the nanotube bundle but still could not quantify the fluorescence quenching as they tend to photobleach and quench faster.

Moreover, this chapter demonstrated that the ultra-structures could be resolved through super resolution microscopy through a non-destructive way of imaging fluorescent dye functionalized SWNTs, one of the critical challenges in biosystems[10]. And, this lays the foundation for the further exploitation of these individual fluorescent dye grafted SWNTs in sensing bioelectronic devices, especially single molecule devices.

4.4 References

(1) Saito, N.; Usui, Y.; Aoki, K.; Narita, N.; Shimizu, M.; Hara, K.; Ogiwara, N.; Nakamura, K.; Ishigaki, N.; Kato, H.; Taruta, S.; Endo, M. Carbon Nanotubes: Biomaterial Applications. *Chem. Soc. Rev.* **2009**, *38* (7), 1897–1903. https://doi.org/10.1039/B804822N.

(2) Liu, Y.; Zhao, Y.; Sun, B.; Chen, C. Understanding the Toxicity of Carbon Nanotubes. *Acc. Chem. Res.* **2013**, *46* (3), 702 - 713. https://doi.org/10.1021/ar300028m.

(3) Kostarelos, K. The Long and Short of Carbon Nanotube Toxicity. *Nat. Biotechnol.* **2008**, *26* (7), 774–776. https://doi.org/10.1038/nbt0708-774.

(4) Richard, C.; Balavoine, F.; Schultz, P.; Ebbesen, T.W.; Mioskowski, C. Supramolecular Self-Assembly of Lipid Derivatives on Carbon Nanotubes. *Science* **2003**, *300* (5620), 775–778. https://doi.org/10.1126/science.1080848.

(5) Nakashima, N.; Tomonari, Y.; Murakami, H. Water-Soluble Single-Walled Carbon Nanotubes via Noncovalent Sidewall-Functionalization with a Pyrene-Carrying Ammonium Ion. *Chem. Lett.* **2002**, *31* (6), 638–639. https://doi.org/10.1246/cl.2002.638.

(6) Chiu, C. F.; Dementev, N.; Borguet, E. Fluorescence Quenching of Dyes Covalently Attached to Single-Walled Carbon Nanotubes. *J. Phys. Chem. A* **2011**, *115* (34), 9579–9584. https://doi.org/10.1021/jp200152z.

(7) Yoshimura, S.H.; Khan, S.; Maruyama, H.; Nakayama, Y.; Takeyasu, K. Fluorescence Labeling of Carbon Nanotubes and Visualization of a Nanotube protein Hybrid under Fluorescence Microscope. *Biomacromolecules* **2011**, *12* (4), 1200–1204. https://doi.org/10.1021/bm101491s.

(8) Berlier, J. E.; Rothe, A.; Buller, G.; Bradford, J.; Gray, D. R.; Filanoski, B. J.; Telford, W. G.; Yue, S.; Liu, J.; Cheung, C. Y.; Chang, W.; Hirsch, J. D.; Beechem, J. M.; Haugland, R. P.; Haugland, R. P. Quantitative Comparison of Long-Wavelength Alexa Fluor Dyes to Cy Dyes: Fluorescence of the Dyes and Their Bioconjugates. *J. Histochem. Cytochem.* **2003**, *51* (12), 1699–1712. https://doi.org/10.1177/002215540305101214.

(9) Jena Bioscience. Click Chemistry Background Information. **2017**, 1–6.

(10) Joshi, D.; Hauser, M.; Veber, G.; Berl, A.; Xu, K.; Fischer, F. R. Super-Resolution Imaging of Clickable Graphene Nanoribbons Decorated with Fluorescent Dyes. *J. Am. Chem. Soc.* **2018**, *140* (30), 9574–9580. https://doi.org/10.1021/jacs.8b04679.

Chapter 5

Click functionalization of single-walled carbon nanotubes with DNA strands

5.1 Introduction

DNA has excellent potential as a building block since it possesses all of the fundamental characteristics required to create nanoscale electrical devices, which may be used in decentralized clinical testing, environmental monitoring, and food safety[1]. The research into biological applications of nanosystems shaped by functionalizing carbon nanotubes with biological molecules has increased exponentially[2]. DNA functionalized carbon nanotubes gained much attention due to the exceptional specificity of the DNA molecule interaction towards the complementary strands[2,3]. This phenomenon widens the application window when coupled with carbon nanotubes to produce novel nanosystems like DNA based biosensors[4] and nanodevices[5,6]. Hazani and co-workers reported about the specific hybridization of the covalently functionalized DNA-SWNTs through confocal fluorescence imaging[7]. Moreover, the single-stranded DNA molecule offers us the advantage of defined length, sequence and feasible opportunity to functionalize with the molecule of our interest[8].

Though DNA molecules can be functionalized non-covalently[9,10], the use of covalent chemistry is expected to provide better stability, accessibility and selectivity[11]. Harmers and co-workers have reported about the covalent attachment of DNA oligonucleotides with amine-terminated single-walled carbon nanotubes[12]. Meyyapan et al. reported the covalent attachment of DNA molecules to oxidized multi-walled carbon nanotubes arrays as a nano electrode platform for sensing applications[13].

Copper-free click chemistry is the most suitable way of functionalizing the SWNTs covalently as they do not involve metal catalyst in the reaction[14]. The interference of these metal ions might cause damage not only to biological processes but also in the area of electrical and optoelectronic phenomena. It had been reported in several pieces of literature that metal ions such as copper influence the genetic structure of the DNA and its process, affecting the fluorescence quenching of quantum dots and can alter the structure of protein repelling organic moieties apart from toxicity[14–16]

One of the significant challenges that we face during the investigation of photophysical properties of the fluorescent dye functionalized SWNTs through advanced microscopic setups such as FLIM and STORM is the grafting efficiency of the fluorophores towards the nanotubes. Limited photon budget of fixed target labels (For e.g., AF647 functionalized SWNTs) makes the single-molecule localization technique like STORM challenging to employ. An alternative technique to generate blinking target molecules is used in the so-called Points Accumulation in Nanoscale Topography (PAINT) technique[17,18].

Fluorescently labeled imagers (ATTO655 imaging strands in our case) freely circulate in solution and bind to targets of interest either statically or transiently in this approach. The target molecule or structure of interest (ss-DNA functionalized SWNTs in our case) seems to "blink" due to binding. This allows for the separation of blinking from the photophysical dye switching features, which solves one of STORM's problems. However, diffusing imagers connect to their targets via electrostatic or hydrophobic contacts, making it difficult to program many target species in a single cell, limiting simple multiplexed detection.

Here, we show a variation of this PAINT technique known as DNA-PAINT[19], which achieves stochastic switching of fluorescence signals between the ON and OFF states by the repetitive, transient binding of fluorescent-labeled strands (ss-DNA

with ATTO655) to complementary strands (DBCO attached ss-DNA) that are conjugated to targets (SWNTs). This technique allows us to localize with nanometer precision and the flexibility to alter the DNA molecule of our interest.

It is significant to know the distance that the fluorophores are attached away to investigate the photophysical properties. One of the main reasons to know this is that the fluorescence quenching is distance-dependent[20]. Recently, Füllbrunn et al. reported that the distance-dependent graphene induced energy transfer (GIET) between the protein and carbon nanomaterial graphene by using DNA strands conjugated with fluorescent dyes[21]. Similarly, we functionalize the single-walled carbon nanotubes with single-stranded DNA of different lengths (~1 nm, ~8 nm and ~15 nm) via the same SPAAC route.

5.2 Results and Discussion

Figure 5.1 shows the super-resolved image of SWNTs functionalized single-stranded DNA molecule of ~1 nm length via DNA-PAINT approach. Imager DNA strand solution of 1 nM is used along with ATTO 655 fluorescent dye coupled to it. Densely packed structures are imaged from the sample solution for 50 K frames.

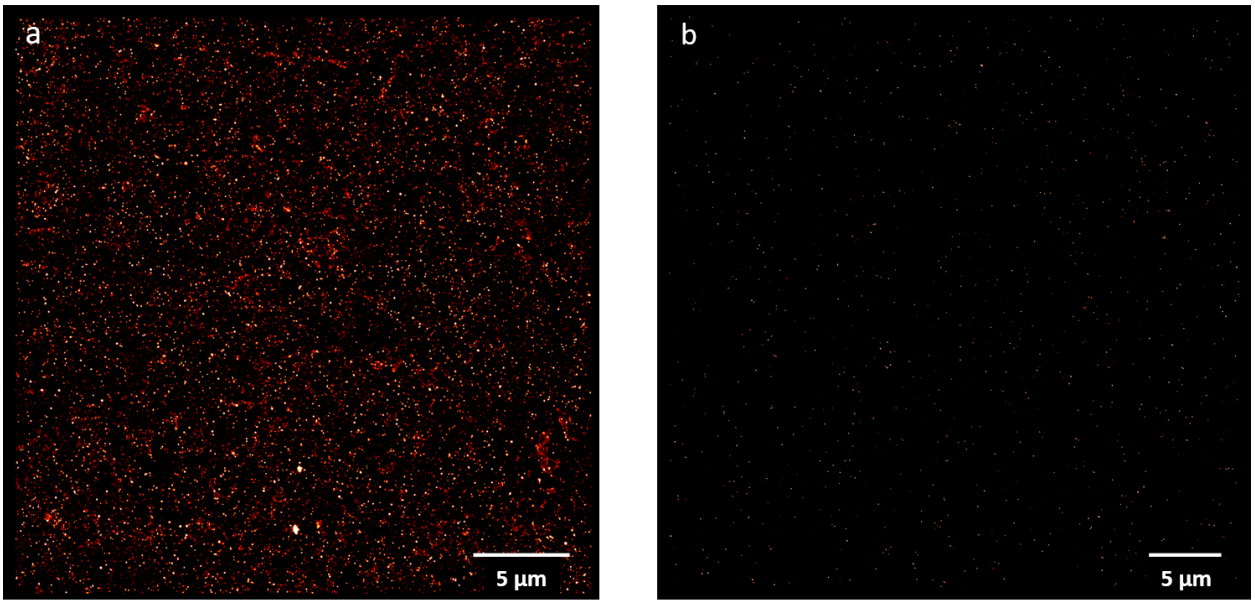

Figure 5.1 a) DNA-PAINT image of functionalized SWNTs with ss-DNA molecule of length ~1 nm (50 K frames) b) Control experiment with 1 nM imager ATTO655 dye conjugated with imager DNA strand without nanotubes (20 K frames).

The first trial clearly shows us the successful grafting of ss-DNA molecules with SWNTs. A control experiment is also carried out to investigate the specificity of the interactions between the complementary DNA strands and imager strands. As expected, there is no effective binding between DNA strands and coverslips, but some spots are imaged in negative control measurements, which might be due to the interaction between the imager strands and the PLL-PEG coated coverslips. PLL-PEG coated coverslips are used to neglect the unspecific binding between the glass

coverslips and the imager strands. We still find them in our control experiments, but they are negligible.

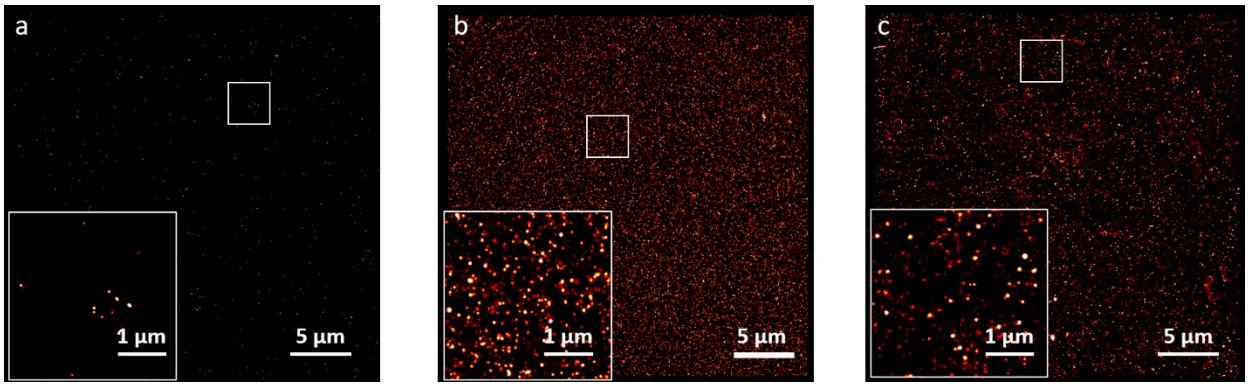

Figure 5.2 DNA-PAINT images of ss-DNA functionalized SWNTs. a) Control experiment image b) Undiluted nanotubes c) 1:100 diluted nanotubes. Sample solutions were drop cast on PLL-PEG coated coverslip and imaged for 20 K frames. Imager strand concentration: 1 nM ss-DNA-ATTO655.

Figure 5.2 shows the comparison between the DNA-PAINT images with different nanotubes concentrations and the control experiment. All the images are recorded for the same frame rate (20 K frames) for better correlation. As illustrated in figure 5.2, a well-diluted solution shows a better view of tubular structures densely grafted with ss-DNA molecules.

To investigate the fluorescence quenching, we choose to have ss-DNA molecules of different lengths, representing the functionalized SWNTs. A single-stranded DNA molecule of a length of ~8 nm and ~15 nm was employed to functionalize with SWNTs along with the short ~1 nm ss-DNA molecule. Figure 5.3 shows the DNA-PAINT images from the different lengths of DNA molecules grafted with SWNTs. Successful functionalization of SWNTs with different ss-DNA molecules was demonstrated. Figure 5.3 (d) shows clear tubular structures are imaged at high

resolution using the same imager strand conjugated with ATTO 655 fluorescent dye for 45K frames.

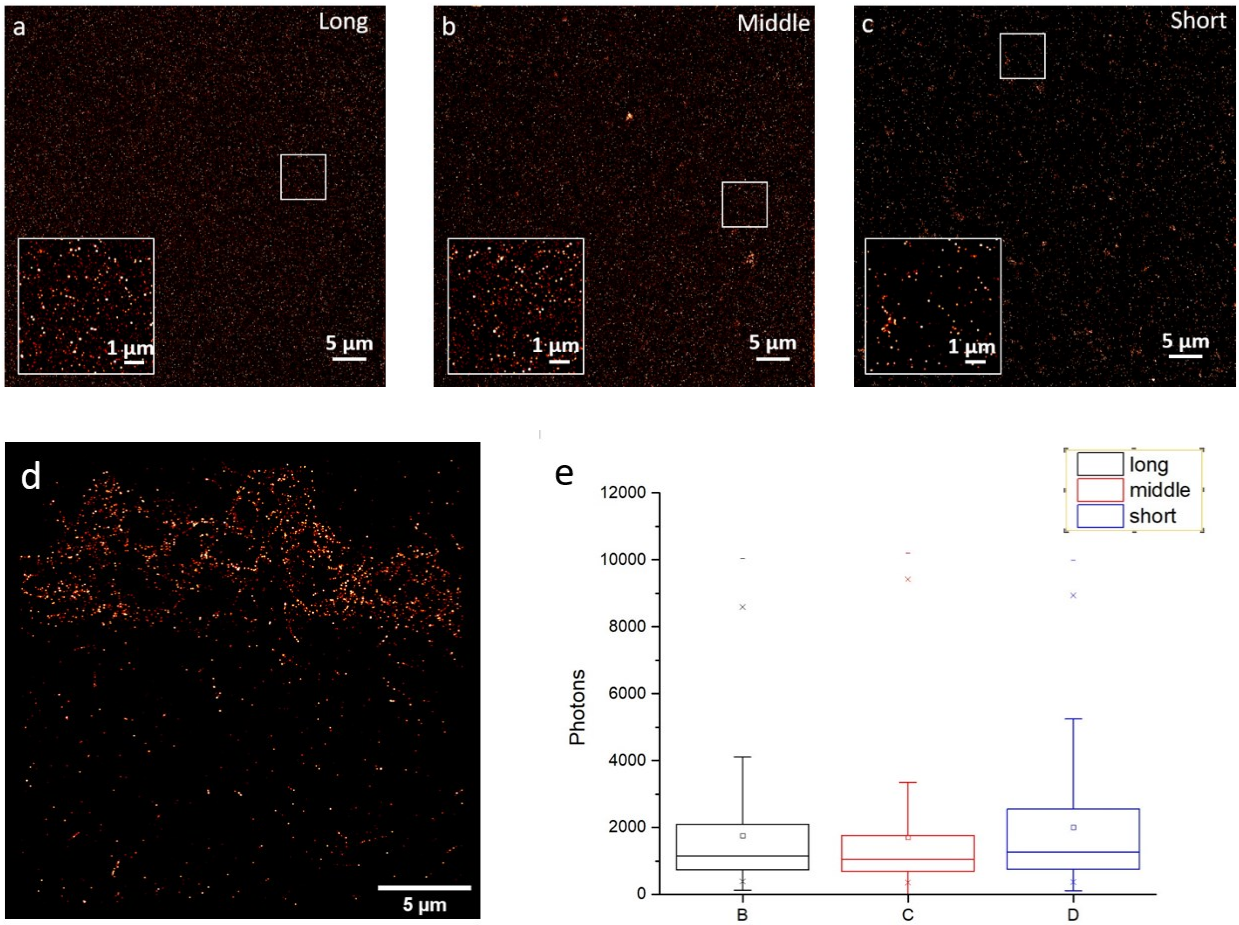

Figure 5.3 DNA-PAINT images of SWNTs functionalized with ss-DNA of different lengths: a) Long (~15 nm), b) Middle (~8 nm) and c) Short (~1 nm). Imaged with 20 K frames on a standard glass coverslip. Imager strand concentration: 1 nM ATTO 655. d) Zoomed in view of the figure. b) Middle ss-DNA SWNTs imaged for 45 K frames. e) Graph illustrates the fluorescence intensity correlation between short, middle and long ss-DNA functionalized SWNTs.

Figure 5.3 (e) shows the correlative analysis of DNA strands functionalized with SWNTs with different lengths. The intensities for the three different lengths of ss-

DNA molecules functionalized SWNTs look similar without much change. We expected a change in intensities as the fluorescence quenching is distance dependent. However, we observed not much of a significant difference in intensities for three different ss-DNA molecules though they are functionalized covalently to the surface of the SWNTs. This might be due to the fact that the ss-DNA molecules are not enough apart from the SWNTs.

5.3 Conclusion

In this chapter, we show that the single-stranded DNA molecule can be functionalized with the SPAAC route. The absence of metal catalyst in this click reaction makes this route effective for attaching DNA molecules in a non-toxic way with SWNTs. Investigation of fluorescent quenching of SWNTs is carried out after functionalizing them with different ss-DNA strands like ~1 nm, ~8 nm and ~15 nm. Successful functionalization of DNA stranded SWNTs was demonstrated through advanced imaging via the DNA-PAINT approach. Due to the unlimited photon budget, we can able to image till 45 K frames.

However, there is no significant change in the intensity correlation of SWNTs functionalized with different ss-DNA molecules of various lengths. This might be due to the fact that the DNA molecules are in close proximity after functionalization. Imager strands that interact transiently to the functionalized SWNTs tend to have ATTO655 dye facing towards the nanotube, reducing the distance between the fluorescent dye and SWNTs. Besides, the length of DNA molecules should be increased even further to observe a significant change in the fluorescence intensity. It should assist in understanding the fluorescence quenching better, which helps design sensors such as DNA based sensors.

5.4 References

(1) Guo, M.; Chen, J.; Liu, D.; Nie, L.; Yao, S. Electrochemical Characteristics of the Immobilization of Calf Thymus DNA Molecules on Multi-Walled Carbon Nanotubes. *Bioelectrochemistry* **2004**, *62* (1), 29– 35. https://doi.org/https://doi.org/10.1016/j.bioelechem.2003.10.005.

(2) Daniel, S.; Rao, T. P.; Rao, K. S.; Rani, S. U.; Naidu, G. R. K.; Lee, H.-Y.; Kawai, T. A Review of DNA Functionalized/Grafted Carbon Nanotubes and Their Characterization. *Sensors Actuators B Chem.* **2007**, *122* (2), 672–682. https://doi.org/https://doi.org/10.1016/j.snb.2006.06.014.

(3) Williams, K. A.; Veenhuizen, P. T. M.; de la Torre, B. G.; Eritja, R.; Dekker, C. Carbon Nanotubes with DNA Recognition. *Nature* **2002**, *420* (6917), 761. https://doi.org/10.1038/420761a.

(4) Mao, S.; Lu, G.; Yu, K.; Chen, J. Specific Biosensing Using Carbon Nanotubes Functionalized with Gold Nanoparticle–Antibody Conjugates. *Carbon N.Y.* **2010**, *48* (2), 479– 486. https://doi.org/https://doi.org/10.1016/j.carbon.2009.09.065.

(5) Dong, X.; Lau, C. M.; Lohani, A.; Mhaisalkar, S. G.; Kasim, J.; Shen, Z.; Ho, X.; Rogers, J. A.; Li, L.-J. Electrical Detection of Femtomolar DNA via Gold-Nanoparticle Enhancement in Carbon - Nanotube - Network Field - Effect Transistors. *Adv. Mater.* **2008**, *20* (12), 2389 – 2393. https://doi.org/https://doi.org/10.1002/adma.200702798.

(6) Chen, Y.; Vedala, H.; Kotchey, G.P.; Audfray, A.; Cecioni, S.; Imberty, A.; Vidal, S.; Star, A. Electronic Detection of Lectins Using Carbohydrate - Functionalized Nanostructures: Graphene versus Carbon Nanotubes. *ACS Nano* **2012**, *6* (1), 760–770. https://doi.org/10.1021/nn2042384.

(7) Hazani, M.; Naaman, R.; Hennrich, F.; Kappes, M. M. Confocal Fluorescence Imaging of DNA-Functionalized Carbon Nanotubes. *Nano Lett.* **2003**, *3* (2), 153–155. https://doi.org/10.1021/nl025874t.

(8) Sánchez - Pomales, G.; Santiago - Rodríguez, L.; Cabrera, C.R. DNA- Functi onalized Carbon Nanotubes for Biosensing Applications. *J. Nanosci. Nanotec hnol.* **2009**, *9* (4), 2175–2188. https://doi.org/10.1166/jnn.2009.se47.

(9) Chen, R.J.; Zhang, Y.; Wang, D.; Dai, H. Noncovalent Sidewall Functionaliz ation of Single-Walled Carbon Nanotubes for Protein Immobilization. *J. Am. Chem. Soc.* **2001**, *123* (16), 3838–3839. https://doi.org/10.1021/ja010172b.

(10) Guo, Z.; Sadler, P.J.; Tsang, S.C. Immobilization and Visualization of DNA and Proteins on Carbon Nanotubes. *Adv. Mater.* **1998**, *10* (9), 701–703. https://doi.org/https://doi.org/10.1002/(SICI)1521- 4095(199806)10:9<701:: AID-ADMA701>3.0.CO;2-4.

(11) Chen, W.; Tzang, C. H.; Tang, J.; Yang, M.; Lee, S. T. Covalently Linked Deoxyribonucleic Acid with Multiwall Carbon Nanotubes: Synthesis and Characterization. *Appl. Phys. Lett.* **2005**, *86* (10), 103114. https://doi.org/10.1 063/1.1880439.

(12) Baker, S.E.; Cai, W.; Lasseter, T.L.; Weidkamp, K.P.; Hamers, R.J. Covalent ly Bonded Adducts of Deoxyribonucleic Acid (DNA) Oligonucleotides with Single - Wall Carbon Nanotubes: Synthesis and Hybridization. *Nano Lett.* **20 02**, *2* (12), 1413–1417. https://doi.org/10.1021/nl025729f.

(13) Nguyen, C.V; Delzeit, L.; Cassell, A.M.; Li, J.; Han, J.; Meyyappan, M. Preparation of Nucleic Acid Functionalized Carbon Nanotube Arrays. *Nano Lett.* **2002**, *2* (10), 1079–1081. https://doi.org/10.1021/nl025689f.

(14) Jewett, J.C.; Bertozzi, C.R. Cu- Free Click Cycloaddition Reactions in Chemi cal Biology. *Chem. Soc. Rev.* **2010**, *39* (4), 1272 – 1279. https://doi.org/10.10 39/b901970g.

(15) Tajmir-Riahi, H. A.; Langlais, M.; Savoie, R. A Laser Raman Spectroscopic Study of the Interaction of Calf-Thymus DNA with Cu(II) and Pb(II) Ions: Metal Ion Binding and DNA Conformational Changes. *Nucleic Acids Res.* **1988**, *16* (2), 751–762. https://doi.org/10.1093/nar/16.2.751.

(16) Shey, M. S.; Hughes, E. J.; de Kock, M.; Barnard, C.; Stone, L.; Kollmann, T. R.; Hanekom, W. A.; Scriba, T. J. Optimization of a Whole Blood Intracellular Cytokine Assay for Measuring Innate Cell Responses to Mycobacteria. *J. Immunol. Methods* **2012**, *376* (1 – 2), 79 – 88. https://doi.org/10.1016/j.jim.2 011.11.011.

(17) Agasti, S.S.; Wang, Y.; Schueder, F.; Sukumar, A.; Jungmann, R.; Yin, P. DNA-Barcoded Labeling Probes for Highly Multiplexed Exchange-PAINT Imaging. *Chem. Sci.* **2017**, *8* (4), 3080 – 3091. https://doi.org/10.1039/C6SC0 5420J.

(18) Lelek, M.; Gyparaki, M.T.; Beliu, G.; Schueder, F.; Griffié, J.; Manley, S.; Jungmann, R.; Sauer, M.; Lakadamyali, M.; Zimmer, C. Single Molecule Localization Microscopy. *Nat. Rev. Methods Prim.* **2021**, *1* (1), 39. https://doi .org/10.1038/s43586-021-00038-x.

(19) Schnitzbauer, J.; Strauss, M.T.; Schlichthaerle, T.; Schueder, F.; Jungmann, R. Super-Resolution Microscopy with DNA-PAINT. *Nat. Protoc.* **2017**, *12* (6), 1198–1228. https://doi.org/10.1038/nprot.2017.024.

(20) Swathi, R. S.; Sebastian, K.L. Excitation Energy Transfer from a Fluorophore to Single-Walled Carbon Nanotubes. *J. Chem. Phys.* **2010**, *132* (10), 104502.

https://doi.org/10.1063/1.3351844.

(21) Füllbrunn, N.; Li, Z.; Jorde, L.; Richter, C.P.; Kurre, R.; Langemeyer, L.; Yu, C.; Meyer, C.; Enderlein, J.; Ungermann, C.; Piehler, J.; You, C. Nanoscopic Anatomy of Dynamic Multi-Protein Complexes at Membranes Resolved by Graphene - Induced Energy Transfer. *Elife* **2021**, *10*, e62501. https://doi.org/10.7554/eLife.62501.

Chapter 6

Substrate functionalization of CVD grown carbon nanotubes

6.1 Introduction

Carbon nanotubes are a primary candidate for biosensors because of their physicochemical characteristics of fast electron transfer between diverse electroactive species and the electrode. They offer good chemical stability and tailorable surface chemistry with versatile functionalization methods to immobilize biomolecules. To recognize specific biomaterials, a synergic hybrid biomaterial comprised of biomolecules and carbon nanotubes with excellent capabilities is necessary[1]. In addition, metal nanoparticles decorated carbon nanotubes are also used in different sensing applications for their exceptional optical, magnetic and electrical properties[2,3]. CNTFET sensors can sense analytes that can be controlled by tuning the functionalization density with a high degree of control[4,5].

Drop casting has been used as the standard method to deposit carbon nanotubes on various substrates because of their cost-effectiveness and simple implementation[6,7]. However, the unreliable positioning and orientation of deposited CNTs often confine the development and extensive scaling of CNTFET biosensors. CVD synthesis offers the opportunity to grow CNTs directly on a substrate. Positioning the catalyst particles on the substrate also plays a significant role in the carbon nanotube's growth as the catalyst residues affect the substrate's further processing, especially device fabrication. Pristine CNTs tend to form bundles when dispersed onto a substrate. Fabrication of electronic devices based on long, individual functionalized SWNTs requires the functionalization to be carried out on tubes directly on a substrate. Selective functionalization of CVD grown nanotubes involves many difficulties as it should be more specific to the surface of the nanotubes. The functionalization procedure may disturb the integrity of the carbon nanotube during the process, and

non-reacted analytes at the surface of the substrate also affect the post-functionalization characterization. Functionalized carbon nanotube-based biosensors have been demonstrated for biomolecular sensing applications, especially label-free CNTFET biosensors, as they are susceptible to variations in the surrounding environment [8,9].

Qi et al. reported that the azide attached SWNTs were functionalized via click chemistry with alkyne modified protein, used as a sensing platform with good sensitivity and stability for the immunoassay[10]. Covalently attached SWNTs and DWNTs TFTs have also reported the concept of electrical sensing with excellent sensitivity and selectivity simultaneously[11]. Li et al. reported enhancing detection sensitivity of single-walled carbon nanotube networks FET through DNA hybridization with gold nanoparticles for sensing application[12].

This chapter demonstrates that the CVD grown nanotubes can be functionalized selectively by various biomolecules and metal nanoparticles in different substrates. Moreover, we show that the carbon nanotubes can be grown through two different catalyst depositions (i) Drop casting the diluted catalyst (ii) Capillary stamping through porous silica stamps. SPAAC route can be transferred with minor changes to a variety of substrates, including transparent substrates, which are feasible for high-resolution imaging and studying photophysical properties. To demonstrate that our route can be transferred to the substrate, we carry out all functionalization steps on carbon nanotubes on different substrates such as Si/SiO_2 substrates, quartz substrates and quartz coverslips.

6.2 Results and Discussion

For substrate functionalization, individual long tubes are preferred as the dense networks might interfere with the functionalization procedure and become complex to fabricate devices further. This can be controlled by diluting the catalyst particles, which eradicates the larger catalyst particles. As illustrated in figure 6.1, carbon nanotubes are grown and imaged to investigate catalyst residues' impact and effect. Figure 6.1 a) shows the SEM image of CVD grown nanotubes from the non-diluted catalyst deposition through drop casting. It formed a very dense network of nanotubes after the CVD process. Figure 6.1 b) represents the CVD grown nanotubes from the well diluted catalyst. As expected, the diluted catalyst produced long elongated single structures, whereas the non-diluted catalyst offered dense networks of nanotubes.

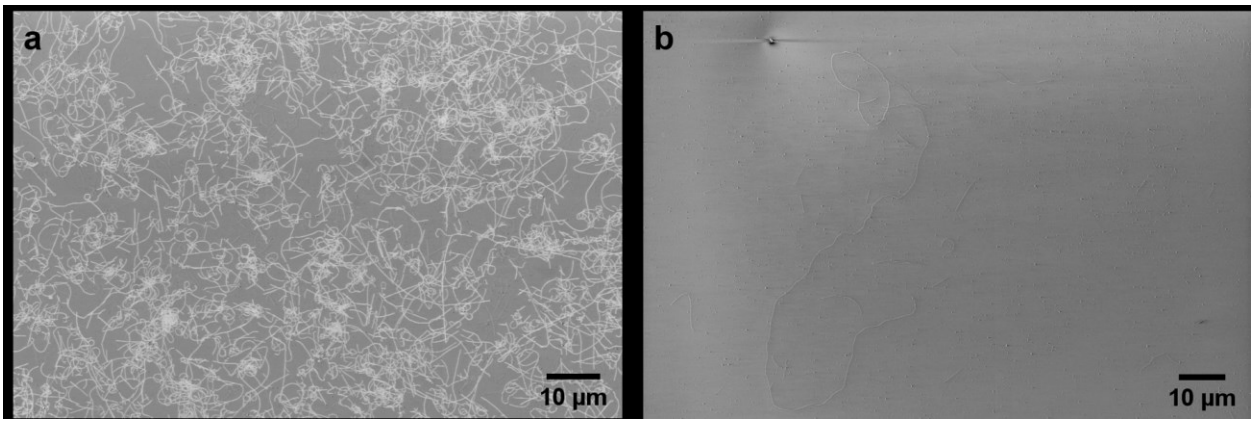

Figure 6.1 SEM images of the CVD grown nanotubes from a) diluted catalyst and b) non-diluted catalyst. Catalysts are deposited on Si/SiO_2 substrate through drop casting.

Another alternative technique to deposit the catalyst particles to produce single, long elongated nanotubes is stamping diluted catalysts through nanoporous silica stamps. In one of our recent publications, we grew nanotubes by stamping the catalyst

particles equidistantly and observed that the nanotubes were grown from the relatively more minor catalyst particles[13].

Firstly, substrate functionalization is carried out on the CVD grown nanotubes with gold nanoparticles on silicon substrates. Carbon nanotubes are grown by CVD on the p-doped Si/SiO_2 substrate from the diluted catalyst to prevent catalyst residue from covering the surface.

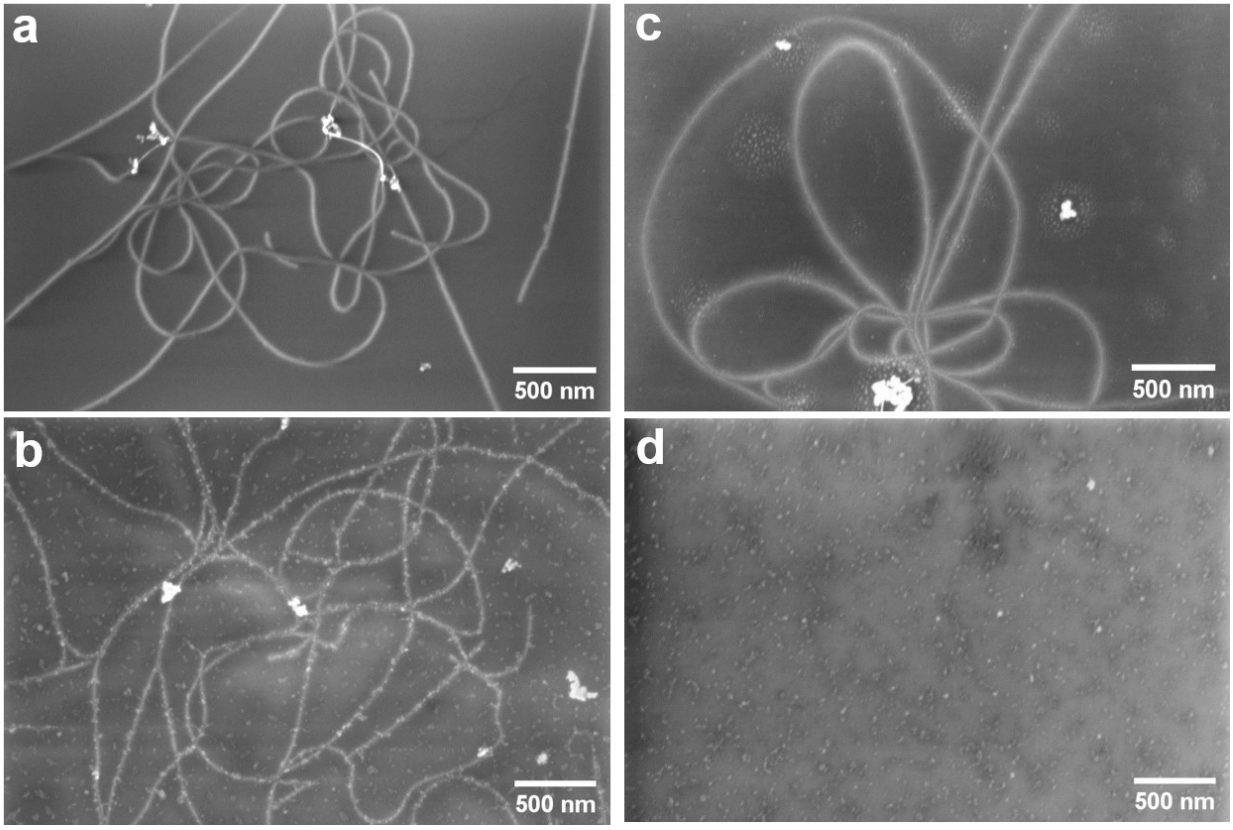

Figure 6.2 SEM images of CVD grew carbon nanotubes functionalization with gold nanoparticles. a) Before and b) After functionalization c) Control experiment-CVD grew nanotubes FDTS silanized and oxidized at 450 °C for 30 minutes and d) Control experiment- FDTS silanized substrate 450 °C for 30 minutes.

Surface passivation of the substrate is necessary since otherwise, the SiO_2 surface of the substrate would be silanized and therefore functionalized along with the CNTs. The passivation layer has to sustain oxidation for 30 minutes in air at T = 450 °C. Therefore, we chose another silane, FDTS, a thermally stable silane, to passivate the SiO_2. Figure 6.2 (a & b) show SEM images before and after functionalization. Here, the CNTs are clearly covered with gold nanoparticles. The SEM image in figure 6.2 (c) shows the CVD grown nanotubes after the oxidation step. While the CNTs look similar to the pristine nanotubes, the oxidized FDTS appears as small dots on the surface. The control experiment is carried out with only FDTS coated substrate after the oxidation step (Figure 6.2 (d)) and confirms that the small dots are from the after oxidation effect of silane.

Gold functionalized nanotubes have the homogeneity and density of the functionalization similar to the one presented in the figure for samples prepared in solution in Chapter 3. After successfully functionalizing CVD grown nanotubes with gold nanoparticles, we implement the same route with fluorescent dye AF647 on optically transparent substrates. Catalyst deposition on the substrate is implemented in two different ways, such as drop casting and stamping.

Quartz substrate of thickness 0.5 mm is employed to grow nanotubes through drop-casting and stamping the diluted catalyst. Thus, the substrate can be used in microscopic techniques like FLIM to study the photophysical properties of the nanotubes. Substrate functionalization is carried out on the quartz substrate, the same as that of Si substrate. Figure 6.3 (a) shows the FLIM images and spectra of catalyst stamped CVD grown nanotubes functionalized with AF647 dye. As expected, there are two fluorescent lifetimes: 1.5 ns and 0.7 ns.

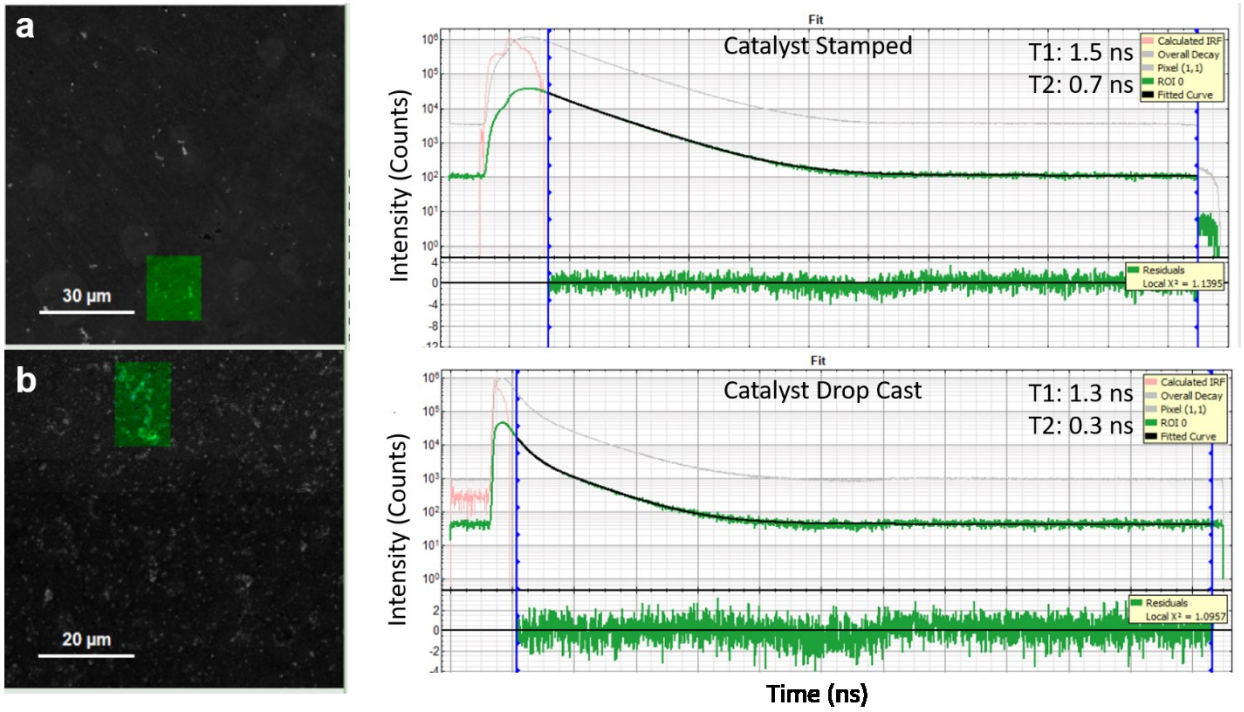

Figure 6.3 FLIM images and analysis of AF647 functionalized CVD grew nanotubes on a quartz substrate of thickness 0.5 mm. a) Catalyst Stamped b) Catalyst Drop Cast. Reference experiment of lifetime analysis with only AF647 dye on quartz substrate and only catalyst on quartz substrate are noted as 1.1 ns and 1.5 ns, respectively.

Comparing this with the AF647 functionalized SWNTs in Chapter 4, a slight increase in lifetimes is detected for the catalyst stamped sample. The reference measurement is carried out with only catalyst particles on quartz to investigate the lifetime and noted as 1.5 ns. We attribute the T_1=1.5 ns to the catalyst particles produced after stamping and the other lifetime T_2=0.7 ns to the fluorescent dye functionalized SWNTs. This increase in both lifetimes might be due to the influence of stamp residues that stick to the substrate's surface along with catalyst particles on the substrate. In addition to this, figure 6.3 (b) shows the FLIM spectra of diluted

catalyst drop cast CVD grown nanotubes functionalized with AF647. The fluorescent lifetimes are noted as T_1=1.3 ns and T_2=0.3 ns, respectively.

Interestingly, both lifetimes look similar to that of AF647 functionalized SWNTs explained in Chapter 4. We attribute this difference in lifetimes to the catalyst and absence stamp residues. There is a drawback as the big catalyst particles affect the functionalization and thus lifetime analysis. It is indeed a complex task to resolve the nanostructures through FLIM setup, and we need to opt for an advanced imaging technique.

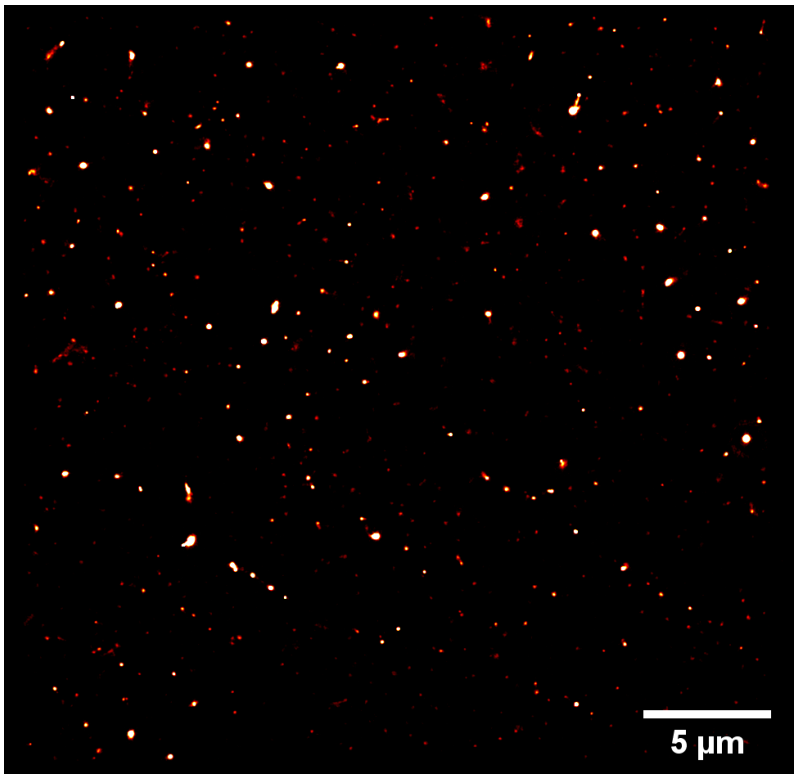

Figure 6.4 d-STORM image of AF647 functionalized CVD grown carbon nanotubes on quartz coverslip.

There is a need to resolve the structure at higher magnification, and quartz substrate of thickness 0.5 mm is not suitable for high-resolution imaging technique to image at nanoscale range. The alternative optically transparent substrate needs to satisfy

the demands of a normal glass coverslip such as thickness and refractive index and have the tendency to withstand the CVD thermal treatment of more than 1000 °C.

Quartz coverslip of the same thickness and refractive index as glass coverslip is employed to grow carbon nanotubes and functionalize them as we did in previous substrates. This allows us to image at high resolution through advanced microscopic techniques like STORM and study the photophysical property in individual nanotube structures. Quartz coverslips are used as the substrate, and the catalyst is deposited through drop-casting. Functionalization is carried out on the quartz coverslip very carefully as they are delicate and can be broken easily.

After functionalizing the coverslip with AF647, we investigated them with STORM microscopy to confirm that the process was successful. As illustrated in figure 6.4, we image nanotube structures densely covered with fluorescent dyes along with some agglomerations of dyes. We could image the nanotubes at higher magnification but not study the photophysical properties as they bleach very fast.

6.3 Conclusion

This chapter demonstrated that the functionalization route we followed for SWNTs could also be transferred to the substrates. Furthermore, the decoration of gold nanoparticles was achieved by the same route on substrate grown nanotubes and thus makes way to fabricate nanoelectronic devices for sensing, transport and other studies. Control experiments suggest that the functionalization is specific to the surface of the nanotubes. Diluted catalyst helps achieve a single elongated nanotube, which is vital for device fabrication, and different forms of catalyst deposition were also explored. Substrate functionalization of CVD grown nanotubes selectively widens the application in sensing applications.

Interestingly, the route can also be successfully transferred to the optically transparent substrates like quartz substrate and coverslips. Fluorescence lifetime analysis correlates the difference between stamped and drop casted CVD functionalized nanotubes. Stamp residues and catalyst agglomeration affect the analysis of fluorescence lifetime as they tend to agglomerate fluorescent dyes. Resolving the fluorescent dye functionalized CVD grown nanotubes is a complex task in substrates with relatively higher thickness. Quartz coverslip functionalization of nanotubes is unique and assisted us to image the nanotubes in higher magnification through the STORM technique. High resolution imaging of ultra-structures not only image at nanoscale but also opens the gate to explore photophysical properties.

6.4 References

(1) Hou, G.; Zhang, L.; Ng, V.; Wu, Z.; Schulz, M. Review of Recent Advances in Carbon Nanotube Biosensors Based on Field-Effect Transistors. *Nano Life* **2016**, *06*, 1642006. https://doi.org/10.1142/s179398441642006x.

(2) Martin, C. R.; Kohli, P. The Emerging Field of Nanotube Biotechnology. *Nat. Rev. Drug Discov.* **2003**, *2* (1), 29–37. https://doi.org/10.1038/nrd988.

(3) Saito, N.; Usui, Y.; Aoki, K.; Narita, N.; Shimizu, M.; Hara, K.; Ogiwara, N.; Nakamura, K.; Ishigaki, N.; Kato, H.; Taruta, S.; Endo, M. Carbon Nanotubes: Biomaterial Applications. *Chem. Soc. Rev.* **2009**, *38* (7), 1897–1903. https://doi.org/10.1039/B804822N.

(4) Gül, O.T.; Pugliese, K.M.; Choi, Y.; Sims, P.C.; Pan, D.; Rajapakse, A.J.; Weiss, G.A.; Collins, P.G. Single - Molecule Bioelectronics and Their Applic ation to Amplification-Free Measurement of DNA Lengths. *Biosensors* **2016**, *6* (3). https://doi.org/10.3390/bios6030029.

(5) Teker, K.; Wickstrom, E.; Panchapakesan, B. Biomolecular Tuning of Electro nic Transport Properties of Carbon Nanotubes via Antibody Functionalizatio n. *IEEE Sens. J.* **2006**, *6* (6), 1422 – 1427. https://doi.org/10.1109/JSEN.2006 .884564.

(6) Oh, J.; Yoo, G.; Chang, Y.W.; Kim, H.J.; Jose, J.; Kim, E.; Pyun, J.C.; Yoo, K.H. A Carbon Nanotube Metal Semiconductor Field Effect Transistor-Based Biosensor for Detection of Amyloid - Beta in Human Serum. *Biosens. Bioele ctron.***2013**,*50*,345 – 350. https://doi.org/https://doi.org/10.1016/j.bios.2013.0 7.004.

(7) Chang, J.; Mao, S.; Zhang, Y.; Cui, S.; Steeber, D. A.; Chen, J. Single-Walled Carbon Nanotube Field-Effect Transistors with Graphene Oxide Passivation

for Fast, Sensitive, and Selective Protein Detection. *Biosens. Bioelectron.* **2013**, *42*, 186–192. https://doi.org/10.1016/j.bios.2012.10.041.

(8) Zanganeh, S.; Khodadadei, F.; Tafti, S. R.; Abdolahad, M. Folic Acid Functionalized Vertically Aligned Carbon Nanotube (FA-VACNT) Electrodes for Cancer Sensing Applications. *J. Mater. Sci. Technol.* **2016**, *32* (7), 617–625. https://doi.org/https://doi.org/10.1016/j.jmst.2016.05.001.

(9) Chen, H.; Choo, T. K.; Huang, J.; Wang, Y.; Liu, Y.; Platt, M.; Palaniappan, A.; Liedberg, B.; Tok, A. I. Y. Label-Free Electronic Detection of Interleukin-6 Using Horizontally Aligned Carbon Nanotubes. *Mater. Des.* **2016**, *90*, 852–857. https://doi.org/https://doi.org/10.1016/j.matdes.2015.11.029.

(10) Qi, H.; Ling, C.; Huang, R.; Qiu, X.; Shangguan, L.; Gao, Q.; Zhang, C. Functionalization of Single-Walled Carbon Nanotubes with Protein by Click Chemistry as Sensing Platform for Sensitized Electrochemical Immunoassay. *Electrochim.Acta,* **2012**,*63*,76 – 82. https://doi.org/https://doi.org/10.1016/j.electacta.2011.12.084.

(11) Huang, J.; Ng, A. L.; Piao, Y.; Chen, C.-F.; Green, A. A.; Sun, C.-F.; Hersam, M. C.; Lee, C. S.; Wang, Y. Covalently Functionalized Double-Walled Carbon Nanotubes Combine High Sensitivity and Selectivity in the Electrical Detection of Small Molecules. *J. Am. Chem. Soc.* **2013**, *135* (6), 2306–2312. https://doi.org/10.1021/ja310844u.

(12) Dong, X.; Lau, C. M.; Lohani, A.; Mhaisalkar, S. G.; Kasim, J.; Shen, Z.; Ho, X.; Rogers, J. A.; Li, L.-J. Electrical Detection of Femtomolar DNA via Gold-Nanoparticle Enhancement in Carbon - Nanotube - Network Field - Effect Transistors. *Adv. Mater.* **2008**, *20* (12), 2389 – 2393. https://doi.org/https://doi.org/10.1002/adma.200702798.

(13) Schmidt, M.; Philippi, M.; Münzner, M.; Stangl, J. M.; Wieczorek, R.; Harneit, W.; Müller-Buschbaum, K.; Enke, D.; Steinhart, M. Capillary Nanostamping with Spongy Mesoporous Silica Stamps. *Adv. Funct. Mater.* **2018**, *28* (23). https://doi.org/10.1002/adfm.201800700.

Chapter 7

Summary and Future perspectives

This thesis presents a design establishment and investigation of carbon nanotubes functionalization to produce highly engineered carbon nanostructures with versatile molecules for numerous applications. Carboxylated single-walled carbon nanotubes are decorated with gold nanoparticles, fluorescent dyes and single-stranded DNA molecules via a non-toxic copper-free click chemistry route. The non-toxic and hybrid way of functionalizing SWNTs offers us the feasibility to integrate them in biosystems. Characteristics of nanotubes after every step in the route are explored through surface characterization techniques such as XPS, Raman and FTIR spectroscopic techniques. We showed that the functionalization density varies drastically concerning the type of solvent, strongly supported by XPS spectra and TEM correlation.

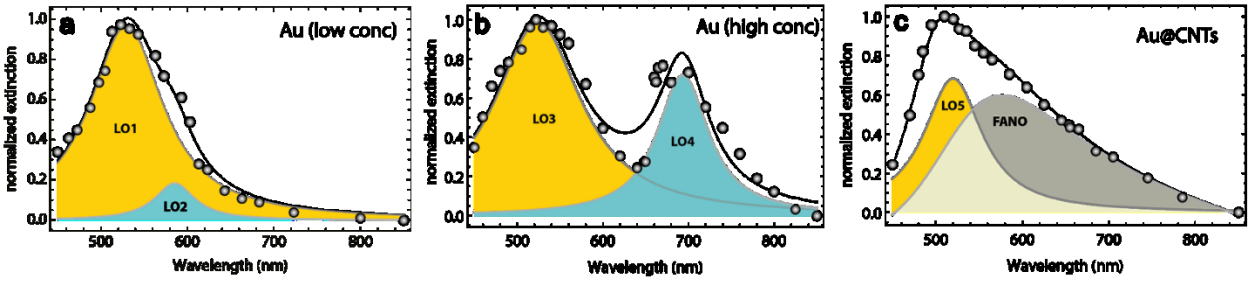

Figure 7.1 a) & b) Extinction coefficient of interaction between gold nanoparticles c) interaction between covalently functionalized SWNTs with gold nanoparticles.

Gold nanoparticles are grafted homogeneously onto the surface of the nanotubes, which has great potential in the field of sensing and catalysis. Gold nanoparticles grafted SWNTs has a wide range of application window in nanomedicine field as well. There is an exciting opportunity to explore the plasmon interactions of gold

functionalized SWNTs after our first experimental extinction coefficient comparison between the gold nanoparticles and AuNP-SWNTs. Figure 7.1 shows the extinction coefficient of both gold nanoparticles and SWNTs functionalized with gold nanoparticles. The extinction coefficient of gold nanoparticles peaked at around 530 nm matches the literature, and the broadened curve represents SWNTs functionalized covalently with gold nanoparticles. This part needs to be calculated theoretically for better understanding.

Fluorescent dyes functionalized nanotubes offer the possibility to investigate the fluorescent lifetime analysis through FRET-FLIM analysis. It is significant to understand the correlation between the structural and optical characteristics of the fluorescent dye functionalized nanotubes as chirality dependent. Raman, SEM and FLIM at the same area of interest assist us to understand the lifetime analysis better, though they were measured on the nanotube bundles.

SWNT bundles are a mix of chirality and behave differently due to their diverse energy band structure. In the future, it is noteworthy to employ chiral selective nanotubes for the analysis to be more accurate. Lifetime analysis of functionalized SWNTs was noted to be 0.4 ns, far less than the free dye lifetime of 1 ns. This phenomenon is attributed to the fluorescence quenching of the nanotubes.

Single molecule localization in an individual bundle is still challenging as the fluorescent dyes bleach fast in the FLIM and the complex task of imaging the structures at the nanoscale level. STORM imaging technique delivers the requirement with ease for the AF647 functionalized carbon nanotubes and resolves the structure at the nanoscale level. This phenomenon is of great interest in biomedical applications, especially cell tracking and labeling and drug delivery.

The results obtained from the fluorescent dye functionalization of SWNTs strongly suggest functionalizing length alterable biomolecules to understand the fluorescence quenching better. DNA functionalized SWNTs offer us to understand the quenching phenomena better as they are distance dependent. DNA-PAINT offers us the super resolved image of DNA functionalized SWNTs of 1 nm, 8 nm and 15 nm lengths. We imaged the SWNTs through the DNA-PAINT approach successfully though the intensity correlation looks similar for different lengths. With this knowledge, to investigate the fluorescence quenching phenomena, it is significant to understand the ss-DNA covalent attachment with SWNTs and employ lengthier DNA strands. In addition, employing different imager DNA strands where the dye faces away from the SWNTs increases the distance further. DNA based biosensors and nanodevices fabrication is the next step to employ the DNA functionalized SWNTs.

From all the above work, we realized that one of the major challenges in functionalizing SWNTs is bundling, as the nanotubes tend to form bundles easily when processed through wet chemistry. CVD-grown nanotubes are the question breaker as they are tunable and can be functionalized selectively and specifically, as we demonstrated in the previous chapter. Successful transfer of our synthetic route to CVD grown nanotubes wide opens the various options for different applications, especially nanoelectronic devices. Catalyst deposition plays a significant role in the CNT growth and influences the optical properties directly. We integrated gold nanoparticles and fluorescent dyes to CVD-grown nanotubes selectively on different substrates such as Si/SiO_2 substrate and optically transparent substrates. Interestingly, we functionalized CVD-grown nanotubes on the quartz coverslip of thickness 0.15 mm, similar to a standard glass coverslip. This clears the way to resolve the fluorescent dye functionalized on CVD-grown individual nanotube at the nanoscale.

Chapter 8
Appendix

8.1 List of Abbreviations

CNTs	Carbon Nanotubes
MWNTs	Multi Walled Carbon Nanotubes
SWNTs	Single Walled Carbon Nanotubes
DNA	Deoxyribose Nucleic Acid
SPAAC	Strain Promoted Azide Alkyne Cycloaddition
CuAAC	Copper catalyzed Azide Alkyne Cycloaddition
FRET	Förster Resonance Energy Transfer
FLIM	Fluorescence Lifetime Imaging Microscopy
CNTFET	Carbon Nanotube Field Effect Transistor
AF647	Alexa Fluor 647
STORM	Stochastic Optical Reconstruction Microscopy
PAINT	Point Accumulation In Nanoscale Topography
BZ	Brillouin Zone
vHSs	van Hove singularities
DOS	Density of States
VOS	Volatile Organic Solvents
DBCO	Dibenzocycloactyne
DMF	N,N-Dimethylformamide
IPA	Isopropanol

DMSO	Dimethylsulfoxide
FDTS	Perfluorodecyltrichlorosilane
CVD	Chemical Vapor Deposition
XPS	X-ray Photoelectron Spectroscopy
RBM	Radial Breathing Mode
DWNTs	Double Walled Carbon Nanotubes
TFTs	Thin Film Transistors
FT-IR	Fourier Transform Infrared Spectroscopy
Au-NPs	Gold Nanoparticles
TEM	Transmission Electron Microscopy
Cy3	Cyanine 3
AFM	Atomic Force Microscopy
EFM	Epi Fluorescence Microscopy
LSM	Laser Scanning Microscopy
ROI	Region of Interest
SEM	Scanning Electron Microscopy
GIET	Graphene Induced Energy Transfer
PLL-PEG	Poly-L-Lysine Poly ethylene glycol

8.2 List of Figures

8.3 Declaration

I hereby declare that the presented thesis

"Click Functionalization of Carbon Nanotubes for Nano-Bio Applications"

was prepared entirely on my own. Outside sources were not used without an explicit declaration in the text. The following persons attributed to this work as a collaboration partner or a student under my supervision.

Dr. Michael Holtmannspötter conducted the FLIM and dSTORM experiments.

Dr. Michael Philippi performed catalyst stamping and SEM experiments.

Jannis Thien conducted the XPS measurements.

Laura Meingast performed Raman measurements.

Alida Meyer conducted FLIM measurements.

I have not attempted a promotion before, and this work was not presented to any other institution before.

Osnabrueck

(11.10.2021) Gririraj Manoharan

8.4 List of Publications and Conference talks

1. Runge, M., Huebner, H., Grimm, A., Manoharan, G., Wieczorek, R., Philippi, M., Harneit, W., Meyer, C., Enke, D., Gallei, M., Steinhart, M., "Capillary Stamping of Functional Materials: Parallel Additive Substrate Patterning without Ink Depletion", Adv. Mater. Interfaces 2021, 8, 2001911'.

2. G. Manoharan, P. Bösel, J. Thien, L. Meingast, M. Runge, H. Eickmeier, M. Haase, J. Maultzsch, M. Steinhart, J. Wollschläger, and C. Meyer., "Click functionalization of Silanized Single-Walled Carbon Nanotubes", JPC-C 2021. (To be submitted).

3. Oral Presentation "Click functionalization of single walled carbon nanotubes" at Nanotube Conference21 at Rice University, 2021.

4. Oral Presentation on "Single walled carbon nanotubes: Functionalization and Characterization" at 2020 Joint Conference of the Condensed Matter Divisions of EPS (CMD) and RSEF (GEFES) 2020.

5. Poster Presentation on "Covalent dye functionalization of carbon nanotubes and their characteristics" at DPG Conference, Berlin, Germany, 2018.

8.5 Curriculum Vitae

2017-2021	**University of Osnabrueck** Department of Physics Electronic Transport Group (Dr. C. Meyer) **PhD in Physics** Doctoral Dissertation: **Click functionalization of carbon nanotubes for nano bio applications.**
2014-2016	**VIT University** Centre for Nanotechnology Research **M.Tech in Nanotechnology** Graduation: Masters of Technology Master thesis at **ARCI**: **High performance Multi Layer Varistors (MLV) from Synthesis and Processing of doped ZnO nanopowders.**
2010-2014	**Pondicherry University** Electronics and Communication Engineering **B.Tech in Electronics and Communication Engineering** Graduation: Bachelor of Technology